

# **GUIDELINES FOR DETERMINING THE CAPACITY OF D-REGIONS WITH PREMATURE CONCRETE DETERIORATION OF ASR/DEF**

John B. Mander  
Zachry Professor of Design and Construction Integration  
Zachry Department of Civil Engineering

Stefan Hurlbaas  
Associate Professor  
Zachry Department of Civil Engineering

Madhu M. Karthik  
Graduate Assistant Researcher  
Zachry Department of Civil Engineering

and

Reece M. Scott  
Graduate Assistant Researcher  
Zachry Department of Civil Engineering

Report 0-5997-P1  
Project 0-5997

Project Title: Structural Assessment of "D" Region Affected by Premature Concrete Deterioration

Performed in cooperation with the  
Texas Department of Transportation  
and the  
Federal Highway Administration

Published: November 2012

TEXAS TRANSPORTATION INSTITUTE  
The Texas A&M University System  
College Station, Texas 77843-3135



## **DISCLAIMER**

This research was performed in cooperation with the Texas Department of Transportation (TxDOT) and the Federal Highway Administration (FHWA). The contents of this report reflect the views of the authors, who are responsible for the facts and the accuracy of the data presented herein. The contents do not necessarily reflect the official view or policies of the FHWA or TxDOT. This report does not constitute a standard, specification, or regulation.

The United States Government and the State of Texas do not endorse products or manufacturers. Trade or manufacturers' names appear herein solely because they are considered essential to the object of this report.

## **ACKNOWLEDGMENTS**

This project was conducted at Texas A&M University in conjunction with the Texas Transportation Institute. The experiments were conducted in the High Bay Structures and Material Testing Laboratory. Mr. Matthew Potter is thanked for his assistance.

Funding for this project was provided via a contract with the Texas Department of Transportation (TxDOT) (Project 0-5997) with Mr. Dingyi Yang serving as Project Director. The guidance of Mr. Yang and the project control group is gratefully acknowledged.

# TABLE OF CONTENTS

1.	Forward.....	1
2.	Analysis Schema.....	3
	2.1 Scope.....	3
	2.2 Stage 1: Analysis Using Beam Theory.....	3
	2.3 Stage 2: Strut-and-Tie Analysis .....	10
	2.4 Stage 3: Analysis Using Compatibility Strut-and-Tie Methods.....	15
	2.4.1 Stage 3.1: C-STM Based on Undamaged Material Properties ....	16
	2.4.2 Stage 3.2: C-STM Allowing for ASR/DEF Damage and Its Effects .....	16
	2.5 Stage 4: Establish Acceptability of Structure.....	17
3.	Compatibility Strut-and-Tie Formulation.....	19
	3.1 Modeling Truss Action.....	19
	3.2 Modeling Arch Action.....	24
	3.3 Modeling the Combined Truss and Arch Action .....	24
	3.4 Stress and Strain Transformation for Flexural Equivalence .....	27
	3.5 C-STM Geometry and Axial Rigidity Assignments .....	31
	3.5.1 Truss Geometry.....	31
	3.5.2 Axial Rigidity.....	32
	3.6 Element Constitutive Material Relations .....	34
	3.6.1 Reinforcing Steel .....	34

3.6.2	Diagonal Concrete Struts .....	34
3.6.3	Concrete Tensile Strength.....	36
3.6.4	Concrete Compression Chord Members.....	38
3.6.5	Modified Material Properties to Account for ASR/DEF .....	38
3.7	Ultimate Strength and Softening of Constitutive Relations .....	45
3.7.1	Strut-and-Tie Strength Checks.....	45
3.8	Computational Implementation.....	45
4.	Worked Example 1 .....	51
4.1	Scope .....	51
4.2	The Structure .....	51
4.3	Stage 1: Strength Analysis Using Beam Theory .....	53
4.4	Stage 2: Strength Analysis Using Strut-and-Tie Modeling.....	57
4.5	Stage 3: Strength and Deformation Capacity Using Compatibility Strut-and-Tie Computational Modeling .....	60
4.6	C-STM Results and Discussion.....	64
4.7	Concluding Remarks on Worked Example 1 .....	67
5.	Worked Example 2 .....	69
5.1	Scope .....	69
5.2	The Structure .....	69
5.3	Stage 1: Strength Analysis Using Beam Theory .....	71
5.4	Stage 2: Strength Analysis Using Strut-and-Tie Modeling.....	74

5.5 Stage 3: Strength and Deformation Capacity Using Compatibility Strut-and-Tie Computational Modeling .....	79
5.6 C-STM Results and Discussion.....	82
5.7 Concluding Remarks on Worked Example 2 .....	87
6. Closure .....	89
References .....	91
Appendix A: Stage 1–3 Analysis–C-Beam Specimen.....	97

## LIST OF FIGURES

Figure 2–1: Flowchart for Analysis Procedure of Bridge Piers.....	4
Figure 2–2: Bridge Pier and Equivalent Beam Model for Flexure Analysis.....	5
Figure 2–3: Joint Arch Mechanism in Beam-Column Joint. ....	11
Figure 2–4: Strut-and-Tie Model of (a) Cantilever Bent (b) Straddle Bent. ....	13
Figure 3–1: Truss Model Idealization for a Fixed-Fixed Beam-Kim and Mander (1999). ....	21
Figure 3–2: Results of Convergence Study for Different Numerical Integration Schemes for C-STM Analysis. ....	22
Figure 3–3: Composition of Classic Arch and Truss Action That Leads to the Overall Compatibility Strut-and-Tie Model.....	25
Figure 3–4: Constitutive Stress-Strain Relationship for Compression Chord Elements. ....	29
Figure 3–5: Diagonal Concrete Web Elements. ....	37
Figure 3–6: Concrete Tension Stiffening Ties.....	37
Figure 3–7: Assumed Arching Mechanism Between Hoops for Rectangular Sections (Mander, 1983). ....	42
Figure 3–8: Confined Strength Determination from Lateral Confining Stresses for Rectangular Sections (Mander, 1983). ....	42
Figure 3–9: Modified Stress-Strain Model for Steel to Account for Prestressing Effects Due to ASR/DEF.....	44
Figure 3–10: SAP2000 Screenshot: Steel Truss (Top); Concrete Truss (Bottom).....	47
Figure 3–11: Nonlinear Constitutive Material Properties (a) Diagonal Web Members, (b) Compression Chord Elements, and (c) Tension Stiffened Elements .....	48
Figure 4–1: Elevation and Cross-Section of Specimen 2A (Bracci et al., 2000).....	52
Figure 4–2: Shear Force and Bending Moment Diagram of Equivalent Beam Model of Bent Cap Specimen 2A. ....	56
Figure 4–3: Strut-and-Tie Model of Reinforced Concrete Bridge Cap Specimen 2A. ....	58
Figure 4–4: C-STM Model and Results for Specimen 2A. ....	61
Figure 4–5: Cracked Reinforced Concrete Material Properties.....	63
Figure 4–6: Failure Analysis of Specimen 2A.....	65
Figure 5–1: Elevation and Cross-Section of the C-Beam Specimens. ....	70



Figure 5–2: Shear Force and Bending Moment Diagram of the Equivalent Beam Model of C-Beam Specimen 1 (Specimen 4). .....	75
Figure 5–3: Strut-and-Tie Model for C-Beam Specimen 1. ....	76
Figure 5–4: Failure Pattern Observed at the Beam-Column Joint of C-Beam Specimen 1. ....	78
Figure 5–5: Modeling the C-Beam Specimens without and with ASR/DEF Damage. ....	80
Figure 5–6: Cracked Reinforced Concrete Material Properties.....	81
Figure 5–7: Actual and Modified Stress-Strain Models for Reinforcing Steel to Account for Prestressing Effects in C-Beam Specimen 4. ....	83
Figure 5–8: Force-Deformation Results for Specimens 1 and 4.....	84
Figure 5–9: Failure Analysis of C-Beam Specimen 1. ....	86

## LIST OF TABLES

Table 3–1: Convergence Study of Higher Order Truss Models for a Cantilever Beam.....	21
Table 3–2: Elastic Truss Member Axial Rigidities.....	33
Table 4–1: Material Properties and Test Results.....	53
Table 4–2: Results for Stage 1 Flexure Analysis.....	55
Table 4–3: Results for Stage 1 Shear Analysis.....	55
Table 4–4: Results for Stage 2 SAT Analysis.....	59
Table 4–5: Axial Rigidity Assignments for Specimen 2A.....	62
Table 4–6: Result for Specimen 2A.....	67
Table 5–1: Material Properties and Test Results.....	71
Table 5–2: Results of Stage 1 Flexure Analysis (Without Deterioration).....	72
Table 5–3: Results of Stage 1 Shear Analysis.....	73
Table 5–4: Results for Stage 2 SAT Analysis.....	79
Table 5–5: Result for C-Beam Specimens 1 and 4.....	88

## 1. FORWARD

When a bridge engineer encounters a design or analysis problem concerning a bridge substructure, that structure will commonly have a mixture of member types, some slender, and some squat. Slender members are generally governed by flexure, and normal beam theory should suffice for analysis and design. Squat members can often be handled by beam theory too, although nowadays designers have a choice and may opt to use strut-and-tie (SAT) models.

When the structure possesses a mixture of beam (B-) regions and deep or disturbed (D-) regions the dilemma facing the structural engineer is: What method should one use for structural analysis and design?

The issue becomes even more murky when a structure already exists, but shows signs of damage and deterioration from the effects of alkali-silica reaction (ASR), delayed ettringite formation (DEF), or other deterioration mechanisms. The engineer is faced with a second dilemma: How do deteriorated material properties get incorporated into the analysis?

It is well-known that the behavior of deep beams or disturbed (or “D”) regions in a structural system cannot be accurately described according to conventional beam theory alone. This is due to the high irregularity of internal stress and strain distributions, accompanied by the interaction of flexure and shear. As a result, the coupled flexure and shear analysis of structural concrete members, especially deep beams, have been a contentious issue to both researchers and structural engineers for decades.

Conventional U.S. design standards for D-regions have historically been based on empirically derived expressions. The concept of strut-and-tie modeling (SAT) was first introduced as a method of strength design in the [AASHTO LRFD Bridge Design Specification \(2010\)](#) in 1994, and the [ACI 318 Building Code Requirements for Structural Concrete \(2011\)](#) in 2002. However, as a SAT model only satisfies force equilibrium and is intentionally formulated as a lower bound (plastic) solution, the critical mode of failure (i.e., element or nodal failure) is often illusive to the designer. Thus the ultimate failure mechanism might lead to an undesirable brittle collapse when imposed to overload scenarios.

Current nonlinear shear analysis models for structural concrete deep beams are generally complicated to use and have limited applicability or appeal to practicing engineers. Clearly, it is desirable to have a model that is derived from rational mechanics and validated with experimental evidence that can be implemented into commercially available structural analysis software. Therefore, a *Compatibility Strut-and-Tie Model* (C-STM) that is intended for the nonlinear analysis of shear critical reinforced concrete structures is presented.

These guidelines seek to demystify the above mentioned dilemmas. More specifically, guidelines are presented for determining the capacity of D-regions without and with premature concrete deterioration, in particular ASR and DEF effects.

In many cases either beam theory, or SAT methods should suffice in assessing the strength and safety of bridge substructures with or without ASR/DEF effects. However, as a supplementary analysis tool the C-STM approach can be used to augment the design process by accurately assessing the force-deformation response and nonlinear failure modes of deep beams with small span to depth ratios or D-regions.

## 2. ANALYSIS SCHEMA

### 2.1 SCOPE

This section presents the analysis methodology to be followed for the analysis of the structural capacity of bridge pier. The flowchart given in [Figure 2–1](#) depicts the procedure and the branching decision points that either terminate the analysis or trigger additional analyses to provide additional insights into expected behavior of bridge piers.

### 2.2 STAGE 1: ANALYSIS USING BEAM THEORY

As a first step in the analysis of a bridge pier as shown in [Figure 2–2](#), it is assumed that flexural plastic hinge forms first, and the analysis is conducted based on flexural bending theory. The steps in this analysis technique can be summarized as described in the following steps:

**Step 1:** Determine first yield flexural capacity,  $M_y^b$ .

Calculate the beam yield moment ( $M_y^b$ ) at first yield of longitudinal steel given by:

$$M_y^b = C_s(d - d') + C_c(d - kd/3) \quad (2-1)$$

in which  $d$  = depth to the centroid of tensile reinforcement from the extreme compression fiber;  $d'$  = depth to the centroid of compression steel from the extreme compression fiber;  $C_s = A'_s f_s$  when  $f_s \leq f_y$  and  $C_c = 0.85 f'_c ab$  where  $A'_s$  = the area of compression reinforcement;  $f_s$  = stress in steel corresponding to strain  $\epsilon_s$ ;  $f_y$  = yield stress of reinforcing steel;  $f'_c$  = concrete compressive strength;  $b$  = breadth of the section; and  $k$  is the elastic compression zone coefficient as given by [Park and Paulay \(1975\)](#):

$$k = \sqrt{(\rho_L + \rho'_L)^2 n^2 + 2(\rho_L + \rho'_L d'/d)n} + (\rho_L + \rho'_L)n \quad (2-2)$$

in which  $\rho_L$  = the ratio of tension reinforcement;  $\rho'_L$  = the ratio of compression reinforcement; and  $n$  = the modular ratio of steel to concrete.

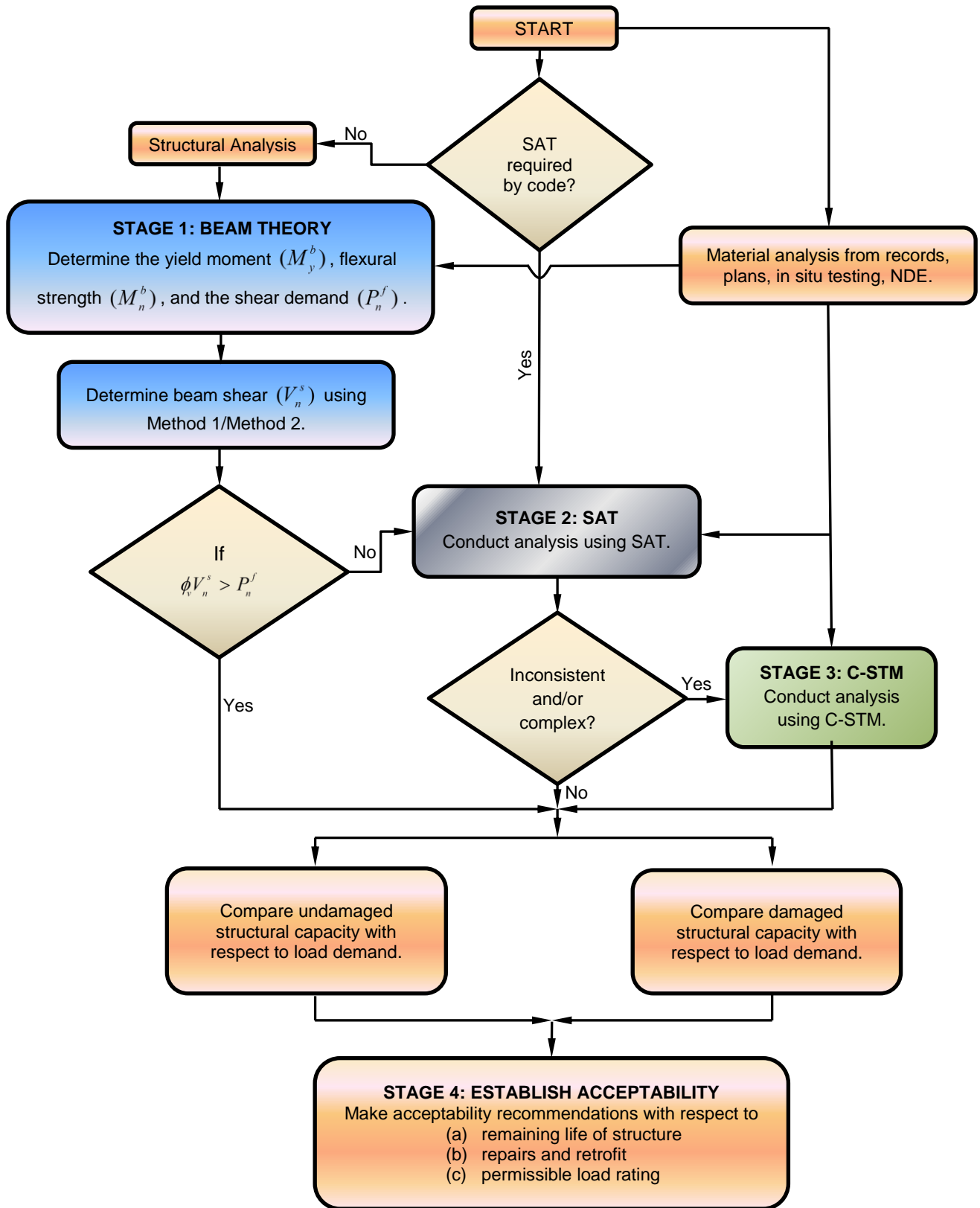
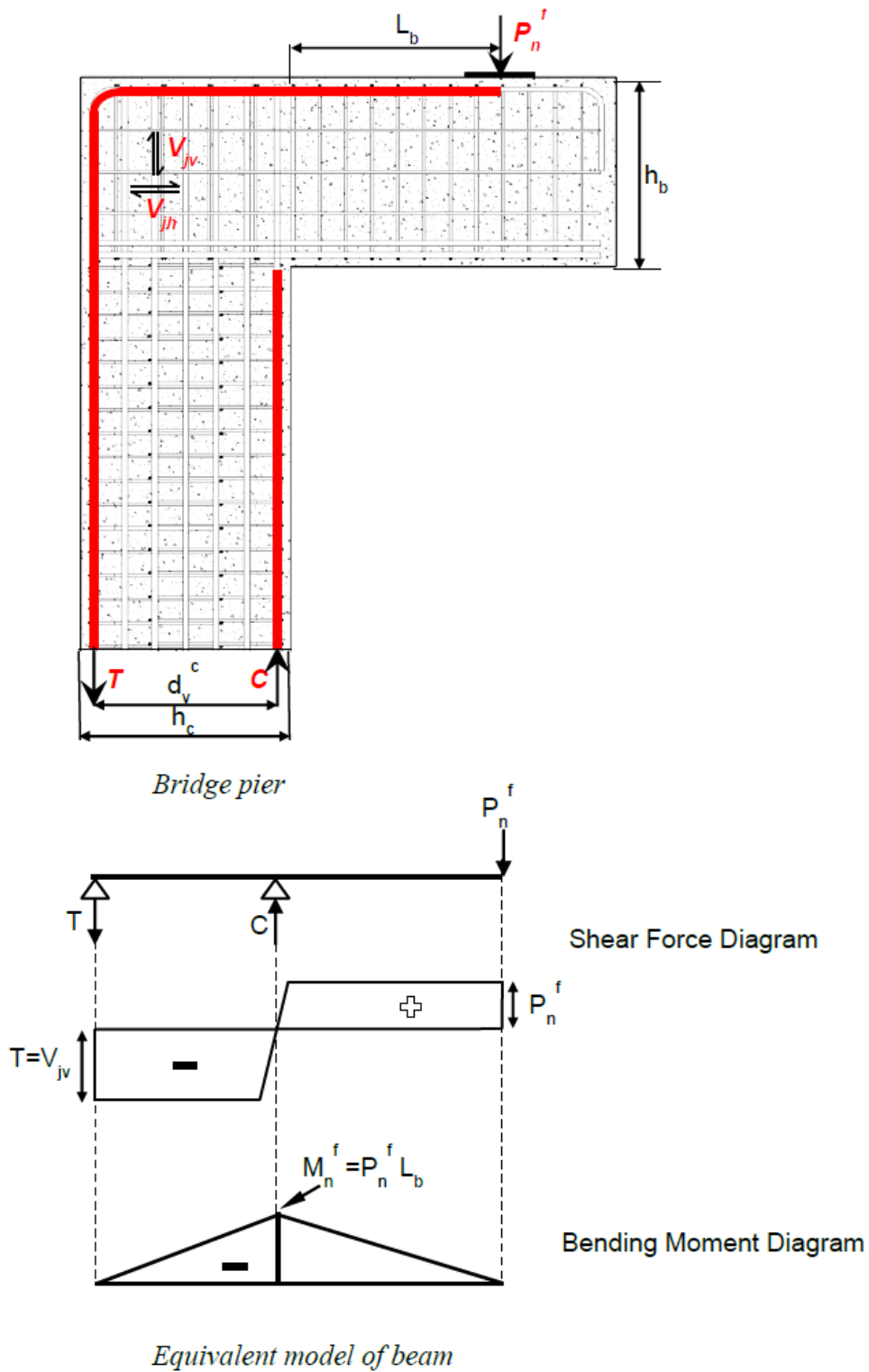


Figure 2–1: Flowchart for Analysis Procedure of Bridge Piers.



**Figure 2-2: Bridge Pier and Equivalent Beam Model for Flexure Analysis.**

The externally applied load that causes first yield is given by:

$$P_y^b = M_y^b / L_b \quad (2-3)$$

where  $L_b$  = distance from the point of application of the load to the face of the column.

**Step 2:** Determine nominal flexural moment,  $M_n^f$ .

The flexural moment ( $M_n^f$ ) of the beam is calculated as:

$$M_n^f = C_s(d - d') + C_c(d - a / 2) \quad (2-4)$$

in which  $a = \beta_1 c$  is the depth of the equivalent rectangular stress-block for which  $c$  is the neutral axis depth and  $\beta_1$  = the equivalent rectangular stress-block parameter given as:

$$0.65 \leq \beta_1 = 0.85 - 0.05(f'_c(\text{ksi}) - 4) \leq 0.85 \quad (2-5)$$

**Step 3:** Determine externally applied load based on flexure,  $P_n^f$ .

Based on the flexural capacity ( $M_n^f$ ), the externally applied load ( $P_n^f$ ) is determined:

$$P_n^f = M_n^f / L_b \quad (2-6)$$

**Step 4:** Determine beam shear capacity,  $V_n^s$ .

The shear capacity ( $V_n^s$ ) of the beam is computed as:

$$V_n^s = V_c + V_s + V_p \quad (2-7)$$

in which  $V_p$  = component of shear carried by prestressing tendons, if any;  $V_s$  = shear carried by steel; and  $V_c$  = shear carried by concrete given by:

$$V_c = 0.0316 \beta \sqrt{f'_c} b_v d_v \quad (2-8)$$

where  $f'_c$  = concrete strength is in *ksi* units;  $b_v$  = section web width across shear plane;  $d_v$  = effective shear depth taken as  $d_v = jd$  or not less than the greater of  $0.9d$  (where  $d$  = effective depth), or  $0.72h$  (where  $h$  = overall depth).



For sections with steel transverse to the longitudinal axis of the member ( $\alpha = 90^\circ$ ), the shear carried by the hoops and /or cross ties is given by:

$$V_s = A_v f_y \frac{d_v}{s} \cot \theta \quad (2-9)$$

where  $A_v$  = cross-sectional area of hoopset;  $s$  = hoopset spacing; and  $\theta$  = shear crack angle inclined from the longitudinal axis.

[AASHTO LRFD \(2010\)](#) specifications permit  $\beta$  and  $\theta$  in Eq. (2-8) and (2-9) to be calculated by one of the following two methods:

Method 1: Simplified Procedure

For reinforced (non-prestressed) concrete members, values of  $\beta = 2.0$  and  $\theta = 45^\circ$  can be used. Thus, the shear carried by concrete is the same as the well-known historic [ACI-318 \(2011\)](#) method.

Method 2: General Sectional Procedure

This method is based on the simplified version of the Modified Compression Field Theory (MCFT) ([Bentz et al., 2006](#)). In this method the parameters  $\beta$  and  $\theta$  can be determined as described below.

For sections containing the minimum amount of transverse reinforcement as specified in [AASHTO LRFD \(2010\)](#),  $\beta$  is determined as:

$$\beta = \frac{4.8}{1 + 750\varepsilon_s} \quad (2-10)$$

where  $\varepsilon_s$  = net longitudinal tensile strain in the section at the centroid of the tensile reinforcement determined as explained later.

For sections that do not contain the minimum amount of shear reinforcement as specified in [AASHTO LRFD \(2010\)](#),  $\beta$  is determined as:

$$\beta = \frac{4.8}{(1+750\varepsilon_s)} \frac{51}{(39+s_{xe})} \quad (2-11)$$

where  $s_{xe}$  = the crack spacing parameter is given by:

$$12.0(in.) \leq s_{xe} = s_x \frac{1.38}{a_g + 0.63} \leq 80.0(in.) \quad (2-12)$$

where  $a_g$  = maximum aggregate size in inches;  $s_x$  = the lesser of either  $d_v$  (effective shear depth) or the maximum distance between layers of longitudinal crack control reinforcement, where the area of the reinforcement in each layer is not less than  $0.003b_v s_x$ .

The crack angle  $\theta$  for any of the above cases is given by:

$$\theta = 29 + 3500\varepsilon_s \quad (2-13)$$

In Eqs. (2-10), (2-11), and (2-13),  $\varepsilon_s$  can be determined from the following expression:

$$\varepsilon_s = \frac{\left( \frac{|M_u|}{d_v} + 0.5N_u + |V_u - V_p| - A_{ps}f_{po} \right)}{E_s A_s + E_p A_{ps}} \quad (2-14)$$

where  $|M_u|$  = factored moment, not to be taken less than  $|V_u - V_p| d_v$ ;  $V_u$  = factored shear force;  $V_p$  = component of shear carried by prestressing tendon;  $N_u$  = factored axial force taken as positive if tensile and negative if compressive;  $A_s$  = area of nonprestressing tensile steel;  $A_{ps}$  = area of prestressing steel on the flexural tension side of the member;  $f_{po}$  (pretensioned members) = stress in strands when concrete is cast around them, and  $f_{po}$  (post-tensioned members) = average stress in the tendons when the post-tensioning is completed, or for usual levels of prestressing  $f_{po} = 0.7f_{pu}$  for both pre and post-tensioning;  $f_{pu}$  = ultimate stress in the prestressing tendon;  $E_s$  and  $E_p$  = modulus of elasticity of reinforcing steel and prestressing steel respectively; and  $A_s$  = area of reinforcing steel.

**Step 5:** Check strength hierarchy.

Once the externally applied load based on flexure ( $P_n^f$ ) and the shear capacity ( $V_n^s$ ) are calculated, the strength hierarchy can be determined based on:

$$\text{IF} \quad \phi V_n^s > P_n^f$$

THEN shear has a measure of reserve capacity and the beam should fail in flexure.

$$\text{IF} \quad \phi_w V_n^s < \phi_f P_n^f$$

THEN the factored shear capacity may be insufficient leading to a shear failure of the bridge pier.

In the above  $\phi = 0.90$  and  $\phi_f = 0.90$  are the strength reduction factors for shear and flexure, respectively, as per [AASHTO LRFD Bridge Design Specifications \(2010\)](#).

**Step 6:** Determine the shear capacity of the beam-column joint regions.

For the beam-column joint regions in bent caps the joint shear capacity needs to be determined in the direction in which the shear steel (hoopsets) is oriented. Thus, the vertical joint shear ( $V_{jv}$ ) determined from the shear force diagram ([Figure 2-2](#)) of the bridge bent cap can be transformed (if necessary) as follows:

$$V_{jh} = \frac{h_c}{h_b} V_{jv} \quad (2-15)$$

in which  $h_b$  and  $h_c$  are the overall depth of the beam and column, respectively.

The joint capacity can be assessed as:

$$V_n^j = V_{arch} + V_{truss} \quad (2-16)$$

where  $V_{arch}$  = shear carried by the corner-to-corner diagonal concrete arch (defined later); and  $V_{truss} = \sum A_{sv} f_y$  = the shear carried by the hoops and/or cross ties, in which  $\sum A_{sv}$  = the total area of steel given by all hoops/ties within the joint region.

There is a parabolic distribution of stress in the corner-to-corner arch in the beam-column zone which can further be simplified as shown in Figure 2-3a and b. From Figure 2-3c,  $V = P \sin \alpha$ . The total tensile force across the arch equals  $P/2 = (jd / \sin \alpha) b_w f_t'$ , which implies the shear contribution from the corner-to-corner joint arch is given by:

$$V_{arch} = 0.253 \sqrt{f_c' (ksi)} b_w jd = 8 \sqrt{f_c' (psi)} b_w jd \quad (2-17)$$

taking  $f_t' = 0.126 \sqrt{f_c' (ksi)} = 4 \sqrt{f_c' (psi)}$ .

For the beam-column joint to be safe in shear the following should be satisfied:

$$\phi V_n^j > V_{jv} \quad (2-18)$$

From the above analysis, if it is determined that the beam has a measure of reserve capacity then the analysis can essentially be stopped at this point. However, if either the beam or the beam-column joint is a shear critical section, then further investigation is warranted. In such a case, or when required by the code, the strut-and-tie technique of analysis can be used for further analysis, which is discussed in the next section.

### 2.3 STAGE 2: STRUT-AND-TIE ANALYSIS

The strut-and-tie modeling technique is a lower bound plastic truss model that is particularly useful for design. It can also be adopted for strength analysis, and may be particularly useful for structures that possess stocky members and a significant number of D (disturbed) regions. Using an SAT approach, a structure with D-regions is modeled as a truss, which consists of three types of elements: struts, ties, and nodes. Struts represent concrete that carries compressive loads while tensile loads are carried by ties representing steel reinforcements. Struts and ties intersect at nodes. Nodes are labeled by the element forces intersecting at the nodes; “C” represents compression while “T” stands for tension. Based on the type of member forces at the node, the nodes can be classified as CCC, CCT, CTT, and so on.

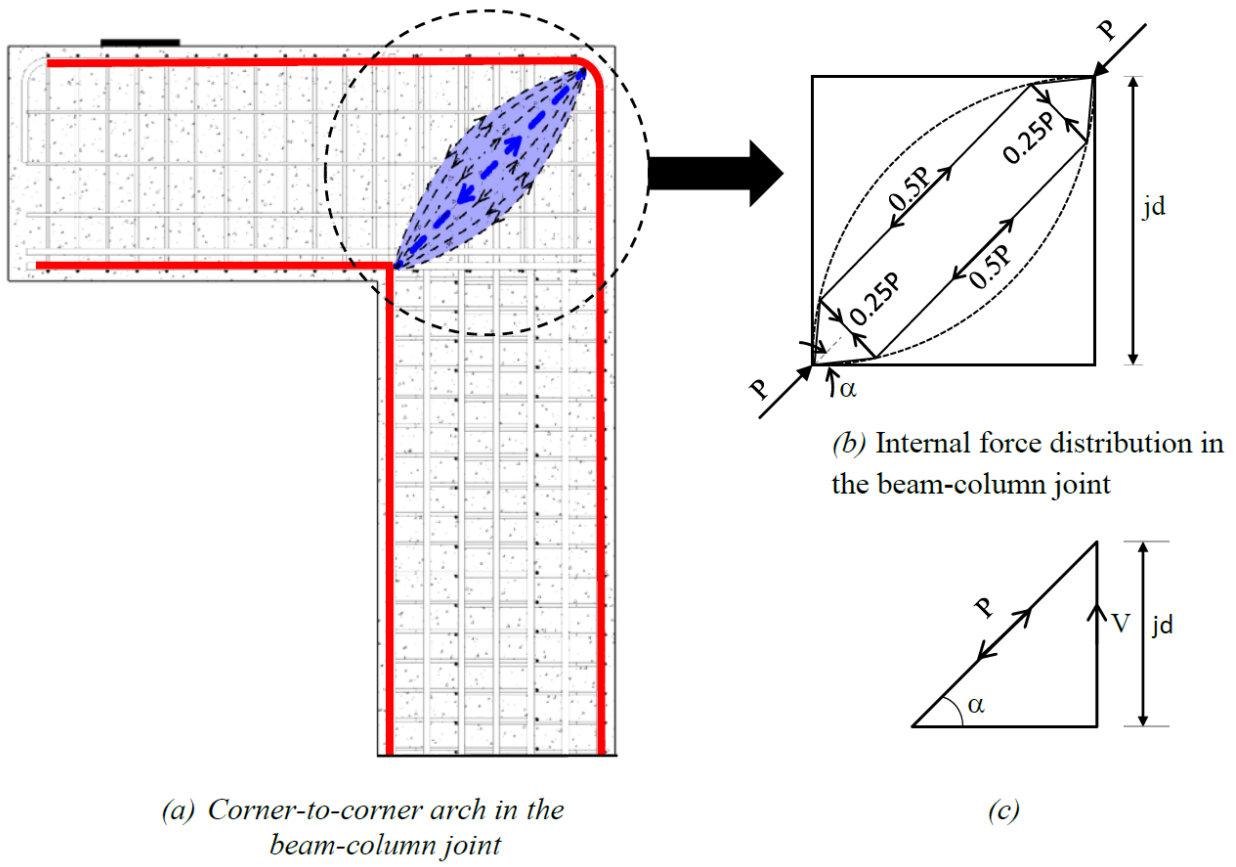


**Figure 2–3: Joint Arch Mechanism in Beam-Column Joint.**

The truss geometry of the strut-and-tie model is based on the direction of stress flow in the D-region. The ties are aligned along the reinforcement layout, whereas the struts are oriented based on the compressive stress flow trajectories. It is also reasonable to determine the truss geometry based on the cracks that can be seen on a structural member as illustrated in [Figure 2–4\(b\)](#).

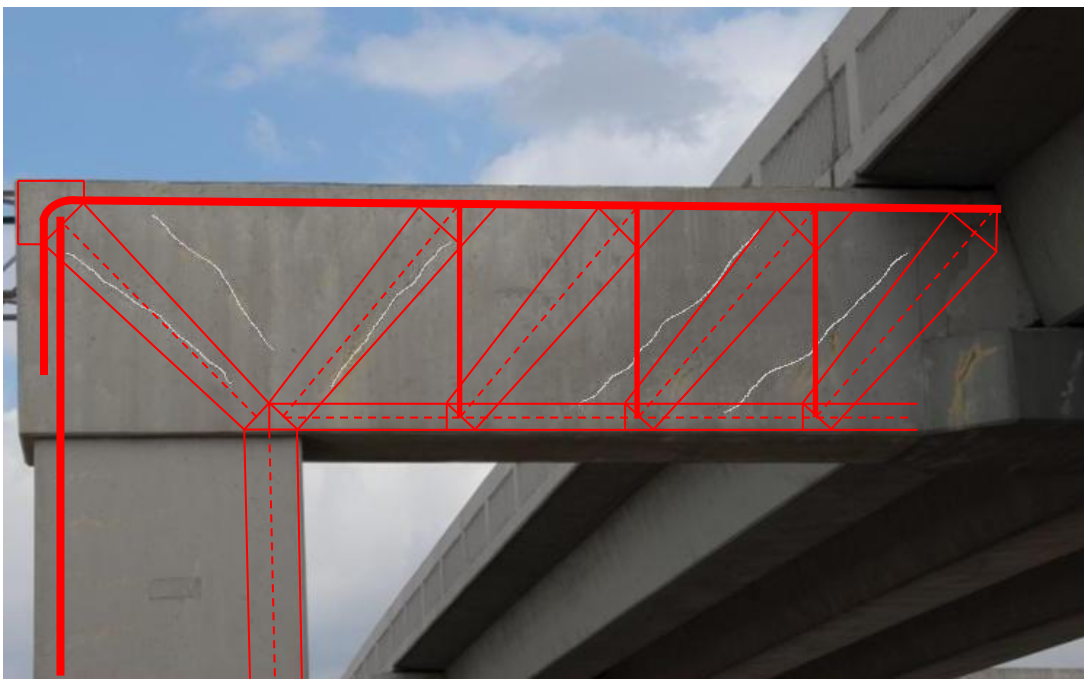
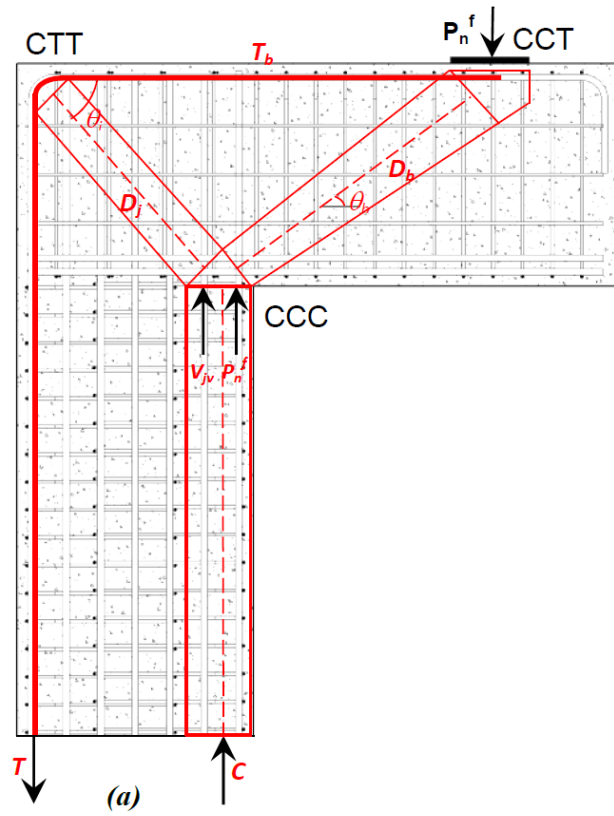
Once the truss geometry is determined, the nodal geometries must be established in order to calculate the stresses on each of the nodal faces. These calculated stresses must not exceed the allowable stresses for each nodal face. The nodes can be proportioned either as a hydrostatic node or as a non-hydrostatic node. In a hydrostatic node the principal stresses are equal on all sides of the node; hence the ratio of each nodal face is directly proportional to the force being applied to the nodal face. However, often the nodal dimensions are inconsistent with the beam details such as the location of the reinforcement and depth of the flexural compression zone. In the case of non-hydrostatic nodes the stresses applied to each nodal face is different as the node is sized based on the beam details. As a result of this the nodal geometry is synchronized with the beam details. Additionally, higher values of shear span-to-depth ratio can also lead to unrealistically large struts in the case of hydrostatic nodes.

Based on the above concepts, a strut-and-tie model for a cantilever bent and a straddle bent are shown in [Figure 2–4](#). The forces in the truss elements can be determined by a simple truss analysis. The stresses in each of the truss elements and nodes are then checked against the allowable stresses.

The allowable concrete compressive stresses on the nodal face depend on the type of node. The allowable stresses in the nodal regions are defined as follows:

For	CCC nodes	$f_{cu} = 0.85f'_c$	
	CCT nodes	$f_{cu} = 0.75f'_c$	(2–19)
	CTT nodes	$f_{cu} = 0.65f'_c$	

The limiting compressive stress within a strut ( $f_{cu}$ ) is given by:



(b)

Figure 2-4: Strut-and-Tie Model of (a) Cantilever Bent (b) Straddle Bent.

$$f_{cu} = \frac{f'_c}{0.8 + 170\varepsilon_1} \leq 0.85f'_c \quad (2-20)$$

in which  $\varepsilon_1$  = principal tension strain given by:

$$\varepsilon_1 = \varepsilon_s + (\varepsilon_s + 0.002) \cot^2 \alpha_s \quad (2-21)$$

where  $\varepsilon_s$  = tensile strain in the direction of the tension tie; and  $\alpha_s$  = the smallest angle between the compressive strut and adjoining tension tie.

The nominal resistance of a strut/node is given as:

$$P_n = f_{cu} A_{cs} \quad (2-22)$$

where  $A_{cs}$  = effective cross-sectional area of the strut/node.

The nominal resistance of a tension tie is given by:

$$P_n = f_y A_{st} + A_{ps} [f_{pe} + f_y] \quad (2-23)$$

where  $f_y$  = yield strength of reinforcing steel;  $A_{st}$  = area of reinforcing steel in the tension tie;  $A_{ps}$  = area of prestressing steel;  $f_{pe}$  = stress in prestressing steel after losses.

A generalized stepwise procedure on how to build a strut-and-tie model for a bridge pier as illustrated in [Figure 2-4](#) is as follows.

**Step 1:** Determine the truss and node geometry.

The first step in doing a strut-and-tie analysis is to determine the geometry of the truss and the nodes. The width of the compression chords in the column and the beam can be determined based on the depth of the triangular stress-block or the equivalent rectangular stress-block. The base of the CCC node can be proportioned based on the externally applied load that causes beam flexure ( $P_n^f$ ) and the vertical component of shear in the beam-column joint ( $V_{jv}$ ). The width of the CCT node is taken to be equal to the width of the bearing pad, and the CTT node is dimensioned based on the bending radius of longitudinal reinforcement. The struts can be drawn based on the dimension of the nodes. This will also provide the inclination angle of the diagonal struts.



**Step 2:** Solve the determinate truss.

It is assumed that the beam tension steel yields, that is,  $T_b = A_s f_y$ . Considering equilibrium of forces at the nodes, the forces in all the members of the truss can be determined.

**Step 3:** Determine critical node.

The critical node can be determined based on the nodal strength of each of the nodes. Based on the nodal dimensions and the allowable stress (Eq. 2-19), the nodal capacity can be determined. Based on this information the critical node is identified.

**Step 4:** Determine shear demand.

The shear demand on the bridge pier can be determined based on the most critical strut/tie or nodal zone.

Though the strut-and-tie modeling technique is an efficient method of analysis for shear critical members, it is observed that there could be inconsistencies or added complexity due to the nature of the structure that is being analyzed. Additionally, further difficulties in reaching a conclusion are likely, if the factored shear capacity based on SAT analysis is lower than the factored capacity from Stage 1 of the analysis even though the nominal capacity from SAT analysis is higher. Also, the results of the SAT analysis are based on reasonable assumptions, which could lead to varying results depending on the assumptions made.

This calls for a more advanced analysis technique that adopts the concepts of the strut-and-tie method and gives an idea about the overall behavior of the structure. One such technique, the compatibility strut-and-tie modeling, is developed in the next chapter.

## **2.4 STAGE 3: ANALYSIS USING COMPATIBILITY STRUT-AND-TIE METHODS**

As mentioned above, strut-and-tie analysis methods are strictly lower bound solutions. Such solutions adhere to the principles of equilibrium, but are both silent on and unable to predict deformations of the structure.

### **2.4.1 Stage 3.1: C-STM Based on Undamaged Material Properties**

To obtain a more holistic view of structural behavior that provides a complete force vs. deformation pathway to failure, compatibility of member deformations must be incorporated into the analysis. This approach is referred to as the *Compatibility Strut-and-Tie Model* (C-STM).

As this approach is relatively new, a complete background and theoretical formulation is presented in the next chapter. As the bookkeeping for this class of nonlinear analysis would be time consuming, it is suggested that nonlinear structural analysis software (e.g., SAP2000) be used for the analysis. In this stage of analysis the undamaged material properties are used in evaluating the behavior of the structure.

### **2.4.2 Stage 3.2: C-STM Allowing for ASR/DEF Damage and Its Effects**

It is well-known that ASR/DEF may cause the concrete to deteriorate. The effects of ASR/DEF on the structure can be explained as follows:

- ASR/DEF effects cause the concrete to swell.
- This in turn may cause the cover concrete to badly crack and in some cases cause spalling.
- Meanwhile swelling of the core concrete occurs, but this is constrained in part by the presence of longitudinal and transverse reinforcement.
- Tensile strains that are induced put the reinforcing steel to be in a state of prestress.
- In turn, this prestress effect, which is similar to adding an axial force, increases the stiffness and can slightly enhance the strength of the members most affected by ASR/DEF.

The effects of ASR/DEF on the structure can be modeled in C-STM by introducing the effects of deteriorated concrete, concrete core confinement, prestressing forces, and modifying the stress-strain relation of steel accordingly.

Based on an assessment of the extent of damage due to ASR/DEF effects observed in the structure, the damage can be categorized into three classes: slight, moderate, and heavy damage. Based on the damage class, the deteriorated concrete properties and the prestressing forces in the

longitudinal and transverse reinforcing steel are determined. A C-STM analysis with the modified properties gives the behavior of the structure with ASR/DEF damage.

Based on the results from the three stages of analysis presented above, the structural capacity of the damaged/undamaged structure can be compared to the load demand on the structure. Based on these comparisons, acceptability criterion can be set for a structure; this constitutes stage 4 of the analysis schema.

## **2.5 STAGE 4: ESTABLISH ACCEPTABILITY OF STRUCTURE**

Based on the analysis conducted on the structure in the previous three stages, a structural engineer must be able to make recommendations and establish the acceptability of an existing structure that may or may not be subjected to any form of deterioration/damage. The engineer must be able to make acceptability recommendations with respect to:

- (a) The remaining life of the structure: This would essentially give ample time to the state DOTs to plan ahead in time on how to deal with the existing structure and/or plan alternate strategies.
- (b) Repairs or retrofit: Such remediation can be done in order to strengthen the existing structure and give it added service life to enable it to perform as designed.
- (c) Permissible load rating: By limiting the permissible loads on the structure, the service life of the structure can be extended.

The first two stages of analysis, using beam theory and SAT analysis, would give the structural engineer just an idea about the maximum load that the structure can withstand before it starts to show signs of distress or even fails. However, stage 3 of the analysis (where the C-STM technique is adopted) gives the overall force-deformation of the structure, which helps to better predict its behavior and make a more definitive engineering judgment on the structure's acceptability condition. The C-STM analysis technique will aid the structural engineer to make a more accurate educated prediction about the behavior of the structure.

Detailed examples of the different stages of analysis are presented in [Chapter 4](#) and [Chapter 5](#).



### 3. COMPATIBILITY STRUT-AND-TIE FORMULATION

It is well-known that the shear resistance in structural concrete elements is resisted by a combination of truss and arch action (Park and Paulay, 1975). Truss action is associated with the shear resistance provided by the transverse reinforcement (Ritter, 1899; Mörsch, 1909; Dilger, 1966; Paulay, 1971; Kim and Mander, 1999, 2000, and 2007). Arch action becomes prevalent in squat reinforced concrete members, particularly those with wide webs where a direct compression load path (arch) exists between the applied load and the supports. These two primary mechanisms are further considered in what follows.

#### 3.1 MODELING TRUSS ACTION

Figure 3–1(a) illustrates a variable angle crack pattern that typically forms in the disturbed regions of a fixed-fixed reinforced concrete deep beam. After the development of first cracking, diagonal concrete compression struts are tied together by the longitudinal and transverse reinforcing steel, thus resembling a truss. Starting with a differential portion of this truss, Kim and Mander (1999, 2007) integrated this over the beam length to develop a “continuum truss” model where cracking was implicitly smeared in order to obtain the shear stiffness in a numerical form.

Alternative numerical integration schemes were then considered by Kim and Mander (1999, 2007) to model the discrete crack patterns typically observed in reinforced concrete beams and are explored further herein. For a fixed-fixed beam, the simplest of these numerical integration schemes uses a two-point Gaussian quadrature solution leading to a so-called two-point Gauss Truss shown in Figure 3–1(b). Note the solid lines represent tension ties (reinforcing steel), and the dashed lines represent diagonal compression struts (concrete). Through experimental and analytical validation, Kim and Mander (1999, 2007) found the two-point Gauss Truss to be a suitably accurate numerical integration scheme for capturing both shear and flexure deformations of disturbed regions with fixed-fixed end conditions. Higher order numerical schemes were also considered; however the two-point Gauss Truss model has the appeal of being statically determinate (due to anti-symmetry).

By taking only one-half of an anti-symmetric fixed-fixed beam that is represented by the two-point Gauss Truss, a statically determinant cantilever remains, which can be represented by a so-called *Single-Point Gauss Truss*. In order to confirm the numerical accuracy of the proposed single-point Gauss Truss, a convergence study of higher order numerical integration schemes was conducted. Based on recommendations of [Kim and Mander \(1999, 2000\)](#), the axial rigidities assigned to each truss member at the  $i^{th}$  integration point are given by:

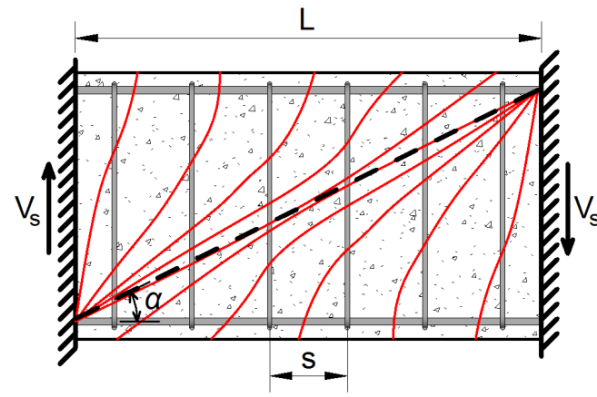
$$(EA)_{Ti} = \omega_i E_s A_{sh} \frac{L}{s} \quad (3-1)$$

$$(EA)_{di} = \frac{0.5\omega_i}{\sqrt{x_i + \tan^2 \theta_i}} E_c A_v \quad (3-2)$$

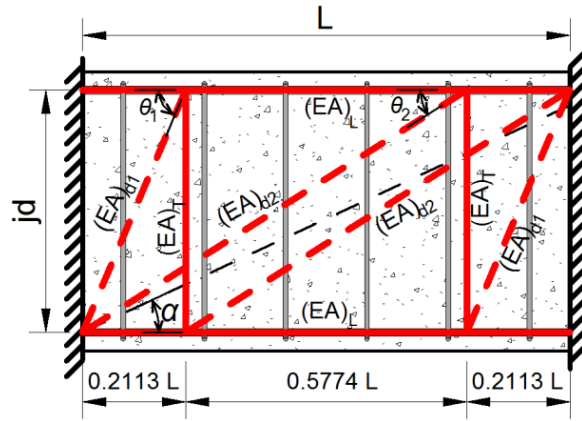
$$(EA)_L = A_L E_s \quad (3-3)$$

in which  $(EA)_{Ti}$  = axial rigidity of the transverse reinforcement ties (where  $\omega_i$  = numerical weight factor for transverse reinforcement defined in [Table 3-1](#),  $E_s$  = Young's Modulus for steel,  $A_{sh}$  = area of one set of stirrups,  $L$  = member length, and  $s$  = stirrup spacing);  $(EA)_{di}$  = axial rigidity of the diagonal concrete struts (where  $x_i$  = normalized coordinate of the  $i^{th}$  integration point,  $\theta_i$  = strut angle relative to longitudinal steel,  $E_c$  = Young's Modulus for concrete,  $A_v = b_w d$  is the shear area of concrete,  $b_w$  = beam width, and  $d$  = the effective depth of the beam from the extreme concrete compression fiber to the centroid of the tension steel); and  $(EA)_L$  = axial rigidity the longitudinal reinforcement ties (where  $A_L$  = is the sectional area of steel assigned to the longitudinal tension tie).

[Table 3-1](#) presents four different numerical integration schemes that were considered in this convergence study: single, two, and three-point Gauss quadrature, and Boole's rule. A 3 ft by 2 ft (900 x 600 mm) cantilevered beam was used as an illustrative example with a span to depth ratio of 1, and longitudinal and transverse reinforcing ratios of 0.010 and 0.003, respectively, where each integration scheme is depicted at the top of [Figure 3-2](#). The right column of [Table 3-1](#) presents the relative elastic shear stiffness ( $K$ ) of each truss normalized



(a) Discrete representation



(b) Two-point Gauss Truss

Figure 3–1: Truss Model Idealization for a Fixed-Fixed Beam—Kim and Mander (1999).

Table 3–1: Convergence Study of Higher Order Truss Models for a Cantilever Beam.

Numerical Scheme	$i$	$x_i$	$\omega_i$	$\frac{K_{Truss}}{K_{2-point}}$
Single-Point Gauss	1	0.42265	1	1.0429
	2	0.57735	1	
Two-Point Gauss	1	0.21132	0.5	<b>1.0000</b>
	2	0.78868	0.5	
Three-Point Gauss	1	0.11270	5/18	1.0007
	2	0.50000	8/18	
	3	0.88730	5/18	
Boole's Rule	1	0.00	7/90	0.9371
	2	0.25	32/90	
	3	0.50	12/90	
	4	0.75	32/90	
	5	1.00	7/90	

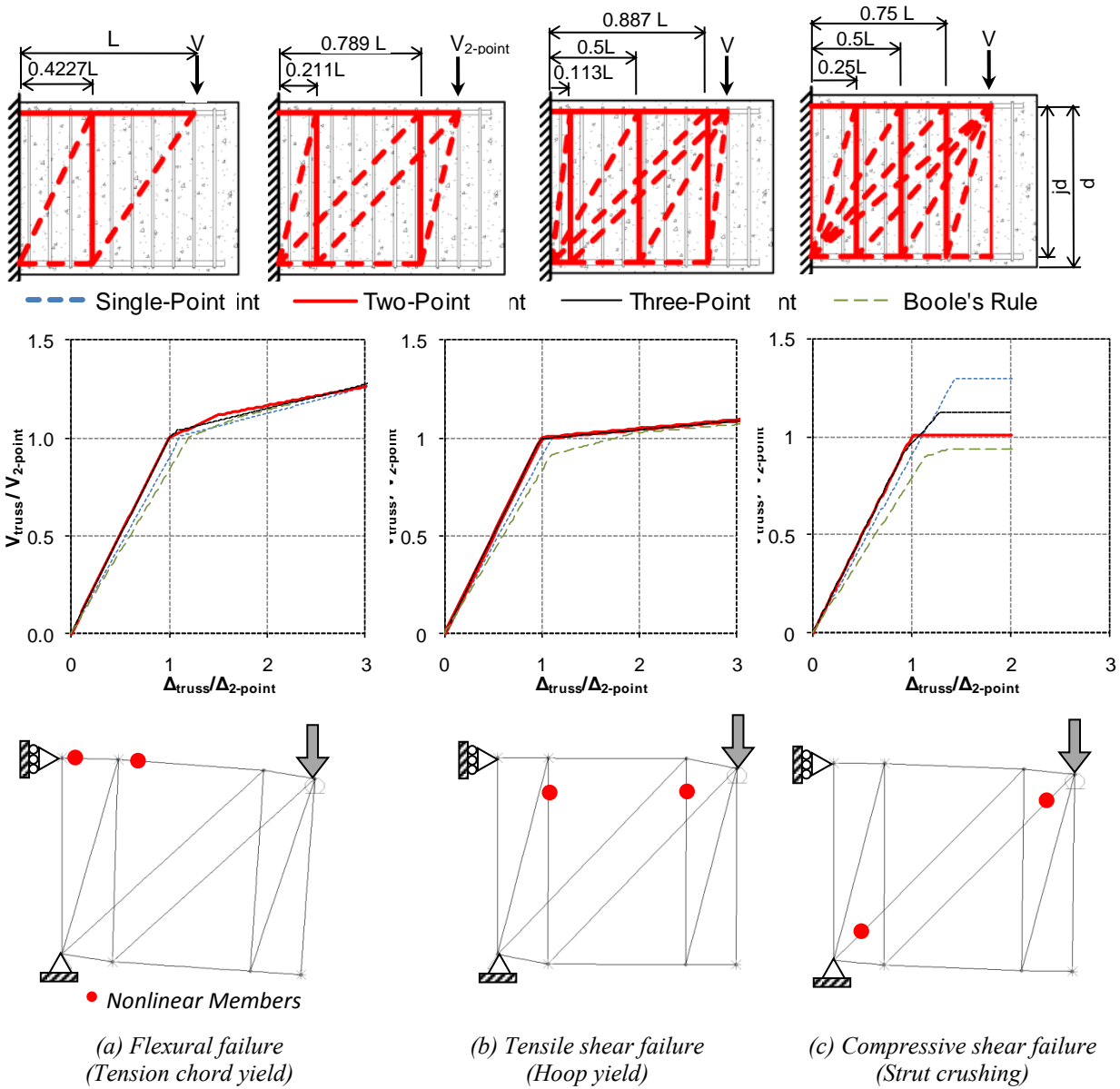


**Figure 3–2: Results of Convergence Study for Different Numerical Integration Schemes for C-STM Analysis.**



with respect to the two-point Gauss Truss. Although some variability between schemes exists, it can be concluded that any reasonable integration scheme may be used to provide a satisfactory representation of shear stiffness. However, a more in-depth study should be considered to compare the flexure-shear interaction between truss models.

Figure 3–2 shows the force-deformation response of each truss model normalized with respect to the two-point Gauss Truss solution considering the following nonlinear mechanisms: (a) flexural steel yielding; (b) transverse steel yielding; and (c) concrete strut crushing. Each truss is modeled using well-known commercial structural analysis software SAP2000™ (1995), and considers a bilinear stress-strain relationship with 3 percent strain hardening stiffness for steel, and an elasto-plastic response with a maximum compression stress of  $0.85f'_c$  for the concrete struts.

When nonlinear behavior is governed by longitudinal tensile steel yielding (Figure 3–2(a)), the post-yield force-deformation response is ductile. Despite similar yield strengths, the single-point Gauss Truss model resulted in a slightly more flexible elastic stiffness than the higher order Gauss quadrature truss models. The Boole's truss was the most flexible of the truss models and provided slightly lower initial yield strength, but had a similar post yield response.

When nonlinear behavior is governed by transverse steel yielding (Figure 3–2(b)), similar stiffness results were obtained. However the post yield stiffness was less than that with longitudinal steel yielding. This shows that yielding of the transverse reinforcement can lead to large shear deformations with small increases in applied load.

When nonlinear behavior is governed by strut crushing (Figure 3–2(c)), the ultimate strength had a variation up to 30 percent with the single-point truss giving the largest difference. An elasto-plastic response of concrete was used for illustrative purposes only and does not accurately model concrete crushing; hence the response of each was stopped at a ductility of two.

In summary, for cantilever modeling, the single-point Gauss Truss is evidently a sufficiently accurate model for considering the nonlinear flexure-shear interaction relative to the higher order truss models when the failure mechanism is controlled by longitudinal and transverse steel yielding. However, for mechanisms controlled by strut crushing, a convergence

study is recommended to ensure the single-point Gauss Truss does not over-estimate the failure mechanism.

### 3.2 MODELING ARCH ACTION

Arch action consists of a compressive stress field forming a diagonal corner-to-corner concrete strut that is tied back by the longitudinal reinforcement as shown in [Figure 3–3\(a\)](#). The strut is assumed to have a parabolic stress distribution with a strut width that is proportional to the depth and length of the beam given below ([Holden et al., 2003](#)):

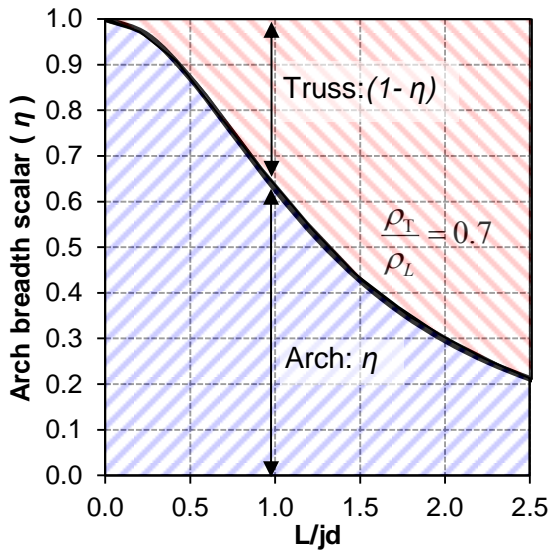
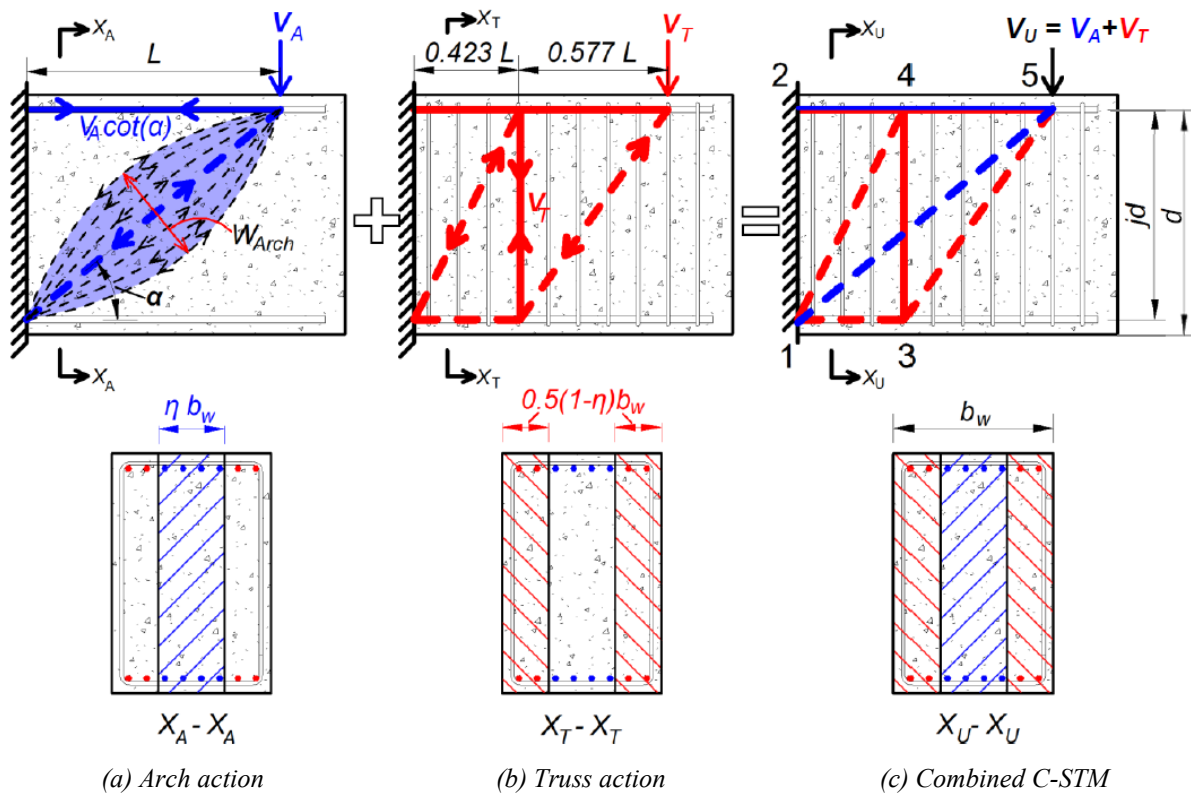
$$W_A = 0.375jd / \cos \alpha \quad (3-4)$$

This approach is similar to that proposed for coupling beams by [Paulay \(1971\)](#).

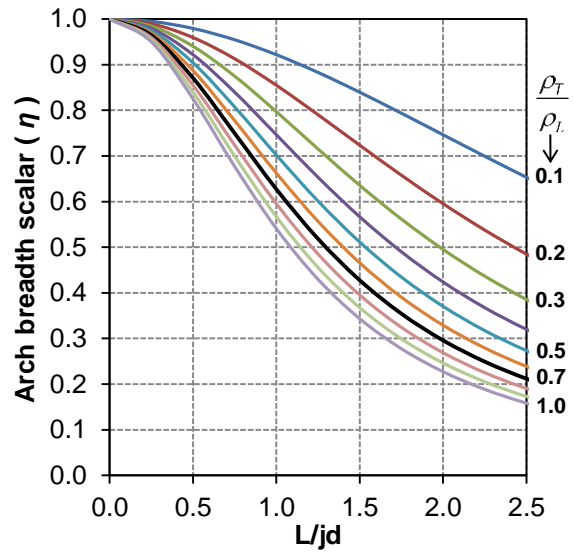
### 3.3 MODELING THE COMBINED TRUSS AND ARCH ACTION

[Figure 3–3](#) presents the combined C-STM that is comprised of: (a) arch action acting through the center of the beam cross-section; and (b) truss action acting along the outside stirrup legs. [Figure 3–3\(c\)](#) shows the amalgamated response of arch and truss action, where displacement compatibility is inherently accounted for such that the two mechanisms work in parallel to one another. A method of apportioning the relative contributions of arch and truss action is described as follows.

Different methods of allocating the shear resisting mechanisms have previously been proposed based on the following parameters: (i) strength ([Paulay, 1971](#); [Kim and Mander, 1999](#)); (ii) stiffness ([Zhu et al., 2003](#)); (iii) geometry ([Hwang et al., 2000](#)); and (iv) the shear span-to-internal lever arm ratio ([FIP-Commission 3, 1996](#)). An investigation into the merits of each of these strategies was conducted, and the following conclusion was drawn: varying the proportions of arch and truss action resulted in minimal differences of the elastic force-deformation response. However, significant differences in the nonlinear response of the flexure and shear failure mechanisms were observed. Hence to accurately model the flexure-shear interaction, it is considered necessary to apportion the arch and truss mechanisms according to the longitudinal and transverse reinforcement ratios in order to account for strength and  $L/jd$  in order to account for geometry.



(d) Arch breadth scalar vs.  $L/jd$  ratio



(e) Arch breadth scalar with varying reinforcement ratios

**Figure 3-3: Composition of Classic Arch and Truss Action That Leads to the Overall Compatibility Strut-and-Tie Model.**

An arch breadth scalar  $\eta$  is proposed to apportion the section breadth (shown in the cross-sections of [Figure 3–3](#)) and is defined by the following ratio:

$$\eta = \frac{V_{Arch}}{V_{Arch} + V_{Truss}} = \frac{\rho_L f_y}{\rho_L f_y + \rho_T f_{yh} j \cot^2 \alpha} \quad (3-5)$$

in which  $V_{Arch}$  = maximum shear force resisted by arch action that is proportional to the longitudinal reinforcement given below; and  $V_{Truss}$  = maximum shear force resisted by truss action that is proportional to the transverse reinforced given as:

$$V_{Arch} = f_y A_L \tan \alpha = \rho_L f_y b_w d \tan \alpha \quad (3-6a)$$

$$V_{Truss} = f_{yh} A_{sh} L / s = \rho_T f_{yh} b_w j d \cot \alpha \quad (3-6b)$$

where  $\alpha$  = the corner-to-corner diagonal angle;  $\rho_L = A_L / b_w d$  is the volumetric ratio of longitudinal steel to concrete;  $A_L$  = is the area of longitudinal reinforcement contributing to the tension tie;  $\rho_T = A_{sh} / b_w s$  is the volumetric ratio of transverse steel to concrete over one hoop spacing;  $f_y$  = yield strength of the longitudinal steel;  $f_{yh}$  = yield strength of the transverse steel; and  $j = (1 - d' / d)$  the internal lever arm coefficient.

The total shear resistance of the combined C-STM  $V_U$ , as shown in [Figure 3–3\(c\)](#), can now be defined as:

$$V_U = V_A + V_T \quad (3-7)$$

where  $V_A$  = is the shear resistance from arch action; and  $V_T$  = is the shear resistance from truss action.

In order to maintain deformation compatibility and equilibrium between the arch and truss mechanisms, it is assumed that the section breadth  $b_w$  is proportioned according to the component strength as follows:

$$\frac{V_A}{V_U} = \frac{\eta b_w}{b_w} \quad ; \quad \frac{V_T}{V_U} = \frac{(1-\eta)b_w}{b_w} \quad (3-8)$$

where  $\eta b_w$  = the arch breadth, and  $(1-\eta)b_w$  = the truss breadth as shown in the cross-sections of Figure 3-3(a) and (b), respectively.

Figure 3-3(d) and (e) illustrates the results of the arch breadth scalar  $\eta$  (Eq. 3-5) when plotted against  $L/jd$  with varying ratios of transverse to longitudinal reinforcement. As one might intuitively expect, this relationship shows that arch action is more prominent in beams with smaller  $L/jd$  and  $\rho_T/\rho_L$  ratios, while truss action has more of an effect in beams with larger  $L/jd$  and  $\rho_T/\rho_L$  ratios. Others have made similar conclusions (Hsu, 1996).

### 3.4 STRESS AND STRAIN TRANSFORMATION FOR FLEXURAL EQUIVALENCE

A primary difficulty associated with truss modeling approaches is the limitation of selecting a single truss model geometry that captures the full elastic and inelastic force-deformation response. For doubly reinforced sections, it is proposed that the longitudinal C-STM flexural chords (members 1-3 (compression), and 2-4-5 (tension) in Figure 3-3(c)) be aligned with the respective compression steel centroids so that the internal lever arm is represented as  $jd = d - d'$ , where  $d$  and  $d'$  are the respective centroids of the tension and compression steel and  $j = (1 - d'/d)$  is the internal lever arm coefficient. A similar approach was used and validated by Kim and Mander (1999, 2000) in order to incorporate cyclic behavior. However, because the centroids of the steel compression force ( $C_s$ ) and the concrete compression force ( $C_c$ ) may not coincide, it is necessary to transform the concrete constitutive material properties accordingly so that the transposition of the concrete element force ( $C_c$ ) will provide a similar moment in order to satisfy the sectional moment capacity throughout the analysis.

Historically the truss geometry for strut-and-tie models has been mostly based on an elastic stress field analysis and typically ignores the presence of compression steel (Hwang et al., 2000; Drucker, 1961; Thürlimann et al., 1983). Other researchers contend that the use of elastic stress analysis is inappropriate when assessing the ultimate limit state of a structure due to highly nonlinear development of strains associated with D-regions (MacGregor, 1992; Salem and Maekawa, 2006; Yun, 2000; Sritharan and Ingham, 2003). The proposed transformation theory

(described below) provides a method that accounts for both compression steel and the nonlinear behavior of concrete compression chord element in accordance with standard stress-block analysis that is incorporated over the entire range of loading. Figure 3–4(a) illustrates a standard flexural stress block analysis performed on a doubly reinforced concrete section, assuming plane sections remain plane purely for the purposes of defining the concrete compression force, where the concrete tensile strength is assumed as zero. The neutral axis depth  $c$  can be defined such that  $c = kd$ , where  $k$  is the elastic compression zone coefficient given by Park and Paulay (1975) as:

$$k = \sqrt{(\rho_L + \rho'_L)^2 n^2 + 2(\rho_L + \rho'_L d'/d)n + (\rho_L + \rho'_L)n} \quad (3-9a)$$

For column members an additional modification is made to allow for the axial force given by Eq. (3-9 b) (Arnold, 2004).

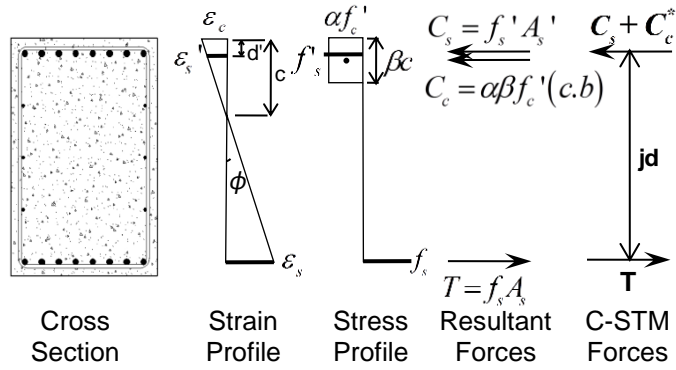
$$k = \sqrt{\left(\rho_L + \rho'_L + \left(\frac{P}{f'_c bd}\right)\left(\frac{f'_c}{f_s}\right)\right)^2 n^2 + 2\left(\rho_L + \rho'_L\left(\frac{d'}{d}\right) + \left(\frac{P}{f'_c bd}\right)\left(\frac{f'_c}{f_s}\right)\right)n - \left(\rho_L + \rho'_L + \left(\frac{P}{f'_c bd}\right)\left(\frac{f'_c}{f_s}\right)\right)n} \quad (3-9b)$$

where  $d$  = the effective depth of the beam from the extreme concrete compression fiber to the centroid of the tension steel;  $d'$  = the depth from the extreme compression fiber to the centroid of the compression reinforcement;  $\rho$  = the ratio of tension reinforcement;  $\rho'$  = the ratio of compression reinforcement;  $n$  = the modular ratio of steel to concrete;  $b$  = the section breadth;  $f'_c$  = concrete compression strength; and  $P$  = axial force plus prestressing force (if any).

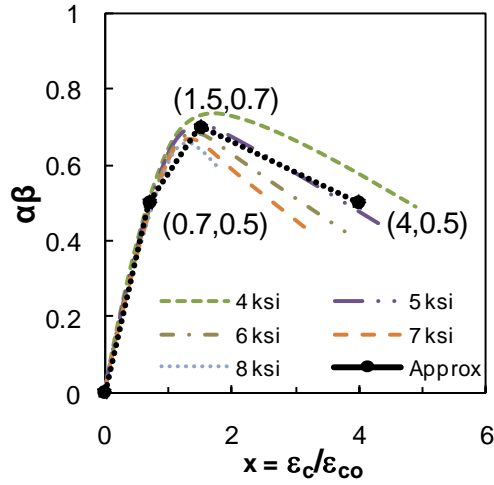
Because the C-STM compression chord member is located at the steel centroid, a transformation of the concrete stress block force  $C_c$  is required to convert it to an equivalent C-STM force that coincides with C-STM compression chord member. Section equilibrium requires:

$$P = (C_s + C_c^*) - T \quad (3-10)$$

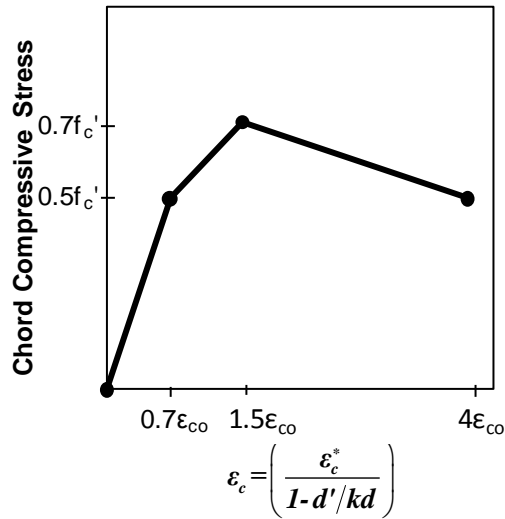
in which  $P$  = the applied axial load ( $P = 0$  for beams);  $T = A_s E_s \varepsilon_s$  (where  $A_s$  = representative area of longitudinal tension steel, and  $\varepsilon_s$  = tensile steel strain);  $C_s = A'_s E_s \varepsilon'_s$  (where  $A'_s$  = representative area of longitudinal compression steel, and  $\varepsilon'_s$  = compression steel strain); and  $C_c^*$  = transformed concrete force discussed below.



(a) Doubly reinforced stress block analysis



(b) Stress block parameters (Karthik and Mander, 2011)



(c) Key stress-strain parameters

Figure 3–4: Constitutive Stress-Strain Relationship for Compression Chord Elements.

The effective concrete strain  $\varepsilon_c^*$  measured by the C-STM chord member can be defined in terms of the extreme compressive concrete strain using the strain compatibility relationships:

$$\varepsilon_c^* = \varepsilon_s' = \varepsilon_c \left( 1 - \frac{d'}{kd} \right) \quad (3-11)$$

Hence, the concrete compression force can be expressed in terms of equivalent concrete stress block and related to  $\varepsilon_s' = \varepsilon_c^*$  as follows:

$$C_c = \alpha\beta f_c' (kd \cdot b) = \varepsilon_c^* \psi E_c A_c \quad (3-12)$$

in which  $\alpha\beta$  = the stress block parameters used to define the equivalent stress block, where  $\alpha$  = effective average concrete stress ratio, and  $\beta$  = effective stress block depth factor;  $f_c'$  = concrete strength;  $\varepsilon_c^*$  = C-STM concrete compression chord strain;  $\psi$  = a compatibility correction scalar; and  $A_c = kd b$  is the area assigned to the concrete chord element.

Rearranging Eq. (3-12) and substituting Eq. (3-11), the compatibility correction scalar can be expressed as:

$$\psi = \frac{\alpha\beta f_c'}{\varepsilon_c^* E_c} = \frac{\alpha\beta}{(1 - d'/kd) x n} \quad (3-13)$$

in which  $x = \varepsilon_c / \varepsilon_{co}$  is the normalized concrete compression strain at the extreme compression fiber;  $\varepsilon_{co} = 0.002$  for unconfined concrete; and  $n = E_c \varepsilon_{co} / f_c'$  (where  $E_c = 60000 \sqrt{f_c'(\text{psi})} = 5000 \sqrt{f_c'(MPa)}$  is the initial tangent modulus) (Mander et al., 1988).

The only remaining unknown variables in Eq. (3-13) are  $\alpha\beta$  and the nonlinear strain,  $x$ . The nonlinear relationship between these two stress block variables is shown in Figure 3-4(b) (Karthik and Mander, 2011), where a tri-linear relationship is used to approximate the stress block parameters. The key stress-strain parameters for obtaining the concrete chord members constitutive relationship can be obtained through a direct axis transformation as shown in Figure 3-4(c): where stress is a function of  $\alpha\beta f_c'$ , and the strain is a function of  $x \varepsilon_{co}$ , as derived



from Eq. (3-13). The transformed constitutive relation used for concrete chord members is then derived by substituting appropriate values of  $f'_c$  and  $(1-d'/kd)$  into Figure 3-4(c). An application of this is presented later.

A similar analysis for singly reinforced beams may be applied where the location of the compression chord member can be defined as follows. For members that do not exceed the elastic limit in the concrete compression stress block, the internal lever arm may be defined such that  $jd = d - kd/3$  (where  $k$  = the elastic compression zone coefficient defined in Eq. (3-9)). For members that do exceed the elastic stresses, a more appropriate representation of the internal lever arm may be defined using an ultimate limit state analysis such that  $jd = d - \beta_1 c/2$  (where  $\beta_1$  is the standard code-based stress block factor, and  $c$  is the neutral axis depth calculated by satisfying section equilibrium).

### 3.5 C-STM GEOMETRY AND AXIAL RIGIDITY ASSIGNMENTS

The C-STM shown in Figure 3-3(c) can be adapted for any deep beam or disturbed region and modeled using structural analysis software. Each member in the C-STM is comprised of two elements that model the individual behavior of steel and concrete in that member. The two elements are constrained together in order to give the combined steel-concrete response. The C-STM requires the following parameters to be defined in order to model the constitutive behavior of truss members: (i) truss geometry to define the member force; and (ii) axial rigidities of the steel and concrete elements to define elastic deformations.

#### 3.5.1 Truss Geometry

As previously discussed, the primary difficulty associated with accurate truss modeling is the limitation of selecting a single truss model geometry that captures the force-deformation over a range of both elastic and inelastic response. The truss geometry is defined by first locating the node coordinates for the compression and tension chord members. This is done in accordance with the foregoing section, where the location of the compression chord member varies for doubly and singly reinforced sections.

The horizontal coordinates of the boundary nodes are either defined by: (i) an applied load/bearing support (i.e., Node 5 in Figure 3–3(c) is defined by the centroid of the applied load); or (ii) at the intersecting lines of thrust from the beam and column members (i.e., Node 1 in Figure 3–3(c) is defined at the intersection of the compression steel in the beam and supporting column represented as a fixed boundary). The transverse tension ties in the truss mechanism are then located according to the selected numerical truss as defined in Figure 3–2 (i.e., Nodes 3 and 4 in Figure 3–3(c) are defined by single-point Gauss quadrature).

### 3.5.2 Axial Rigidity

For each C-STM member, the expected composite steel-concrete response is modeled using separate elements for steel and concrete, respectively. Each element is assigned elastic axial rigidities as specified in Table 3–2, where the member numbers refer to Figure 3–3(c). Some comments on Table 3–2 follow.

For tension chord members (row 1 of Table 3–2), the presence of longitudinal distribution steel along the web may be accounted for by using an effective steel area:

$$A_s^* = \frac{\bar{A}_s \bar{d}}{d} \quad (3-14)$$

where  $\bar{A}_s$  = the total area of longitudinal plus distribution reinforcement acting in tension;  $\bar{d}$  = the effective depth to the centroid of  $\bar{A}_s$ ; and  $d$  = section depth to the longitudinal tension reinforcement.

For tension and compression chord members (row 1 and 2 of Table 3–2), the concrete area is assumed to be the same so that cyclic effects can to be accounted for, if necessary.

For transverse truss members (row 3 of Table 3–2), the total area of transverse reinforcement is evaluated as the number of hoops actively participating in the truss mechanism  $N_h$ , where  $N_h = \text{int}[L/s - 1]$  is the number of hoopsets. Also, the effective tension area of concrete for the transverse tie is taken as twice the cover depth ( $c_c$ ) plus the stirrup hoop diameter ( $d_h$ ), multiplied

over the length of actively participating hoops ( $N_h s$ ), thus defining the area of concrete surrounding the stirrup legs.

**Table 3–2: Elastic Truss Member Axial Rigidities.**

Member	Steel		Concrete		Comments
	$E$	$A$	$E$	$A$	
2 – 4 4 – 5	$E_s$	$A_s$	$E_c$	$b.kd$	Tension Chord
1 – 3	$E_s$	$A_s'$	$\psi_E E_c$	$b.kd$	* Compression Chord
3 – 4	$E_s$	$N_h A_{sh}$	$E_c$	$(4c + 2d_h) N_h s$	<sup>†</sup> Active Hoop steel including tension stiffening effect
1 – 5	–	–	$E_c$	$\frac{0.375 \eta b_w j d}{\cos \alpha}$	Concrete Strut in Arch Mechanism
1 – 4	–	–	$E_c$	$\frac{0.5(1-\eta)b_w j d}{\sqrt{0.423 + \tan^2 \alpha}}$	Concrete Strut in Truss Mechanism
3 – 5	–	–	$E_c$	$\frac{0.5(1-\eta)b_w j d}{\sqrt{0.577 + \tan^2 \alpha}}$	Concrete Strut in Truss Mechanism

$$^* \psi_E = \text{strain compatibility coefficient} = \frac{\sqrt{f_c'(\text{psi})}}{168(1-d'/kd)} = \frac{\sqrt{f_c'(\text{MPa})}}{14(1-d'/kd)}$$

In lieu of a more precise analysis it is recommended that  $\psi_E = 0.6$

<sup>†</sup>  $N_h = \text{int}[L/s-1]$  is the integer part of active hoops in truss mechanism

For the concrete arch member (row 4 of Table 3–2), the strut width is given by Eq. (3–4) and is multiplied by the apportioned arch strut width  $\eta b_w$  to obtain the strut area.

For the concrete strut members in the truss mechanism (row 5 and 6 of Table 3–2), the strut width is defined using Eq. (3–2) (Kim and Mander, 1999, 2000), where the normalized coordinate of the  $i^{\text{th}}$  integration point  $x_i$  is taken as 0.423 and 0.577 (in accordance with Table 3–1) for the concrete elements 1-4 and 3-5, respectively. These are multiplied by the apportioned truss strut width  $(1-\eta)b_w$  to obtain the respective strut areas.

### 3.6 ELEMENT CONSTITUTIVE MATERIAL RELATIONS

The elastic parameters of the C-STM model are defined by the truss geometry and axial rigidities. In order to define the strength of each element, nonlinear constitutive material relationships for cracked reinforced concrete are applied as follows.

#### 3.6.1 Reinforcing Steel

For simplicity, the reinforcing steel is approximated using a bi-linear stress-strain relationship with 3 percent strain hardening beyond yielding. Where necessary, a more accurate material model may be applied in order to allow for bond slip or where a bilinear slope does not provide suitable accuracy.

#### 3.6.2 Diagonal Concrete Struts

From the works of [Vecchio and Collins \(1986\)](#), [Mau and Hsu \(1987\)](#), and [Hsu and Zhang \(1997\)](#) it is well-known that the compression strength of diagonal concrete struts in reinforced concrete beams and panel elements is reduced as a result of the tensile strain acting orthogonal to the compression strain. This concrete softening phenomenon was investigated by Collins and his research group; one rendition of their work is modeled by the following relationship ([Vecchio and Collins, 1986](#)):

$$\zeta = \frac{f_{2,\max}}{f'_c} = \frac{1}{0.8 + 0.34 \left| \frac{\varepsilon_1}{\varepsilon_{co}} \right|} \leq 1.0 \quad (3-15)$$

where  $\zeta$  = the softening coefficient;  $f_{2,\max}$  = the “softened” concrete strength;  $\varepsilon_{co}$  = the principal compression strain typically taken as 0.002; and  $\varepsilon_1$  = the principal tensile strain acting perpendicular to compression strut.

This relationship is typically incorporated in each step of a hand analysis, or directly embedded into a nonlinear Finite Element Modeling (FEM) formulation where the softening coefficient is continuously updated to satisfy equilibrium ([Rots et al., 1985](#)). However, when applying this in commercial structural analysis software (such as [SAP2000<sup>TM</sup>, 1995](#)), the user is

restricted to the initial input parameters and hence a more direct approximation is required. Accordingly, Eq. (3–15) can be conveniently recast as:

$$\zeta = \frac{1}{1 + \left\langle \frac{\varepsilon_1 - 0.0012}{3\varepsilon_{co}} \right\rangle} \quad (3-16)$$

where  $\langle \bullet \rangle$  are Macaulay brackets, and the value 0.0012 can be thought of as a fracture strain such that only when  $\varepsilon_1 > 0.0012$  the concrete softens.

The strain  $\varepsilon_1$  can be assessed from dummy strain elements (with  $EA=I$ ) perpendicular to the diagonal concrete struts as described later. An alternate to Eq. (3–16), based on the compression softening data obtained from panel test results presented in Vecchio (2000), is given by:

$$\zeta = \frac{1}{1 + 0.25 \frac{\varepsilon_1}{\varepsilon_2}} \quad (3-17)$$

where  $\varepsilon_2$  is the strain in the diagonal member. However, it is noted that the softened model for concrete is somewhat sensitive to  $\varepsilon_1$ , and the value of  $\varepsilon_1$  is dependent on where the transverse strain member is placed relative to the diagonal concrete element.

The softened constitutive relations for the diagonal concrete struts can now be defined by modifying the Mander et al. (1988) model to reduce the concrete stress and strain given by:

$$f_c = \frac{\zeta f'_c x^r}{r - 1 + x^r} \quad (3-18)$$

in which  $\zeta f'_c$  = softened concrete stress;  $x = \varepsilon_c / (\zeta \varepsilon_{co})$  is the softened concrete strain coefficient (where  $\varepsilon_{co} = 0.002$ ); and  $r = E_c / (E_c - E_{sec})$  (where  $E_{sec} = f'_c / \varepsilon_{co}$ ). The softened concrete stress-strain relationship is shown in Figure 3–5 by the dotted line and approximated as a linear response in accordance with Vecchio and Collins (1993).

### 3.6.3 Concrete Tensile Strength

The contribution provided by the concrete tensile strength, commonly referred to as “tension stiffening” (Vecchio and Collins, 1986), is typically ignored in many force-based strut-and-tie models (MacGregor, 1992; Collins and Mitchell, 1991; Collins, 1978; Hwang et al., 2000). By assuming strain compatibility between concrete and steel, the overall member tensile force is simply the summation of the steel and concrete forces for a given strain (Collins and Mitchell, 1991; Vecchio and Collins, 1986). Thus the combined steel and concrete elements that make up the tension members 2-4-5, and 3-4 in Figure 3–3(c), intrinsically provide the overall tension stiffened response.

Tension stiffening models vary for different situations and structures; hence the following three approaches are recommended for the C-STM:

- For longitudinal and transverse reinforcing steel bars, tension stiffening is modeled by considering a fracture energy method (Petersson, 1980) as shown in Figure 3–6. The fracture energy  $G_f$  is defined as the energy required to create one unit area of cracking in which  $G_f = h g_f$ , where  $h = 3d_a$  is the crack band width taken as three aggregate diameters; and  $g_f =$  the area under the stress-strain softening diagram. The stress-strain relationship is defined using a tri-linear stress-strain relationship given by:

$$f_t = E_c \varepsilon_t \quad \text{for} \quad \varepsilon_t \leq \varepsilon_t' \quad (3-19a)$$

$$f_t = \frac{f_t'}{3} \quad \text{for} \quad \varepsilon_t = \frac{2}{3} \varepsilon_u \quad (3-19b)$$

$$f_t = 0 \quad \text{for} \quad \varepsilon_t = \varepsilon_u \quad (3-19c)$$

in which  $f_t =$  average concrete tensile stress;  $\varepsilon_t =$  average concrete tensile strain;  $\varepsilon_t' =$  strain at peak tensile stress;  $f_t' = 4\sqrt{f_c'}$  (psi) is typically used to define the concrete tensile strength (Collins and Mitchell, 1991); and  $\varepsilon_u =$  ultimate tensile strain where stress can no longer be transferred and is defined by Eq. (3–20).

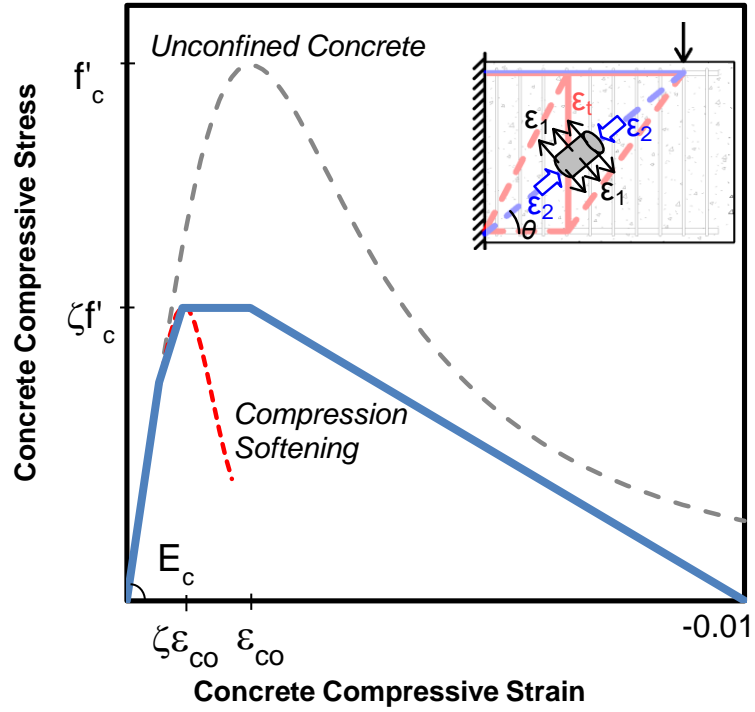


Figure 3-5: Diagonal Concrete Web Elements.

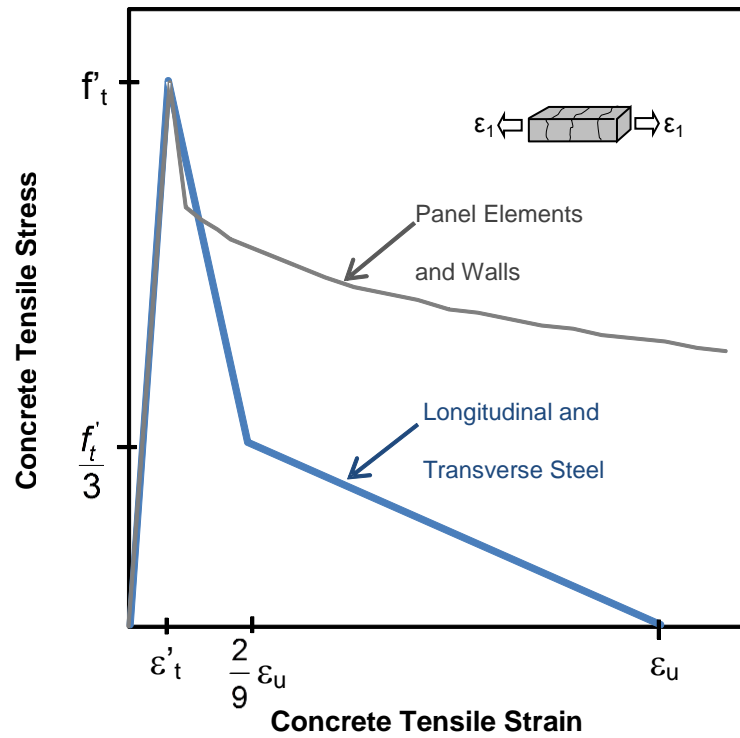


Figure 3-6: Concrete Tension Stiffening Ties.

$$\varepsilon_u = \frac{18 G_f}{5 f'_t h} \quad (3-20)$$

Based on experimental results, [Petersson \(1980\)](#) noted that the fracture energy  $G_f$  for normal-weight concrete typically ranges from  $0.343 - 0.571(\text{lbs}/\text{in}) \equiv 60 - 100(\text{N}/\text{m})$ . Alternatively, for simplicity,  $\varepsilon_u$  is assumed as the steel yield strain in this work.

- In the case of panel and wall structures with a dense network or reinforcing steel, the descending branch model proposed by [Vecchio and Collins \(1986\)](#) may be more appropriate as shown in [Figure 3-6](#). That is:

$$f'_t = \frac{\alpha_1 \alpha_2 f'_t}{1 + \sqrt{500 \varepsilon_t}} \quad \text{for} \quad \varepsilon_t > \varepsilon'_t \quad (3-21)$$

where  $\alpha_1$  and  $\alpha_2$  = factors to account for bond characteristics of reinforcement.

- For structures with experimental results, parameterized models can be applied to model the stress-strain relations used for concrete tension stiffening.

### 3.6.4 Concrete Compression Chord Members

As previously discussed, the transformed constitutive relation used for concrete chord members is derived by substituting appropriate values of  $f'_c$  and  $(1 - d'/kd)$  into [Figure 3-4\(c\)](#) to obtain the stress-strain relationship of the concrete compression chord member.

### 3.6.5 Modified Material Properties to Account for ASR/DEF

The effects of ASR/DEF on the structure can be taken into account in the C-STM analysis technique by modifying the material properties based on observations and experimental data. The extent of damage on the structure can be categorized into three classes: *slight*, *moderate*, and *heavy* damage. Based on this assessment the following material properties should be adopted in the analysis.



1. Diagonal truss concrete:

The concrete strength in the diagonal truss members have to be detuned to account for the damages in cover concrete due to deterioration of concrete by ASR/DEF effects. The modified concrete strength is given as:

$$f'_{cASR} = \lambda f'_c \quad (3-22)$$

where  $\lambda$  = the strength reduction factor defined according to the extent of damage as follows:

- slight damage  $\lambda = 0.85$
- moderate damage  $\lambda = 0.70$
- heavy damage  $\lambda = 0.60^*$

\*Caveat: This value is assessed based on incomplete trends in data at the time of writing (2012). Results of experiments currently in progress are expected in 2014 and will provide a final value.

2. Assess concrete core confinement and modify the concrete properties:

ASR/DEF effect causes the concrete to swell. The swelling of core concrete is constrained by longitudinal and transverse reinforcement, which effectively confines the core concrete. To account for this effect the confinement ratio ( $K_{cc} = f'_{cc} / f'_{co}$  where  $f'_{co}$  = in situ concrete strength) has to be determined to obtain the confined concrete stress ( $f'_{cc}$ ). The procedure to evaluate the confinement ratio is described below ([Mander et al., 1988](#)).

The effective confining stress in the x and y direction  $f'_{lx}$  and  $f'_{ly}$  are given as:

$$\begin{aligned} f'_{lx} &= k_e \rho_x f_y \\ f'_{ly} &= k_e \rho_y f_x \end{aligned} \quad (3-23)$$

where  $k_e$  = confinement effectiveness coefficient (defined below);  $f_y$  = yield stress of reinforcing steel;  $\rho_x$  and  $\rho_y$  are the volumetric ratio of lateral confining steel parallel to the x and y axis, respectively, given as:

$$\rho_x = \frac{A_{sx}}{sd_c} \quad (3-24)$$

$$\rho_y = \frac{A_{sy}}{sb_c}$$

in which  $A_{sx}$  and  $A_{sy}$  = total area of lateral reinforcement parallel to the x and y axes, respectively;  $s$  = spacing of hoop sets;  $d_c$  = core dimension in y direction; and  $b_c$  = core dimension in the x direction. The confinement effectiveness coefficient ( $k_e$ ) is the ratio of area of effectively confined core concrete ( $A_e$ ) to the concrete core area of the section ( $A_{cc}$ ).

$$k_e = \frac{A_e}{A_{cc}} \quad (3-25)$$

In rectangular sections the transverse steel bows outward between the longitudinal bars, hence arching action will occur between the longitudinal bars that are fully supported in position by an angle bend in the transverse steel as shown in [Figure 3-7](#). The arching action is assumed to take the form of a second degree parabola with an initial tangent slope of 45°. The area of one such parabola is given by  $(w'_i)^2 / 6$ , where  $w'_i$  is the  $i^{\text{th}}$  clear transverse spacing between longitudinal bars in which arching action of concrete develops. In the case of a lightly confined rectangular section, the parameter  $w'$  along the y axis is taken as the depth of the neutral axis ( $kd$ ) minus the distance from the extreme compression fiber to the longitudinal bar. The net area of ineffectively confined concrete for the  $n$  longitudinal bars supported in the corners of the bent transverse hoops is given by:

$$\sum_{i=1}^n (w_i)^2 / 6 \quad (3-26)$$

The total effectively confined core concrete area is defined as:

$$A_e = \left[ b_c d_c - \sum_{i=1}^n (w_i)^2 / 6 \right] \left( 1 - 0.5 \frac{s'}{b_c} \right) \left( 1 - 0.5 \frac{s'}{d_c} \right) \quad (3-27)$$

in which  $s'$  = clear longitudinal spacing between hoop bars in which arching action of concrete develops.

The concrete core area of the rectangular section is given by:

$$A_{cc} = b_c d_c (1 - \rho_{cc}) \quad (3-28)$$

where  $\rho_{cc}$  = volumetric ratio of longitudinal steel in the confined core. Note that the term  $(1 - \rho_{cc})$  in the above equation effectively removes the presence of longitudinal bars from the confined concrete area. From these the confinement effectiveness coefficient ( $k_e$ ) can be determined from [Eq. \(3-25\)](#).

The ratios  $f'_{lx} / f'_{co}$  and  $f'_{ly} / f'_{co}$  are determined, the smaller of these ratios is taken as  $f'_{l1} / f'_{co}$ , and the larger is taken as  $f'_{l2} / f'_{co}$ . The confinement ratio ( $K_{cc} = f'_{cc} / f'_{co}$ ) is determined from the chart shown in [Figure 3-8](#). Thus, the confined concrete stress is then determined as  $f'_{cc} = K_{cc} f'_{co}$ , where  $f'_{co}$  = in situ concrete strength.

The strain ( $\varepsilon_{cc}$ ) corresponding to the maximum confined concrete stress ( $f'_{cc}$ ) is defined as:

$$\varepsilon_{cc} = \varepsilon_{co} (1 + 5(K_{cc} - 1)) \quad (3-29)$$

in which  $\varepsilon_{co}$  = the strain corresponding to the unconfined concrete strength (usually  $\varepsilon_{co} = 0.002$ ).

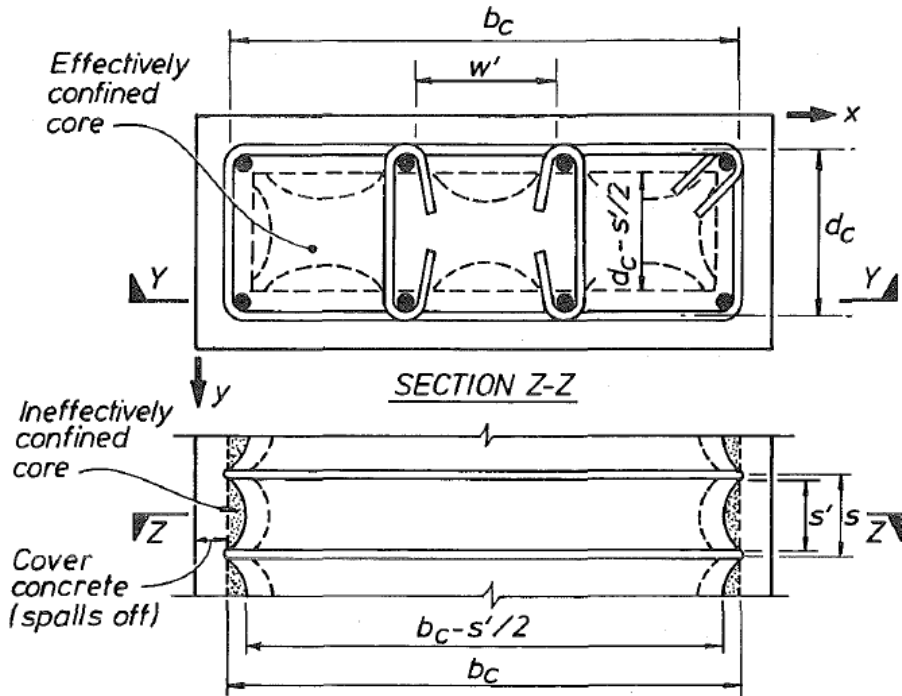


Figure 3-7: Assumed Arching Mechanism Between Hoops for Rectangular Sections (Mander, 1983).

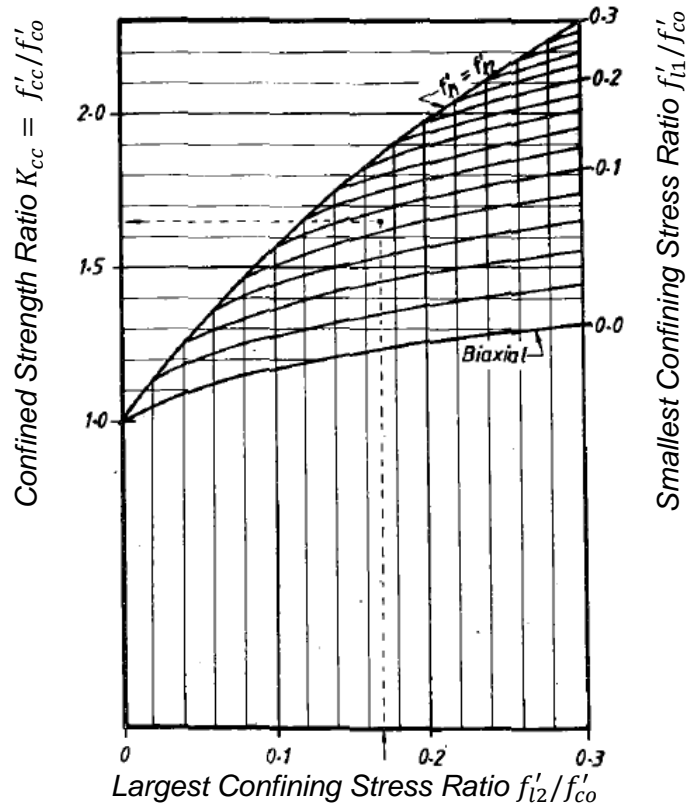


Figure 3-8: Confined Strength Determination from Lateral Confining Stresses for Rectangular Sections (Mander, 1983).

### 3. Prestress effects in longitudinal bars and hoops:

The constraint offered by longitudinal reinforcement and transverse hoops to swelling of core concrete puts tensile strains on the reinforcing steel. This effectively puts the longitudinal and transverse reinforcement in a state of prestress.

The prestressing forces on the reinforcement can be evaluated from the prestressing stresses, which depend on the extent of damage (slight, moderate, or heavy) due to ASR/DEF effects. Based on experimental observations the following recommendations are made for prestressing stresses ( $f_{ps}$ ) in longitudinal reinforcement:

- slight damage  $f_{ps} = 0.3f_y$
- moderate damage  $f_{ps} = 0.5f_y$
- heavy damage  $f_{ps} = 0.8f_y^*$

in which  $f_y$  = yield stress of longitudinal reinforcement.

Recommendations for prestressing stresses in hoops are:

- slight damage  $f_{ps} = 0.5f_{yh}$
- moderate damage  $f_{ps} = 1.0f_{yh}$
- heavy damage  $f_{ps} = 1.1f_{yh}^*$

in which  $f_{yh}$  = yield stress of transverse hoops.

\*Caveat: This value is assessed based on incomplete trends in data at the time of writing (2012). Results of experiments currently in progress are expected in 2014 and will provide a final value.

Appropriate modifications to the stress-strain behavior of the reinforcing steel have to be made to account for the prestressing effects. The modified stress-strain relation of steel is shown in [Figure 3–9](#) in which  $\varepsilon_{ps}$  = prestrain corresponding to prestressing stress ( $f_{ps}$ ).

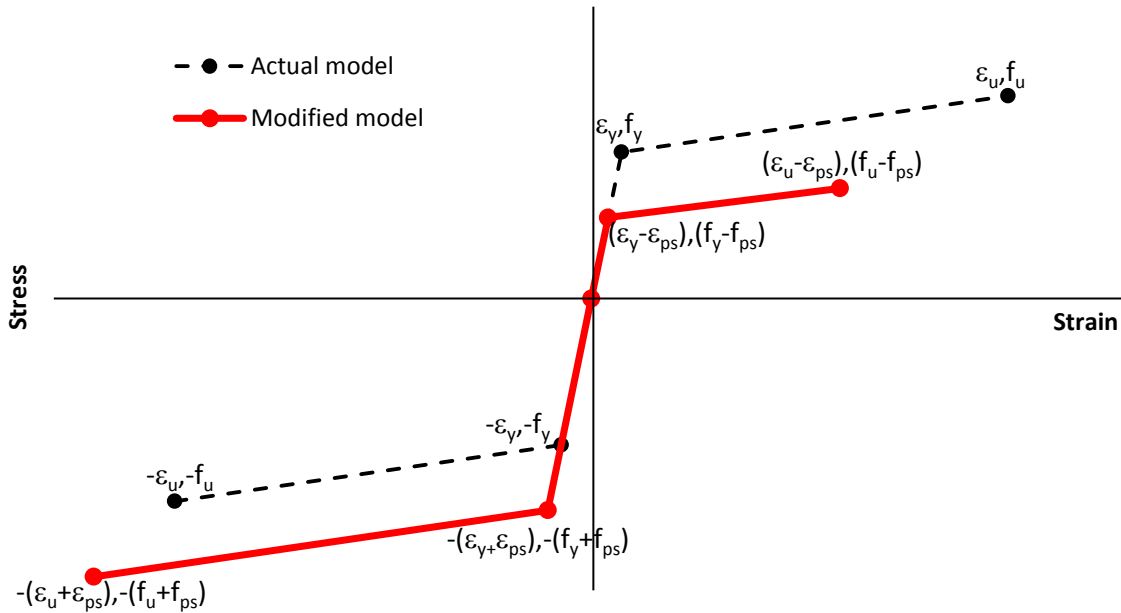


**Figure 3–9: Modified Stress-Strain Model for Steel to Account for Prestressing Effects Due to ASR/DEF.**

### 3.7 ULTIMATE STRENGTH AND SOFTENING OF CONSTITUTIVE RELATIONS

The exact failure mechanism for deep beams or disturbed regions is difficult to define due to unknown (a priori) hierarchy of failure mechanisms, particularly given the fact that shear failure alone can be of four types: diagonal tension, web crushing, nodal failure, or sliding shear. In reality the type of failure is heavily dependent on the member geometry and reinforcement detailing, and is often a combination of events that lead to the formation of the final collapse mechanism. In the C-STM, steel yielding, concrete crushing, and concrete softening are intrinsically accounted for through the material constitutive relationships previously described. However, a more thorough post analysis assessment may be required in order to assess other possible critical failure mechanisms.

#### 3.7.1 Strut-and-Tie Strength Checks

Strut-and-tie modeling predisposes itself to defining failure as either: yielding of reinforcing ties, crushing of a strut, anchorage failure of reinforcing ties, or nodal failure. The member forces in the C-STM can be used to check that the force does not exceed the strength defined using conventional SAT design procedures for anchorage and nodal failures.

### 3.8 COMPUTATIONAL IMPLEMENTATION

The computational analysis of the C-STM described in the above sections can be implemented using structural analysis software and carried out in six steps as discussed in what follows.

#### Step 1: Assign node coordinates

For doubly reinforced sections the longitudinal chord members (members 2-4-5 tension, and 1-3 compression of [Figure 3-3\(c\)](#)) are defined at the respective longitudinal steel centroids. The horizontal coordinates of the boundary nodes are either defined by: (i) an applied load/bearing support (i.e., Node 5 in [Figure 3-3\(c\)](#) is defined by the centroid of the applied load); or (ii) at the intersecting lines of thrust from the beam and column members (i.e., Node 1 in [Figure 3-3\(c\)](#) is defined at the intersection of the compression steel in the beam and supporting column represented as a fixed boundary). The transverse tension ties in the truss mechanism are then located according to the selected numerical truss scheme (i.e., Nodes 3 and 4 in [Figure 3-3\(c\)](#) are defined by single-point Gauss quadrature).

## Step 2: Assign steel and concrete elements

The steel and concrete elements of the C-STM can be modeled using separate trusses with nodes constrained together to give the combined steel-concrete member response. This is most easily simulated by duplicating the assigned nodes in the out-of-plane axis to form two separate trusses, and constraining the degrees of freedom for each of the duplicate nodes. Steel and concrete elements are then drawn with pinned-end connections between the appropriate node points as shown in [Figure 3–10](#).

The expressions presented in [Table 3–2](#) are used to define the stiffness and axial area assignments for each steel and concrete element of the C-STM model. The arch breadth scalar  $\eta$  is used to apportion the contribution of arch and truss action defined as a function of the longitudinal and transverse reinforcement and members' span-to-depth ratio given by [Eq. \(3–5\)](#).

Alternatively, the arch breadth scalar can be obtained graphically using [Figure 3–3\(e\)](#), where the span to depth ratio is used to determine the arch breadth scalar according to the ratio of transverse to longitudinal reinforcement. Once defined, element areas are assigned as axial cross-sectional areas with an associated material property that defines the elastic stiffness, thus defining the element's axial rigidity.

## Step 3: Assign nonlinear constitutive material relationships

At this stage, the elastic response of the C-STM is defined by steps 1 and 2; hence nonlinear constitutive material relations for cracked reinforced concrete are now used to define the element's nonlinear behavior. [Figure 3–11](#) shows the theoretical stress-strain relationships used to define the concrete constitutive relations for: (a) diagonal concrete struts; (b) concrete chord members; and (c) concrete tension behavior used in conjunction with all truss elements that also possess steel. To account for the ASR/DEF effects, the modified material properties as discussed in [section 3.6.5](#) have to be considered.



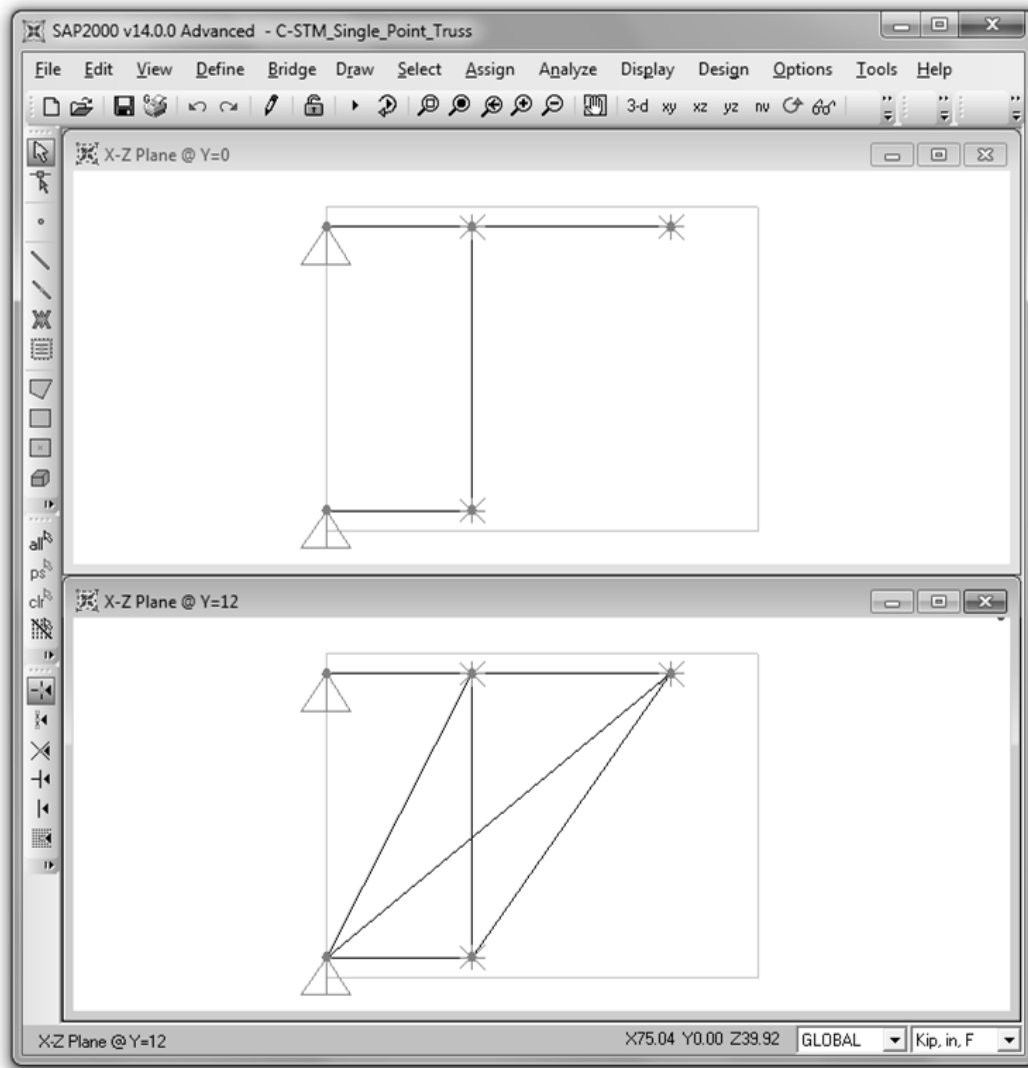
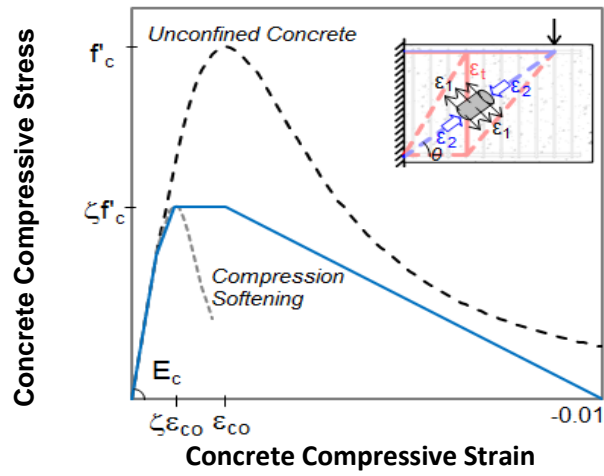
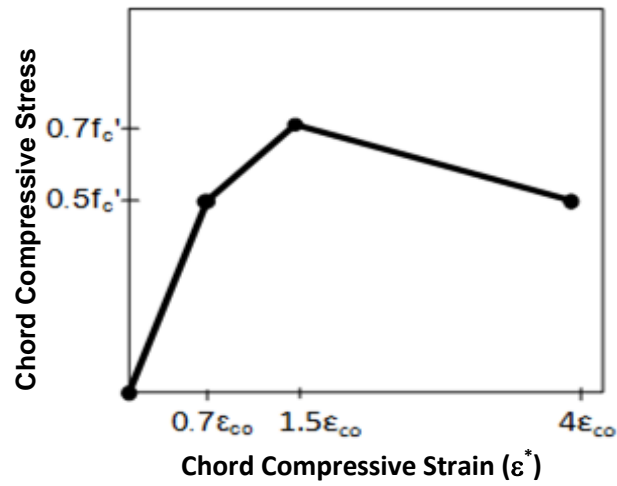


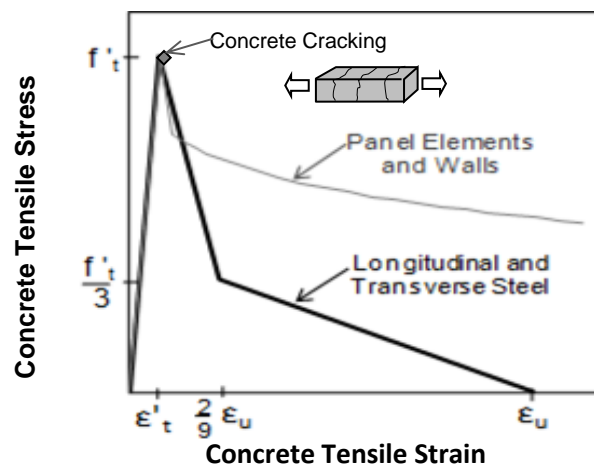
**Figure 3–10: SAP2000 Screenshot: Steel Truss (Top); Concrete Truss (Bottom).**



(a)



(b)



(c)

Figure 3–11: Nonlinear Constitutive Material Properties (a) Diagonal Web Members, (b) Compression Chord Elements, and (c) Tension Stiffened Elements.

#### **Step 4: Assign load cases**

Load patterns are assigned at node locations as either forces or displacements in order to replicate the structure's loading pattern. Other parameter inputs include: loading control either specified as *load* or *displacement* control; incremental step size; results saved at final load or incremental load steps; and other nonlinear parameters. However in [SAP2000™ \(1995\)](#), in order to perform an analysis in displacement control, additional joints have to be introduced without altering the structural behavior of the system. Joint displacements are provided at these joints, and the corresponding forces are calculated to obtain the overall force-deformation behavior of the system.

#### **Step 5: Run analysis**

The analysis can now be run for the desired load cases as input by the user. Once complete, the user can progressively step through the deformed shape to review the formation of nonlinear behavior.

#### **Step 6: Post analysis investigation**

Axial forces, displacements, and other output parameters can then be exported to a spreadsheet so that a post analysis investigation can be conducted. The axial force in each member can be individually assessed in order to ensure that the force does not exceed any other strength failure criteria (i.e., anchorage failure, nodal crushing, concrete softening, etc.). Because element strains are not given as an explicit output in [SAP2000™ \(1995\)](#), an alternative means of defining the strain is required. This can be done using one of the following techniques:

- (a) The element strain can be defined in terms of the element force divided by the axial rigidity as shown below:

$$\varepsilon = \frac{F}{EA} \quad (3-30)$$

where  $EA$  is constant in the elastic range, hence this can only be applied prior to nonlinear behavior.

- (b) For members that reach nonlinear deformations, the strain can be obtained from the link deformations. The link deformations can be divided by their actual member length to obtain the strain in that member.
- (c) Alternatively to the above methods, a third truss called a ‘strain-meter truss,’ can be defined in the out-of-plane axis similar to the steel and concrete trusses such that each node is constrained accordingly. Truss elements with a unit axial rigidity (i.e.,  $EA = 1$ ) can be drawn between the desired nodes as *Strain Members* so that the (small) force resisted is equal to the strain as shown in Eq. (3–30). This will provide the composite steel-concrete axial strain associated between the selected two node points. Note: this method was verified in this research using the previously mentioned methods providing identical comparisons for vertical and horizontal members. However, some minor numerical discrepancies were observed in the diagonal concrete members where the results from step (b) would deviate with highly nonlinear behavior.

Application of the C-STM modeling technique is presented in the following sections with examples.

## 4. WORKED EXAMPLE 1

### 4.1 SCOPE

In this section a specimen tested by [Bracci et al. \(2000\)](#), [Young et al. \(2002\)](#), and [Powanusorn and Bracci \(2006\)](#) to investigate the causes of excessive cracking in deep reinforced concrete bent caps is used to illustrate the analytical procedures. The structure is first analyzed using beam theory, and from this a strut-and-tie model is developed. Finally the structure is modeled using the C-STM technique. All results are compared with the experimental results.

### 4.2 THE STRUCTURE

Full-scale models of prototype bents used in Texas that had shown sign of distress near the column-to-bent cap negative moment connection were tested in order to determine their performance and investigate the causes of the cracks. [Figure 4–1](#) presents the reinforcing layout and cross-section of Specimen 2A selected for the analysis. The specimen has compression reinforcement consisting of eight No. 8 (25 mm) bars and a specified cover concrete depth of 2.25 inches (57 mm).

The reported force-deformation responses are based on the actuator forces that were run in parallel to one another in a stepped force-controlled configuration, versus the average displacement of the two experimental beam displacement responses. This was justified using the FEM model presented by [Bracci et al. \(2000\)](#), [Young et al. \(2002\)](#), and [Powanusorn and Bracci \(2006\)](#), as well as the C-STM (described below), where the end displacements of the two cantilevered ends were calculated within 1 percent of each other.

[Table 4–1](#) presents the reported material strength data and experimental test results for Specimen 2A ([Bracci et al., 2000](#)), in which:  $P_{Yield}^{Expt}$  and  $P_{Failure}^{Expt}$  = applied load at first yield and ultimate failure, respectively;  $\Delta_{Yield}^{Expt}$  and  $\Delta_{Failure}^{Expt}$  = vertical tip displacement at first yield and ultimate failure, respectively; and  $\mu = \Delta_{Failure}^{Expt} / \Delta_{Yield}^{Expt}$  = structural displacement ductility. Note: as no test day strength results were provided, the 28-day strength was assumed for the analysis of Specimen 2A.

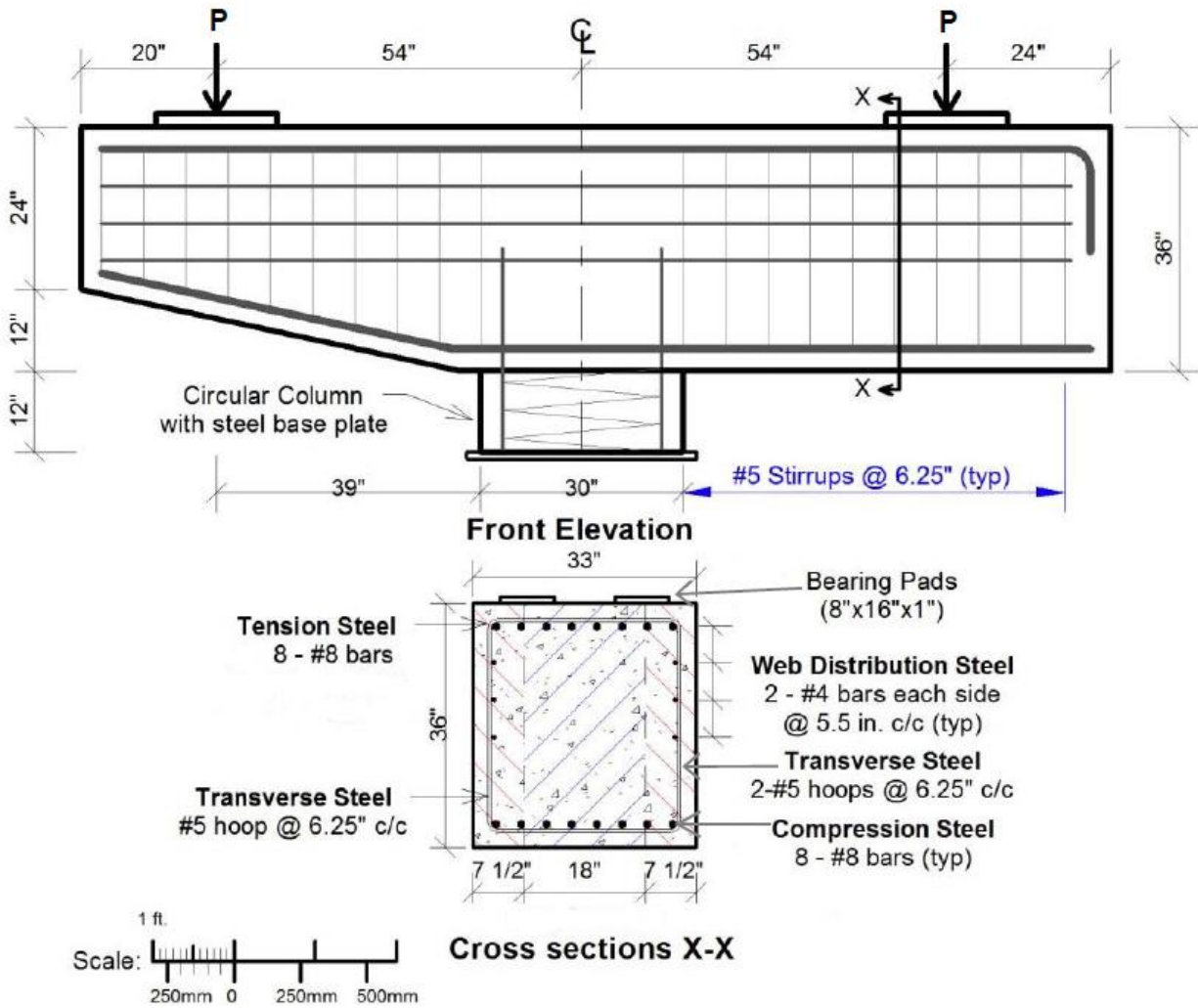


Figure 4-1: Elevation and Cross-Section of Specimen 2A (Bracci et al., 2000).

**Table 4–1: Material Properties and Test Results.**

<b>Material Properties</b>	$f'_c$ (ksi)	6.2 <sup>#</sup>
	$f'_t$ (ksi)	0.32
	$E_c$ (ksi)	4490
	n*	6.46
<b>Experimental Results</b>	$P_{Yield}^{Expt}$ (kip)	330
	$P_{Failure}^{Expt}$ (kip)	404
	$\Delta_{Yield}^{Expt}$ (in)	0.25
	$\Delta_{Failure}^{Expt}$ (in)	0.77
	$\mu$	3.08

<sup>#</sup>TxDOT Class C Concrete-Average compression strength of three 28-day cylinder tests (Section 15.3, ACI 318-99).

\*Modular ratio = Young's modulus of steel to concrete, were  $E_s = 29000ksi = 200GPa$

General observations reported during testing were as follows: 1) vertical flexural cracking initiated near the column face at the top of the bent cap around 100 kip; 2) at approximately 160 kip the vertical flexural cracks began to incline toward the applied load; 3) with increased loading, inclined flexure-shear cracks initiated, propagated, and widened while the original flexural cracks stabilized; 4) ultimate failure was very sudden and typically occurred along the diagonal shear plane, extending from the load point inclined toward the column support (Bracci et al., 2000).

#### 4.3 STAGE 1: STRENGTH ANALYSIS USING BEAM THEORY

The code based design approaches that were described in detail in Chapter 2 are used to predict the response of Specimen 2A. Results from the application of each of these approaches are presented as follows.

**Step 1:** Determine first yield flexural capacity,  $M_y^b$ .

The yield moment and the externally applied load causing first yield are calculated using Eqs. (2–1) and (2–3), respectively. The parameters required by the analysis are presented in

[Table 4–2](#). The analysis results in a yield moment of  $M_y^b = 1028$  kip-ft and an external yield load of  $P_y^b = 316$  kip.

**Steps 2:** Determine nominal flexural moment,  $M_n^f$ .

The nominal flexural moment ( $M_n^f$ ) was calculated based on [Eq. \(2–4\)](#). The flexural capacity  $M_n^f = 1197$  kip-ft.

**Step 3:** Determine externally applied load based on flexure,  $P_n^f$ .

Based on the nominal flexural moment ( $M_n^f$ ), and knowing that the shear span to the face of the column  $L_b = 39$  inches, the external load causing beam flexure is found to be  $P_n^f = 368$  kip. The results are presented in [Table 4–2](#).

**Step 4:** Determine beam shear capacity,  $V_n^s$ .

The shear capacity ( $V_n^s$ ) is calculated from [Eq. \(2–7\)](#). Since there are no prestressing tendons, the component of shear carried by tendons is  $V_p = 0$ . The parameters  $\beta$  and  $\theta$  are calculated based on Method 1. The beam shear capacity was found to be  $V_n^s = 341$  kip. The results of this analysis are presented in [Table 4–3](#).

**Step 5:** Check strength hierarchy.

The strength reduction factor for shear and flexure are  $\phi_v = 0.90$  and  $\phi_f = 0.90$ , respectively. It is observed that  $\phi_v V_n^s = 0.90 \times 341 = 307$  kip is less than  $\phi_f P_n^f = 0.90 \times 368 = 331$  kip. That is, the factored shear capacity is insufficient, which could lead to a shear failure of the bridge pier.

**Step 6:** Determine the shear capacity of the beam-column joint regions.

From the shear force diagram of the equivalent beam model of the bent cap shown in [Figure 4–2](#), it is observed that there is no shear in the beam-column joint. Hence, the beam-column joint is not critical.



**Table 4–2: Results for Stage 1 Flexure Analysis.**

$L_b(in)$	39	
$b_w(in)$	33	
$d'(in)$	3 1/4	
$\rho_L'$	0.00581	
$d(in)$	32 3/4	
$\rho_L$	0.00581	
$n$	6.46	
$k$	0.222	<i>Eq. (2–2)</i>
$C_c(kip)$	-344	
$C_s(kip)$	-64	
$T(kip)$	408	
$M_y^b(kip.ft)$	1028	<i>Eq. (2–1)</i>
$P_y^b(kip)$	<b>316</b>	<i>Eq. (2–3)</i>
$\beta_t$	0.74	<i>Eq. (2–5)</i>
$M_n^f(kip.ft)$	1197	<i>Eq. (2–4)</i>
$P_n^f(kip)$	<b>368</b>	<i>Eq. (2–6)</i>

**Table 4–3: Results for Stage 1 Shear Analysis.**

$d(in)$	32.75	
$A_{sh}(in^2)$	0.614	
$f_c'(ksi)$	6.2	
$f_y(ksi)$	65	
$V_c(kip)$	153	<i>Eq. (2–8)</i>
$V_s(kip)$	188	<i>Eq. (2–9)</i>
$V_n^s(kip)$	<b>341</b>	<i>Eq. (2–7)</i>

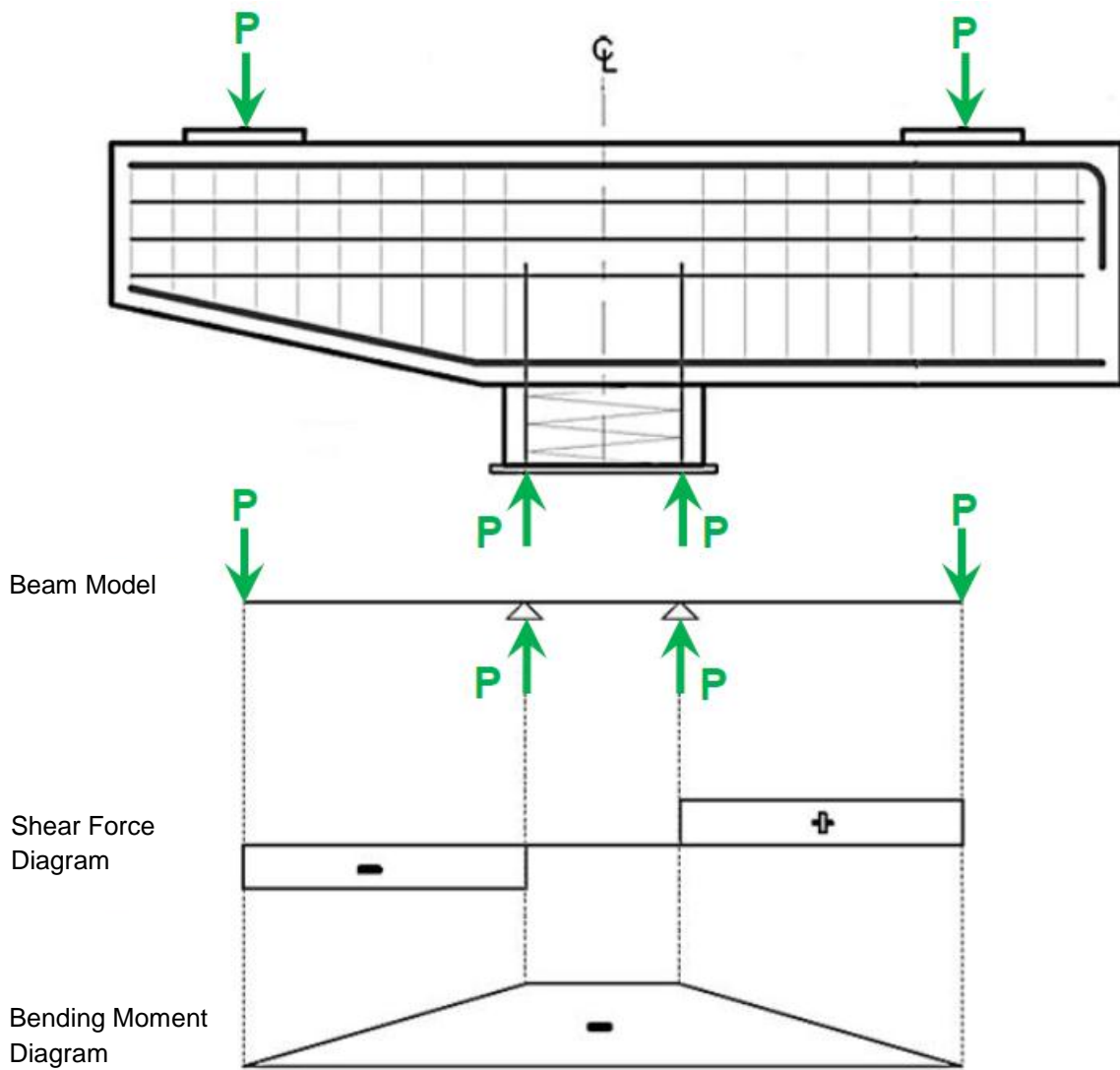


**Figure 4-2: Shear Force and Bending Moment Diagram of Equivalent Beam Model of Bent Cap Specimen 2A.**

From the above computations it is observed that the factored shear capacity of the bent cap is insufficient. This warrants further investigation, and the strut-and-tie technique is used for further analysis.

#### 4.4 STAGE 2: STRENGTH ANALYSIS USING STRUT-AND-TIE MODELING

The strut-and-tie model predictions are based on the procedure detailed in Chapter 2. No reduction factors are used in order to predict the actual response. The strut-and-tie model for the bent cap Specimen 2A is shown in Figure 4-3. Both the single panel and two panel strut-and-tie models are shown. The steps involved in the construct and analysis of the single panel strut-and-tie method are given below.

**Step 1:** Determine the truss and node geometry.

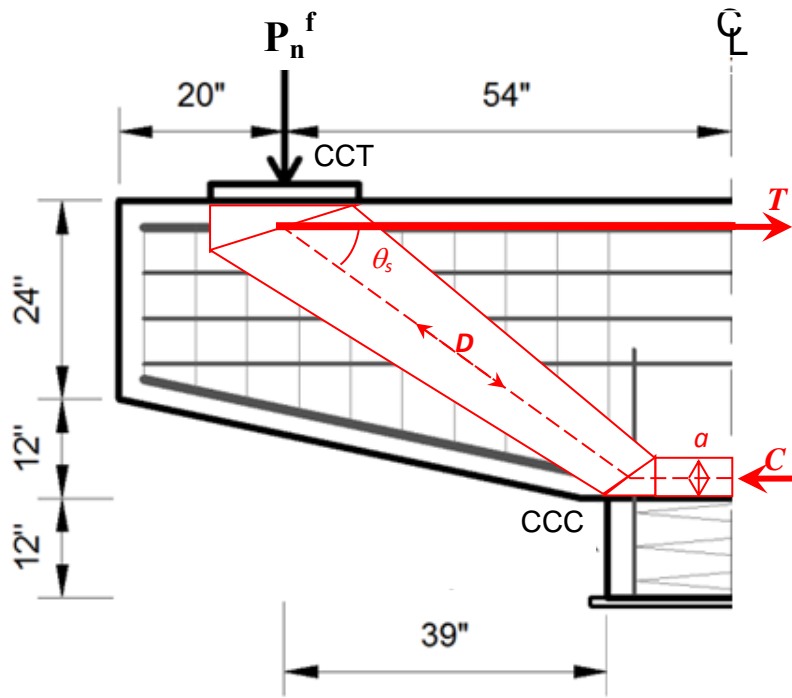
By equating the horizontal forces  $C$  and  $T$  in Figure 4-3(a), the height ( $a$ ) of the CCC node is determined to be:

$$a = \frac{T}{0.85f'_c b_w} = \frac{A_s f_y}{0.85f'_c b_w} = 2.4 \text{ in.} \quad (4-1)$$

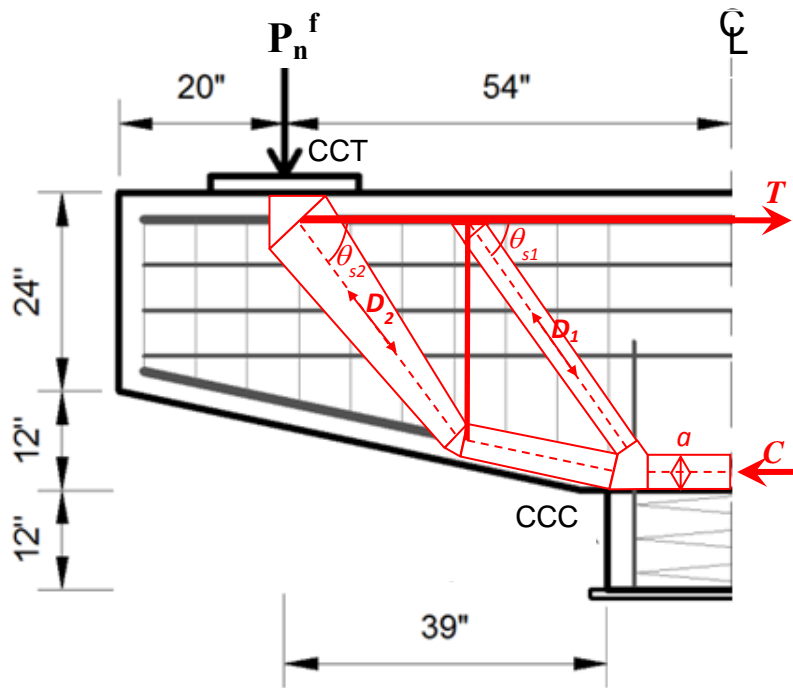
where the variables are as described earlier. The width of the CCT node equals the width of the bearing pad, which is 16 inches. The depth of the back face of the CCT node is taken as twice the distance from near face of the beam to the centroid of the tension reinforcement = 6.75 inches. The angle of inclination of the compression strut  $\theta_s = \tan^{-1}\left(\frac{jd}{\text{shear span}}\right) = 36.8^\circ$ .

**Step 2:** Solve the determinate truss.

Taking moment equilibrium about the CCC node the beam shear  $P_n^f = T(\tan \theta_s) = 306$  kip. Thus based on longitudinal steel yield,  $P_y^{SAT} = 306$  kip. Based on equilibrium of vertical forces at the CCT node the strut force  $D = 510$  kip. The bottom face of the CCC node is proportioned based on the vertical component of the strut force  $D$  and compressive force  $C$ , and is found to be 1.75 inches.



(a) One panel model



(b) Two panel model

Figure 4-3: Strut-and-Tie Model of Reinforced Concrete Bridge Cap Specimen 2A.

**Step 3:** Determine critical node.

Based on the geometry of the nodes it is evident that the CCC node is the most critical node. The strength of the critical CCC node is found to be  $0.85f'_c A_{node} = 510$  kip, where  $A_{node}$  = the cross-sectional area of the inclined face of the CCC node.

**Step 4:** Determine external load causing node failure.

Incidentally it is found that the strut force  $D$  is exactly equal to the node strength of the CCC node. Therefore, the externally applied load based on node capacity  $P_n^{SAT} = 368$  kip  $= P_n^f$ . However, the factored capacity  $\phi_v P_n^{SAT} < \phi_f P_n^f$ . The results obtained from the strut-and-tie analysis are presented in [Table 4-4](#).

**Table 4-4: Results for Stage 2 SAT Analysis.**

Specimen 2A		Comments
$a$ (in)	2.4	
$\theta_s$ (degrees)	36.8	
$T$ (kip)	408	
$D$ (kip)	510	
$P_y^{SAT}$ (kip)	306	Based on longitudinal steel yield.
$\phi_v P_y^{SAT}$ (kip)	214	
$P_n^{SAT}$ (kip)	368	Based on node capacity.
$\phi_v P_n^{SAT}$ (kip)	258	
$\phi_f P_n^f$ (kip)	331	

[Figure 4-4\(b\)](#) shows the experimentally obtained force-deformation response along with each of the code-based predictions as well as the computational response from the proposed C-STM (discussed in subsequent sections). As each of the code-based techniques is only a strength-based approach, no predictions of the structure's global deformation can be made; hence the predicted forces are represented by horizontal lines.

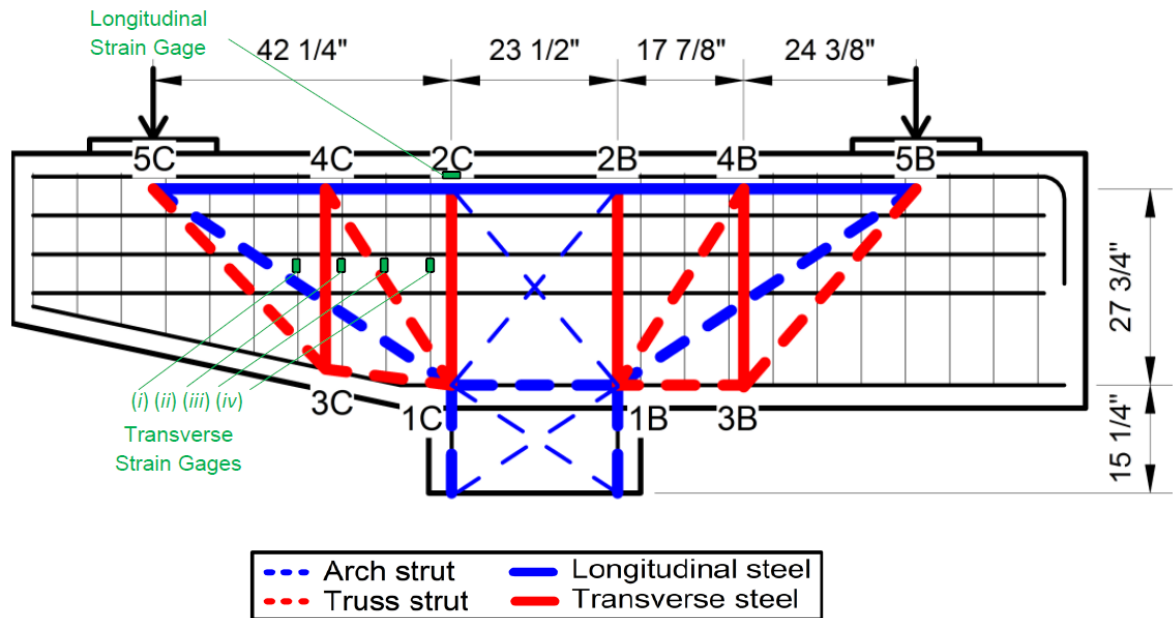
From the SAT analysis it can be concluded that the joint capacity is undependable even though  $P_n^{SAT} = P_n^f$ . The results are inconclusive, and this warrants a more advanced analysis be conducted using C-STM; clearly it is desirable to have a more insightful analysis that can overcome these shortcomings. This is now the subject of the following section.

#### **4.5 STAGE 3: STRENGTH AND DEFORMATION CAPACITY USING COMPATIBILITY STRUT-AND-TIE COMPUTATIONAL MODELING**

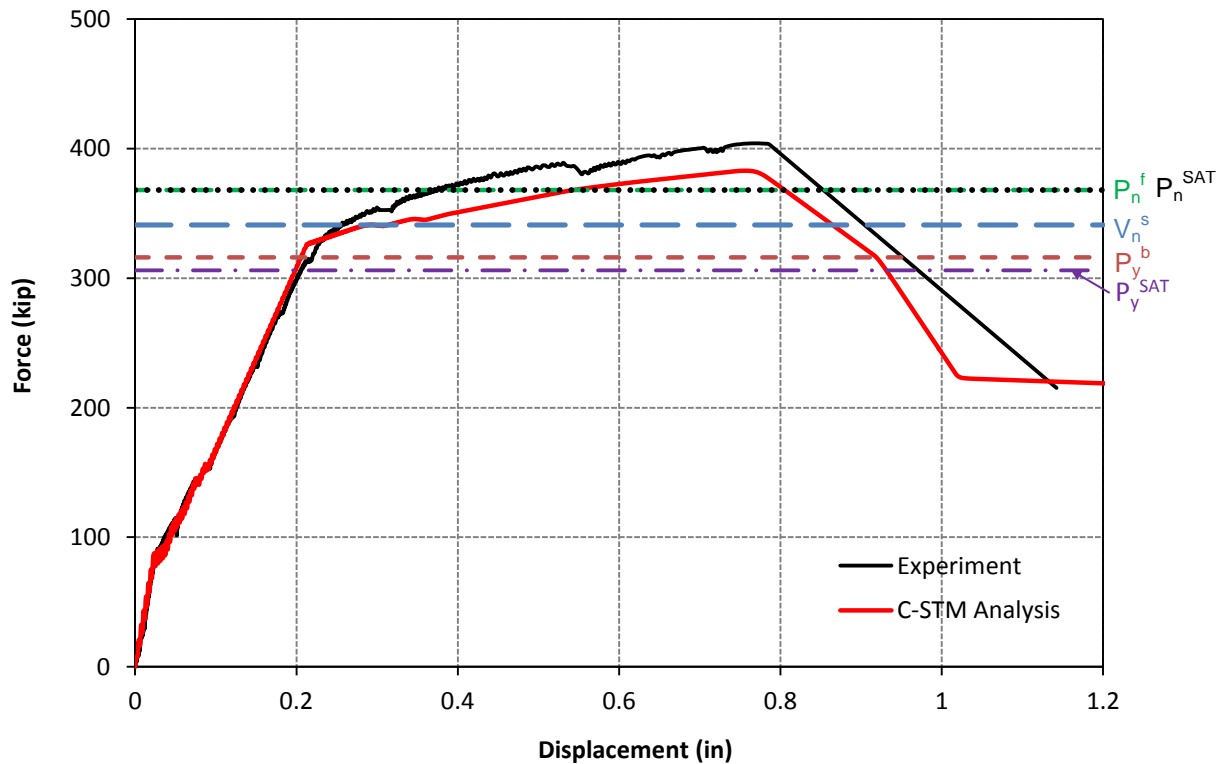
Using the modeling procedure described in [Chapter 3](#) in detail, the proposed C-STM can be applied to the experimental reinforced concrete bent caps in order to provide a more informative analysis. [Figure 4-4\(a\)](#) shows the applied C-STM described earlier. The numbered node points in [Figure 4-4\(a\)](#) correspond to the cantilevered example shown in [Figure 3-3\(c\)](#), as well as suffixes *C* and *B* that refer to the tapered cantilever and beam ends, respectively.

The representative area of longitudinal tension reinforcement (labeled 5C-5B) ([Figure 4-4\(a\)](#)) was defined as the centroid of the No. 8 longitudinal bars plus the three sets of two No. 4 web distribution bars. The internal lever arm of the column support was taken as the internal diameter of the longitudinal reinforcement, thus defining the horizontal coordinates of nodes 1 and 2. The horizontal coordinates of the vertical transverse reinforcement member (member 3-4) were defined according to the single-point Gauss quadrature model.

As an example, [Table 4-5](#) presents the variables used for Specimen 2A to calculate the area assignments of each element described in Step 2. For a  $L/jd$  ratio of 1.52 and a transverse to longitudinal reinforcement ratio of 0.41, the corresponding arch breadth scalar can be calculated as 0.55 using [Eq. \(3-5\)](#), or graphically interpolated as illustrated in [Figure 3-3\(e\)](#).



(a) C-STM model for Specimen 2A



(b) Comparison of force-deformation results of Specimen 2A  
**Figure 4-4: C-STM Model and Results for Specimen 2A.**

**Table 4-5: Axial Rigidity Assignments for Specimen 2A.**

Member	Steel		Concrete		Comments
	$E - ksi$ (GPa)	$A - in.^2$ ( $mm^2$ )	$E - ksi$ (MPa)	$A - in.^2$ ( $mm^2$ )	
2-4 4-5	$E_s = 29000$ (200)	$A_s = 7.46$ (4813)	$E_c = 4490$ (30,960)	$b.kd = 250.7$ (161,740)	†Tension Chord
1-3	$E_s = 29000$ (200)	$A_s' = 6.28$ (4051)	$\psi_E E_c = 3680$ (25,373)	$b.kd = 250.7$ (161,740)	†* Compression Chord
3-4	$E_s = 29000$ (200)	$N_h A_{sh} = 2.46$ (1584)	$E_c = 4490$ (30,960)	$(4c + 2d_h) N_h s = 256.3$ (165,350)	Active Hoop steel including tension stiffening effect
1-5	-	-	$E_c = 4490$ (30,960)	$\frac{0.375 \eta b_w j d}{\cos \alpha} = 224.2$ (144,645)	Concrete Strut in Arch Mechanism
1-4	-	-	$E_c = 4490$ (30,960)	$\frac{0.5(1-\eta)b_w j d}{\sqrt{0.423 + \tan^2 \alpha}} = 220.7$ (145,390)	Concrete Strut in Truss Mechanism
3-5	-	-	$E_c = 4490$ (30,960)	$\frac{0.5(1-\eta)b_w j d}{\sqrt{0.577 + \tan^2 \alpha}} = 203.2$ (131,100)	Concrete Strut in Truss Mechanism

**Variables**

$L$ in (mm)	$jd$ in (mm)	$L/jd$	$\rho_T$	$\rho_L$	$\eta$	$A_s$ $in^2$ ( $mm^2$ )	$A_s'$ $in^2$ ( $mm^2$ )	$N_h$	$A_{sh}$ $in^2$ ( $mm^2$ )	$b_w$ in (mm)	$d$ in (mm)	$kd$ in (mm)	$d'$ in (mm)	$\alpha$
42.25 (1073)	27.76 (705)	1.52	0.0030	0.0073	0.55	7.46 (4813)	6.28 (4051)	4	0.614 (396)	33 (838)	31 (787)	7.60 (193)	3.25 (83)	33.3°

$$\dagger k = \sqrt{(\rho_L + \rho_L')^2 n^2 + 2(\rho_L + \rho_L' d'/d)n} + (\rho_L + \rho_L')n = 0.245 * \psi_E = \frac{\sqrt{f'_c} \text{ (psi)}}{168(1-d'/kd)} = \frac{\sqrt{f'_c} \text{ (MPa)}}{14(1-d'/kd)} = 0.82$$

Row 2 of Figure 4-5 shows the three different nonlinear concrete stress-strain relationships derived for Specimen 2A from the material properties presented in Table 4-1, and are described as follows.

Figure 4-5(a) shows the softened stress-strain relationship for the diagonal concrete struts that were applied to the diagonal web elements. This was obtained by first running an analysis with strain truss members perpendicular to the diagonal concrete strain elements. This provides with the strain transverse to the diagonal concrete members,  $\epsilon_1$ . Using Eq. (3-16) the concrete softening coefficient is evaluated, and the softened stress-strain relation is obtained using Eq. (3-18). The resulting softened stress-strain model may then be simplified in a tri-linear form for ease of implementation in SAP2000™ (1995), as shown in Figure 4-5(a).



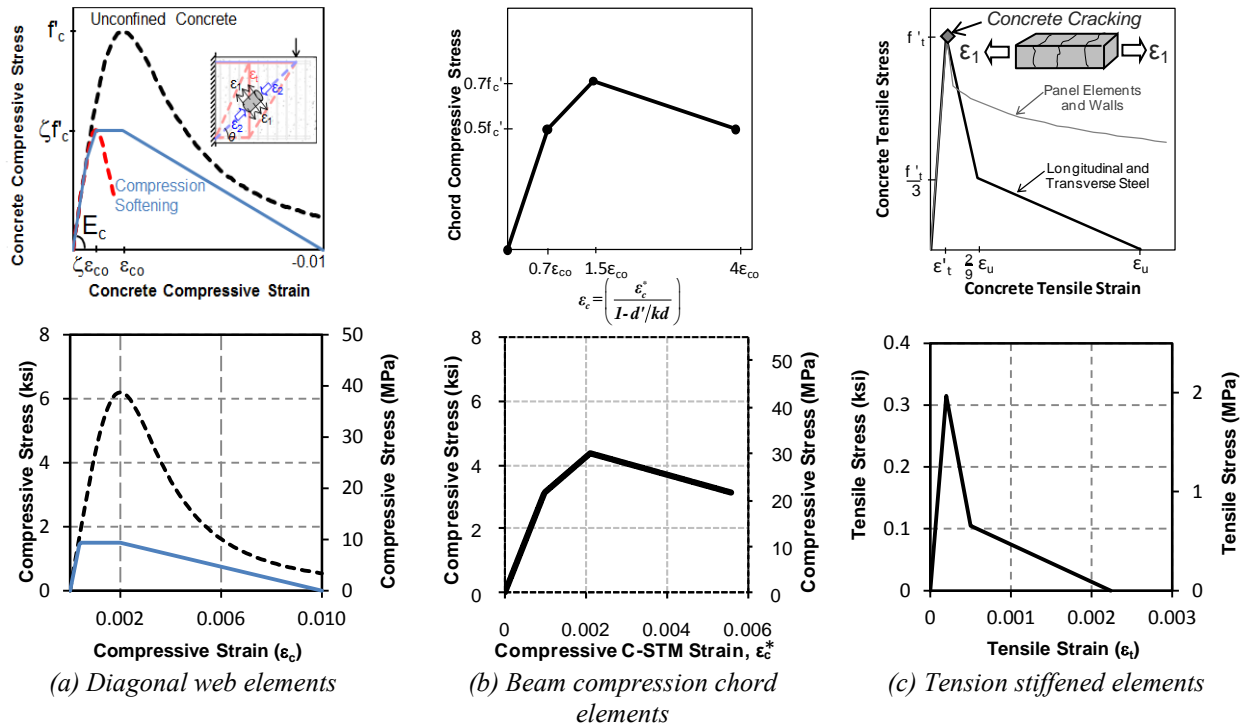


**Figure 4-5: Cracked Reinforced Concrete Material Properties.**

**Top row: Theoretical nonlinear behavior**

**Center row: Specimen 2A modeled behavior**

Figure 4–5(b) shows the transformed concrete chord stress-strain relationship applied to the longitudinal compression chord members. This was obtained by multiplying the tri-linear stress ( $\sigma_c$ ) and strain ( $\varepsilon_c$ ) coefficients by  $f'_c$  and  $\varepsilon_{co}$ , respectively; where  $\varepsilon_{co} = 0.002$  is typically used for unconfined concrete. A further strain transformation of  $\varepsilon_c$  is then required to obtain the compressive C-STM strain ( $\varepsilon_c^*$ ) that applies to the actual position of the C-STM compression chord member. This is achieved by multiplying the values of  $\varepsilon_c$  by  $(1 - d'/kd)$ .

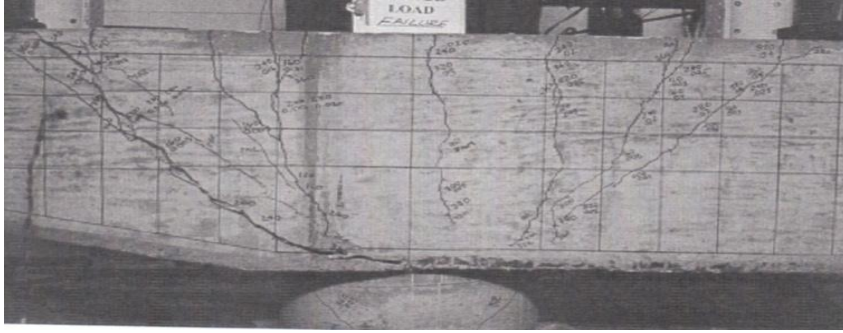
Figure 4–5(c) shows the concrete tensile strength, which is directly related to the concrete material strength properties, as well as the type of structure under consideration.

#### 4.6 C-STM RESULTS AND DISCUSSION

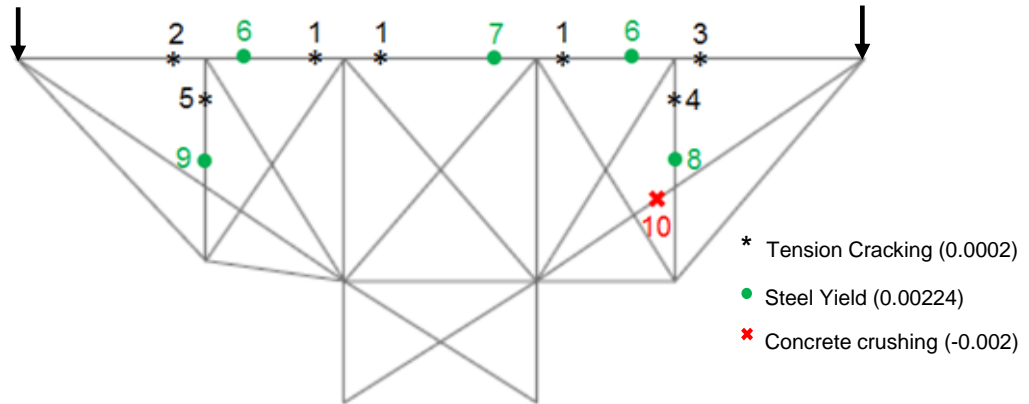
Figure 4–4(b) shows a comparison of the experimental results with the simulated analytical C-STM response for Specimen 2A. These comparisons illustrate the interaction of flexural and shear behavior that occurs in deep beams. It can be observed that the analytical results are in good agreement with the experimental results. It is also to be noted that the C-STM was able to accurately model the failure of the specimen. It was, however, observed that this failure point was dependent on the softened stress-strain model of concrete that was used for the arch elements.

The photograph showing the crack pattern of Specimen 2A is presented in Figure 4–6(a). Figure 4–6(b) shows the order of nonlinear hinge formation observed by the C-STM analysis. These points are indicated on the force-deformation curve (Figure 4–6(c)), which gives an insight into the progression of the nonlinear hinges relative to the global force-deformation behavior of the structure. Each member is comprised of steel and concrete elements. Chronological progression of nonlinear behavior for Specimen 2A is described as follows.

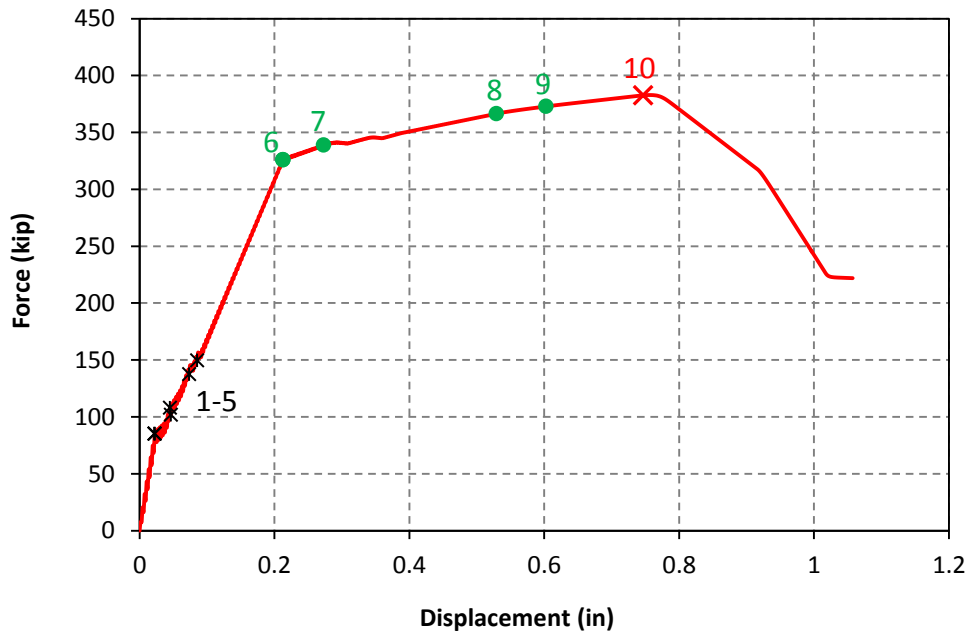
1. Concrete cracking first occurs in the longitudinal concrete element closest to the center-line when the concrete tensile strength  $f'_t$  is exceeded. This signifies the vertical flexural cracking at the column face of the beams observed in Figure 4–6(a).



(a) Experimental photo showing failure crack pattern



(b) Order of nonlinear hinge formation



(c) Force-deformation with nonlinear hinge formation events

**Figure 4-6: Failure Analysis of Specimen 2A.**

2. Concrete cracking slowly extends along the longitudinal concrete element as the applied load increases. This signifies the formation of small vertical flexural cracks observed along the beam closer to the applied load.
3. Concrete cracking of the transverse concrete element shortly follows. This signifies the propagation of shear cracking across the diagonal shear plane, where the cracks incline toward the column support. These cracks were typically observed at approximately 160 kip.
4. Steel yielding first occurs in the longitudinal steel elements closest to the center-line when the yield stress  $f_y$  is exceeded. This corresponds to the flexural moment capacity of the critical section and drastically changes the member's force-deformation response resulting in the nonlinear bilinear slope observed.
5. Steel yielding extends along the longitudinal steel elements with increased loading.
6. Steel yielding of the transverse steel elements occurs when the average stress of the stirrups exceeds the yield stress  $f_y$ . This results in large shear deformations and indicates the widening of the diagonal shear crack observed close to the ultimate load.
7. Once the transverse steel yields, the load-carrying capacity of the truss decreases. Stress flow occurs mainly through the corner-to-corner arch diagonal. This mechanism of stress flow provides additional load-carrying capacity (point 9 to 10 in [Figure 4-6\(c\)](#)) to the specimen. With further loading the peak stresses are reached in the softened diagonal arch member.
8. It was observed that after the arch diagonal on the beam side of the specimen reached its peak softened stress, the strains in the arch diagonal on the cantilever portion of the beam increased. The specimen finally failed when the strains in this member started dropping, leading to the final collapse of the specimen, which is in agreement with the photograph of the specimen shown in [Figure 4-6\(a\)](#).

#### 4.7 CONCLUDING REMARKS ON WORKED EXAMPLE 1

A summary of the results from the three stages of analysis is presented in [Table 4–6](#).

**Table 4–6: Result for Specimen 2A.**

Stage		Capacity (kip)	Factored Capacity (kip)	Comments
Stage 1: Beam Theory	$P_y^b$	316	---	Externally applied load based on yield flexural resistance of the beam.
	$P_n^f$	368	331	Externally applied load based on nominal flexural capacity of the beam.
	$V_n^s$	341	290	Beam shear capacity.
Stage 2: SAT	$P_n^{SAT}$	368	N/A	Externally applied load based on critical CCC node.
	$P_y^{SAT}$	306	214	Externally applied load based on yield of longitudinal steel in beam.
Stage 3: C-STM	$P_{C-STM}$	<b>383</b>	268	Externally applied load based on C-STM analysis.
Experiment	$P_{Failure}^{Expt}$	404	---	Maximum load at incipient failure.

The code-based prediction shows the difficulties associated with trying to predict the failure mechanism using present conventional strength-based analysis techniques. Hence when used alone, these strength-based approaches are unable to provide satisfactory insight into the expected behavior in order to identify the progression of failure modes along with any post-yield capacity. Interestingly, the flexural analysis methods provided the most consistent predictions of the yield force despite the common perception that plane sections no longer remain plane in disturbed regions.

It is observed that the C-STM simulates the behavior of the specimen fairly accurately and gives the entire force vs. deformation behavior of the specimen. It also overcomes the difficulties associated with trying to predict the failure mechanism using present conventional strength-based analysis techniques. Clearly, C-STM has an upper hand when compared to the code-based analysis techniques.



## 5. WORKED EXAMPLE 2

### 5.1 SCOPE

In this section a reinforced concrete bridge pier tested by the authors in order to investigate the effect of premature concrete deterioration in bridge bents currently used in practice, specifically cantilever bents and straddle bents, is selected to illustrate the procedure of analysis detailed in [Chapter 2](#). Additionally, the structure is modeled using the C-STM technique without and with the effects of ASR/DEF. All results are then compared with the experimental results.

### 5.2 THE STRUCTURE

The experimental specimen was designed as a “C” shape sub-assembly such that two large-scale bridge bent components were placed back-to-back so they could be tested as a self-reacting system. The C-Beam specimen had a constant cross-section of 3 ft deep and 2 ft wide that was symmetrical with the exception of the beam compression steel. More specifically the physical model scale factors representing the singly reinforced cantilevered bent and the doubly reinforced straddle bent were approximately 0.5 and 0.75, respectively.

[Figure 5–1](#) presents the reinforcing layout and cross-section of C-Beam Specimen. The longitudinal reinforcement consisted of 10 No. 8 bars running continuously around the outside and hooked at the end of each beam. The singly reinforced beam had two No. 8 straight compression bars for construction purposes. The doubly reinforced beam had symmetrical compression and tension reinforcement.

The longitudinal beam distribution steel (distributed along the beam web) consisted of three sets of No. 4 straight bars equally spaced. Transverse beam reinforcement consisted of closed stirrups with a center-to-center spacing of 4.5 inches starting at the column face. The longitudinal column distribution steel consisted of five sets of No. 8 bars equally spaced. Transverse column reinforcement had overlapping No. 4 stirrups spaced 4.5 inches centers. The beam-column joint was reinforced with four No. 4 U-bars at 8 inch centers continuing from the transverse beam reinforcement.

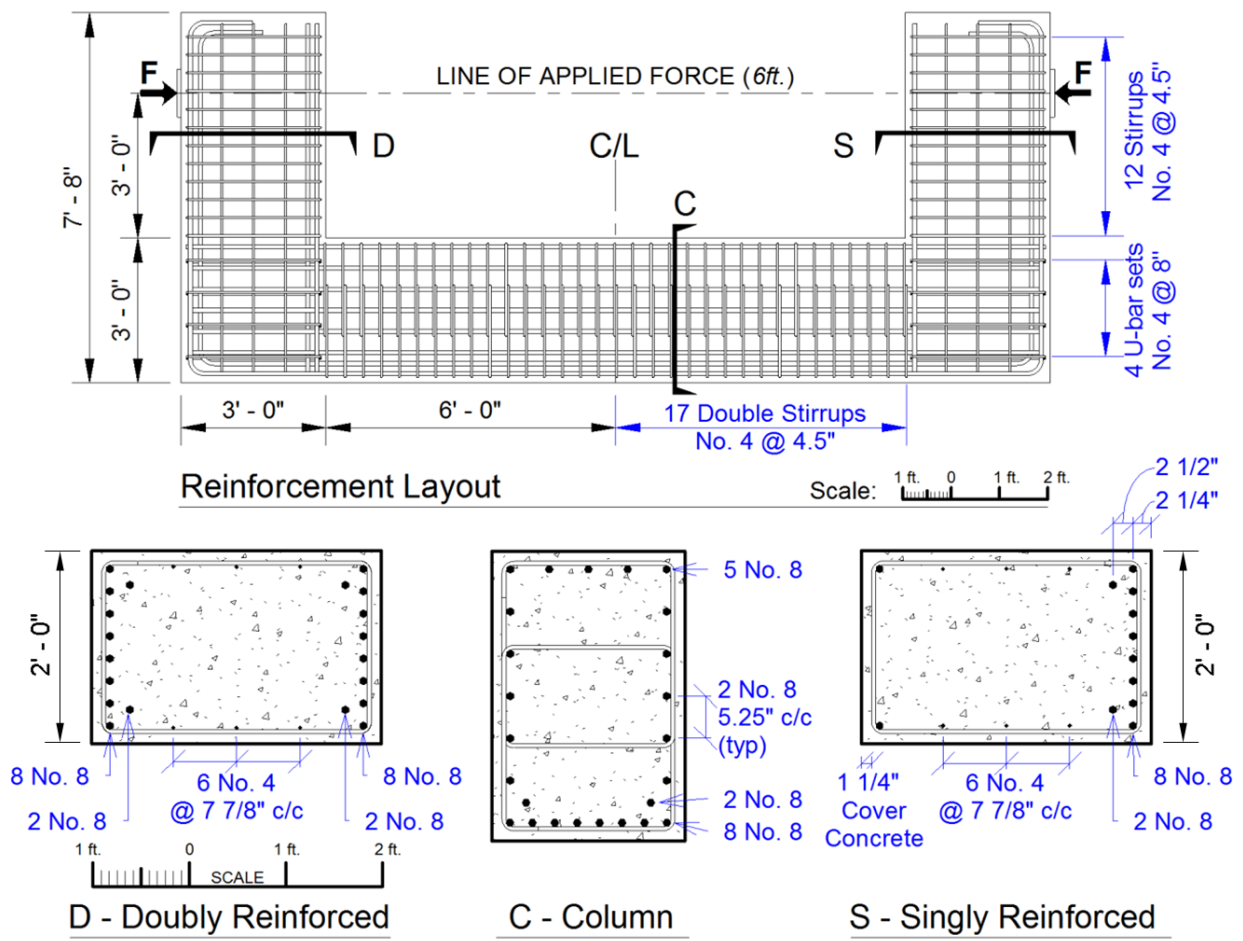


**Figure 5-1: Elevation and Cross-Section of the C-Beam Specimens.**



Table 5–1 presents the reported material strength data on the test day and experimental test results. Specimen 1 is the control specimen and does not have any ASR/DEF induced damage, whereas Specimen 4 showed *moderate* amount of damage due to ASR/DEF effects. The experimental setup, procedure, and general observations from the test can be found in Scott (2010).

**Table 5–1: Material Properties and Test Results.**

		<b>Specimen 1</b>	<b>Specimen 4</b>
<b>Material properties</b>	$f'_c$ (ksi)	5.40	4.00
	$f'_t$ (ksi)	0.30	0.23
	$E_c$ (ksi)	4190	3605
	n*	6.92	8.04
<b>Experimental results</b>	$P_{Yield}^{Expt}$ (kip)	440	440
	$P_{Failure}^{Expt}$ (kip)	474	503
	$\Delta_{Yield}^{Expt}$ (in)	1.49	1.1
	$\Delta_{Failure}^{Expt}$ (in)	1.69	2.17
	$\mu$	1.13	1.97

\*Modular ratio = Young's modulus of steel to concrete, where  
 $E_s = 29000ksi = 200GPa$

### 5.3 STAGE 1: STRENGTH ANALYSIS USING BEAM THEORY

The code-based design approaches that were described in detail in Chapter 2 are used to predict the response of C-Beam Specimens 1 and 4. Results from the application of each of these approaches are presented as follows. Computations are presented in Appendix A.

**Step 1:** Determine first yield flexural capacity,  $M_y^b$ .

The yield moment and the external load causing first yield are calculated using Eqs. (2–1) and (2–3), respectively. The parameters required by the analysis of both Specimen 1 and 4 are presented in Table 5–2. For Specimen 1 the analysis resulted in a yield moment of  $M_y^b = 1290$  kip-ft and a yield force of  $P_y^b = 430$  kip for the doubly reinforced beam.

**Table 5–2: Results of Stage 1 Flexure Analysis (Without Deterioration).**

	Specimen 1		Specimen 4		
	Doubly reinforced	Singly Reinforced	Doubly reinforced	Singly Reinforced	
$k$	0.271	0.299	0.285	0.317	<i>Eq. (2–2)</i>
$C_c(kip)$	-377	-480	-366	-474	
$C_s(kip)$	-132	-34	-144	-37	
$T(kip)$	511	511	511	511	
$M_y^b(kip.ft)$	1290	1276	1285	1269	<i>Eq. (2–1)</i>
$P_y^b(kip)$	<b>430</b>	<b>425</b>	<b>428</b>	<b>423</b>	<i>Eq. (2–3)</i>
$\beta_1$	0.78	0.78	0.85	0.85	<i>Eq. (2–5)</i>
$M_n^f(kip.ft)$	1442	1416	1428	1383	<i>Eq. (2–4)</i>
$P_n^f(kip)$	<b>481</b>	<b>472</b>	<b>476</b>	<b>461</b>	<i>Eq. (2–6)</i>

**Steps 2:** Determine nominal flexural moment,  $M_n^f$ .

The nominal flexural moment ( $M_n^f$ ) was calculated based on [Eq. \(2–4\)](#). The flexural capacity,  $M_n^f = 1442$  kip-ft for the doubly reinforced beam of Specimen 1.

**Step 3:** Determine externally applied load based on beam flexure,  $P_n^f$ .

Based on the nominal flexural moment ( $M_n^f$ ), and knowing that the shear span to the face of the column  $L_b = 36$  inches, the external load causing beam flexure on the bent cap is found to be  $P_n^f = 481$  kip for the doubly reinforced beam of Specimen 1. The results for both Specimen 1 and 4 are presented in [Table 5–2](#).

**Step 4:** Determine beam shear capacity,  $V_n^s$ .

The shear capacity ( $V_n^s$ ) is calculated from [Eq. \(2–7\)](#). Since there are no prestressing tendons, the component of shear carried by tendons  $V_p = 0$ . The parameters  $\beta$  and  $\theta$  are calculated based on

Method 1. For the doubly reinforced side of Specimen 1 the shear capacity for the beam was found to be  $V_n^s = 281$  kip and for the joint was found to be  $V_n^j = 532$  kip. The results of this analysis for both Specimen 1 and 4 are presented in [Table 5–3](#).

**Table 5–3: Results of Stage 1 Shear Analysis.**

	Specimen 1		Specimen 4		
	Singly	Doubly	Singly	Doubly	
$A_{sh}(in^2)$	0.393		0.393		
$f'_c(ksi)$	5.40		4.00		
$f_y(ksi)$	65		65		
$s^b(in)$	4.5		4.5		
$s^j(in)$	8		8		
	Singly	Doubly	Singly	Doubly	
$jd(in)$	31	30.5	31	30.5	
$V_c(kip)$	109	108	94	93	<i>Eq. (2–8)</i>
$V_s(kip)$	176	173	176	173	<i>Eq. (2–9)</i>
$V_{arch}(kip)$	437	430	376	370	<i>Eq. (2–17)</i>
$V_{truss}(kip) = \sum A_{sv}f_y$	102	102	102	102	
$V_n^s(kip)$	<b>285</b>	<b>281</b>	<b>270</b>	<b>266</b>	<i>Eq. (2–7)</i>
$V_n^j(kip)$	<b>539</b>	<b>532</b>	<b>478</b>	<b>472</b>	<i>Eq. (2–16)</i>

**Step 5:** Check strength hierarchy.

The strength reduction factor for shear and flexure are  $\phi_s = 0.90$  and  $\phi_f = 0.90$ , respectively. It is observed that for the doubly reinforced beam of Specimen 1,  $\phi_s V_n^s = 0.90 \times 281 = 253$  kip is less than  $\phi_f P_n^f = 0.90 \times 481 = 433$  kip. This result shows that the factored shear capacity for the beam is insufficient, which can lead to a shear failure in the beam.

**Step 6:** Determine the shear capacity of the beam-column joint regions.

The beam-column joint shear can be found from the shear force diagram of the equivalent beam model of the C-Beam specimen shown in [Figure 5–2](#). The joint shear was found to be  $V_{jv} = 558$  kip. The joint shear capacity of the joint is calculated based on [Eq. \(2–16\)](#) and is found to be  $V_n^j = 532$  kip. For the joint it is observed that  $\phi V_n^j = 0.90 \times 532 = 479$  kip is less than  $\phi_f V_{jv} = 0.90 \times 558 = 502$  kip.

From this analysis it can be concluded that the factored shear capacity for both the beam and the joint is insufficient. This is true for both Specimens 1 and 4, and hence warrants further investigation, and a strut-and-tie analysis is performed.

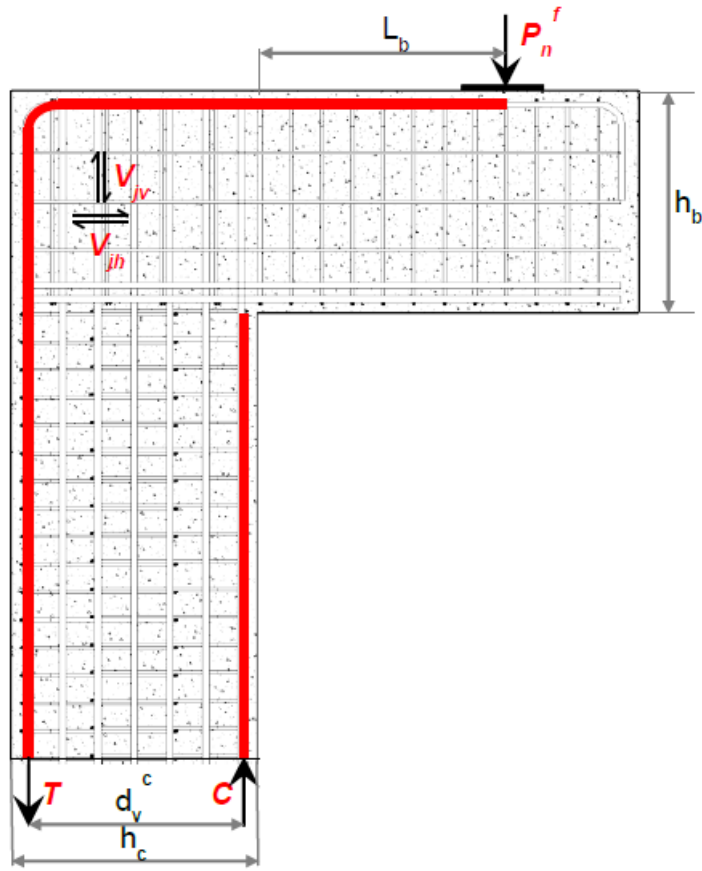
#### 5.4 STAGE 2: STRENGTH ANALYSIS USING STRUT-AND-TIE MODELING

The strut-and-tie model developed for C-Beam Specimen 1 is shown in [Figure 5–3](#). The steps involved in the construct and analysis of the strut-and-tie method are shown below.

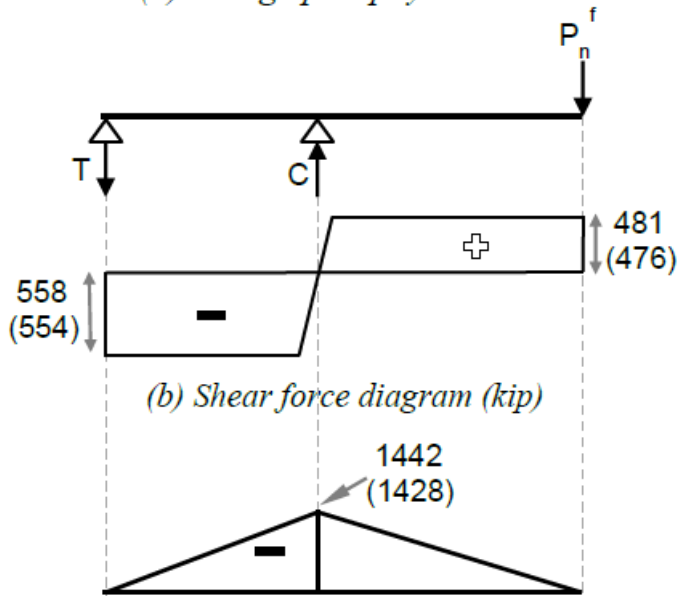
**Step 1:** Determine the truss and node geometry.

The width of the bottom face of the CCC node is equal to the depth of compression zone of the column ( $kd$ ), which is determined based on the equation for the elastic compression zone coefficient  $k$  ([Eq. \(2–2\)](#)) and was found to be equal to 9.53 inches. The bottom face of the CCC node can be proportioned based on the ratio of  $V_{jv} / P_n^f = 558 / 481 = 1.16$  (from the shear force diagram in [Figure 5–2](#)). The width of the CCT node is taken to be equal to the width of the bearing pad, which is 12 inches. The width of the CTT node is based on the bar bending radius ( $R = 4"$ ) and the radius ( $d_b / 2$ ) of the longitudinal column reinforcement.

The height of the CCC node is assumed to be equal to the depth of the back face of the CCT node (which equals two times the distance from the tension face to the centroid of the tension reinforcement). The crack angle in the beam-column joint is assumed to be  $45^\circ$ . After the node geometries are determined, all the SAT model dimensions and inclination angle can be obtained.



(a) Bridge pier physical model



(b) Shear force diagram (kip)

(c) Bending moment diagram (kip-ft) of cap beam

Figure 5–2: Shear Force and Bending Moment Diagram of the Equivalent Beam Model of C-Beam Specimen 1 (Specimen 4).

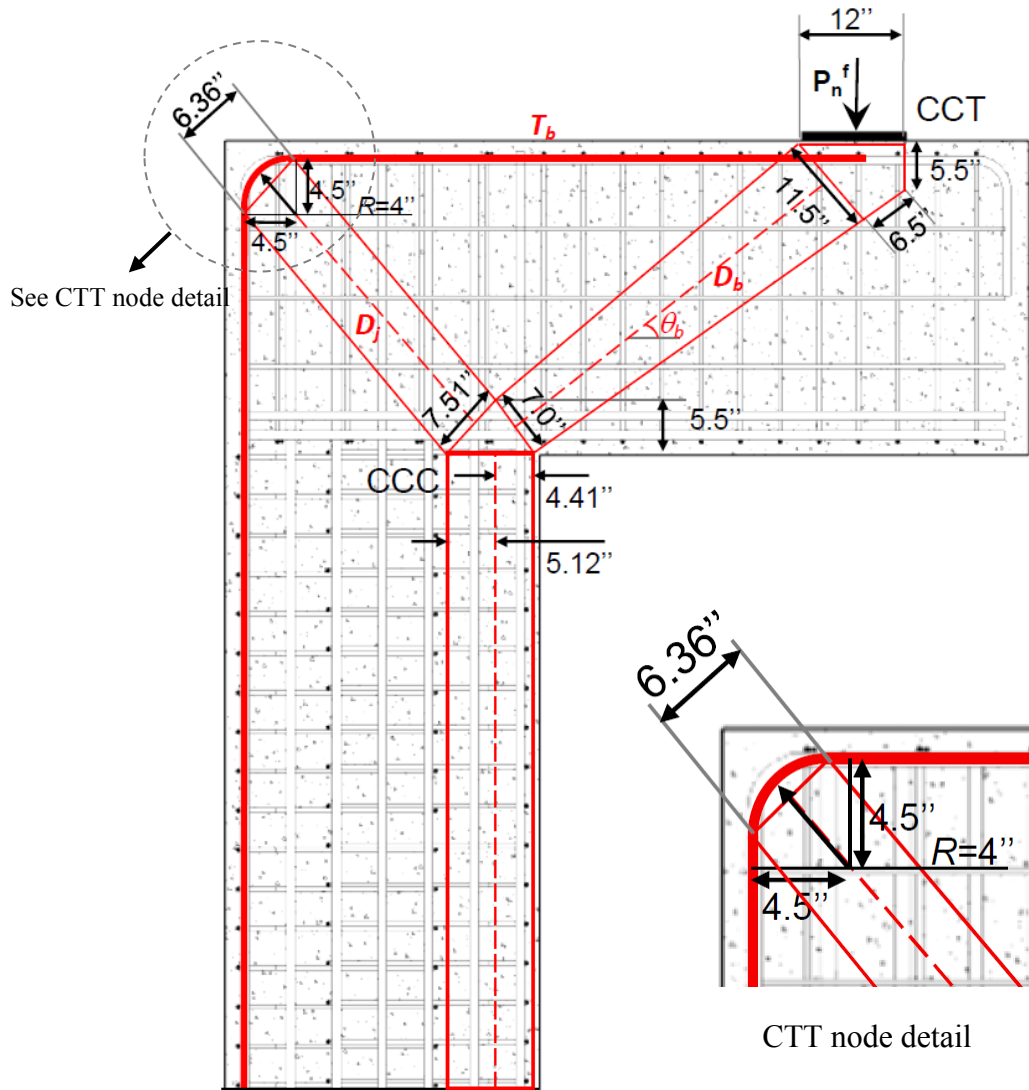


Figure 5-3: Strut-and-Tie Model for C-Beam Specimen 1.

**Step 2:** Solve the determinate truss.

All the member forces can be determined based on joint equilibrium assuming that the tension tie has yielded, that is  $T = A_s f_y$ . The externally applied load based on steel yield was found to be  $P_y^{SAT} = 429$  kip. However, this is most unlikely to be the critical load, as the critical node needs to be identified as follows.

**Step 3:** Determine critical node.

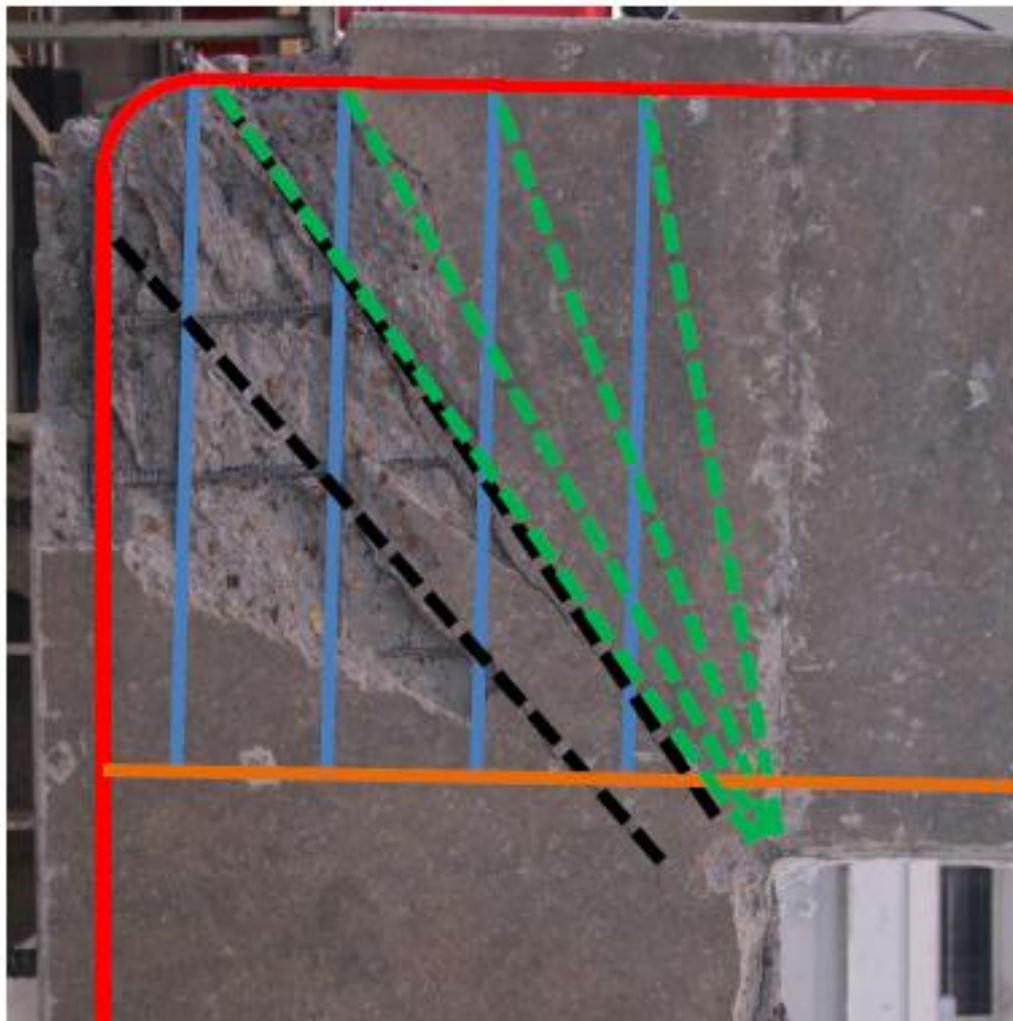
Based on the geometry of the nodes it is determined that the CTT node is the most critical node with allowable stress in this node given as  $0.65 f_c'$  (Eq. 2-19). The node strength of the CTT node is found to be  $F_{cu} = 536$  kip and 397 kip for Specimen 1 and 4, respectively.






**Step 4:** Determine external load causing node failure.

The external load causing node failure for Specimen 1 based on the node capacity of the CTT node can be back calculated and is found to be  $P_n^{SAT} = 318$  kip. It is noted that for both the specimen  $P_n^{SAT} < P_n^f$  and also the factored capacities  $\phi_v P_n^{SAT} < \phi_f P_n^f$ . Therefore, joint capacity is technically undependable. The results of the strut-and-tie analysis are summarized in Table 5-4.

Figure 5-4 shows that indeed the beam-column joint is most critical and that the CTT node is the most critical node. The joint is overlaid with the truss and the arch members as was observed from the crack pattern.

The results show that it is somewhat inconclusive as to what the failure mode for Specimen 1 will be because the joint capacity is technically undependable. It is observed that the specimen also have undependable joint capacity. Additionally, the SAT analysis does not take into account the effects of ASR/DEF damage. This justifies the use of an advanced analysis technique where the C-STM method comes in handy.



-  Tension ties
-  Beam chord
-  Transverse ties
-  Truss action
-  Arch action

**Figure 5-4: Failure Pattern Observed at the Beam-Column Joint of C-Beam Specimen 1.**



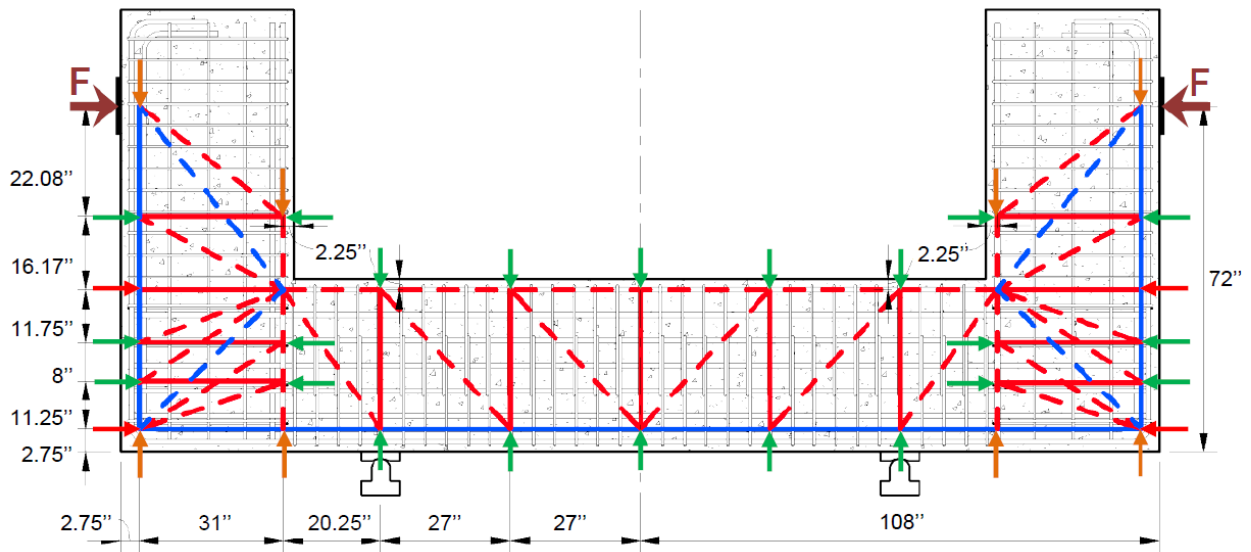
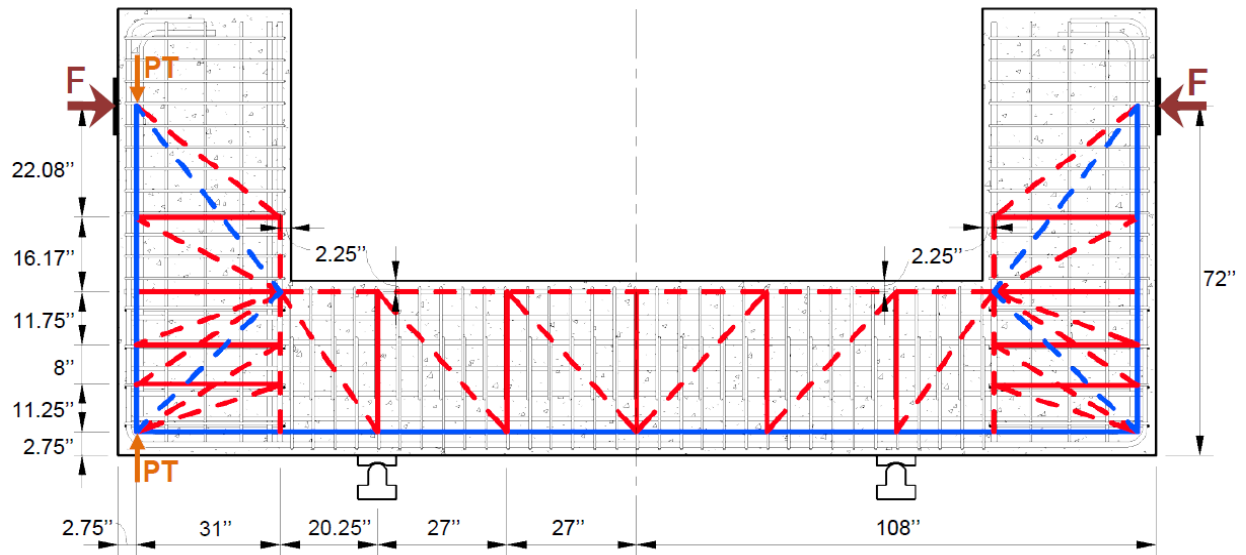
**Table 5–4: Results for Stage 2 SAT Analysis.**

	<b>Specimen 1</b>	<b>Specimen 4</b>	<b>Comments</b>
$D_b(kip)$	667	667	
$D_j(kip)$	723	723	
$\theta_b(degrees)$	40	40	
$\theta_j(degrees)$	45	45	
$P_y^{SAT}(kip)$	429	429	Based on longitudinal steel yield.
$\phi_y P_y^{SAT}(kip)$	300	300	
$P_n^{SAT}(kip)$	<b>318*</b>	<b>236*</b>	Based on node capacity.
$\phi_y P_n^{SAT}(kip)$	223	165	
$\phi_f P_n^f(kip)$	433	428	

\*Expected critical failure mode capacity.

### 5.5 STAGE 3: STRENGTH AND DEFORMATION CAPACITY USING COMPATIBILITY STRUT-AND-TIE COMPUTATIONAL MODELING

Figure 5–5 shows the C-STM model for C-Beam specimen (a) without and (b) with ASR/DEF damage. The cantilever beams were modeled using a single-point Gauss quadrature model. The joints were modeled using a two-point Gauss model (Kim and Mander, 1999) where the transverse ties were aligned with the U-bar reinforcement to provide a more exact representation of the reinforcement. The representative areas of reinforcement for the tension chord were defined as the sum of longitudinal steel and three sets of web distribution steel for tension. The compression chord was defined as the compression longitudinal steel. Rows 2 and 3 of Figure 5–6, respectively, show the different nonlinear concrete stress-strain relationships that were derived for C-Beam Specimens 1 and 4 from the material properties presented in Table 5–1.



(b) Specimen 4: With ASR/DEF damage

**Figure 5–5: Modeling the C-Beam Specimens without and with ASR/DEF Damage.**

Note the additional forces in (b) represent the prestress effect actively induced in the reinforcing steel caused by ASR/DEF induced concrete swelling.

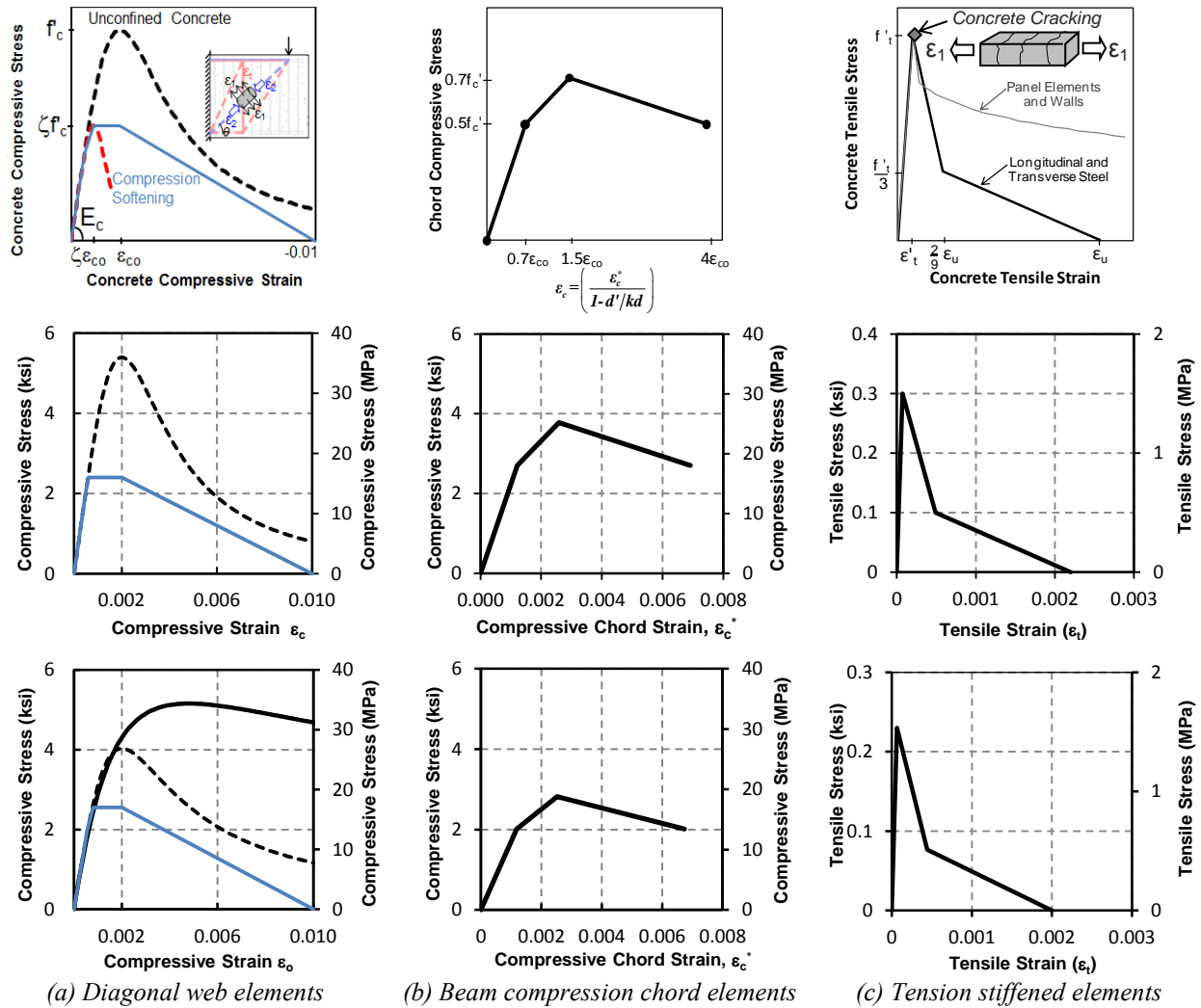


**Figure 5-6: Cracked Reinforced Concrete Material Properties.**

**Top row: Theoretical nonlinear behavior**

**Center row: Specimen 1 modeled behavior**

**Bottom row: Specimen 4 modeled behavior**

### Stage 3.1: C-STM without ASR/DEF damage

Figure 5–5(a) shows the C-STM model that was developed for C-Beam Specimen 1. Specimen 1 is the control specimen and had no ASR/DEF induced damages. To simulate the experimental test setup as accurately as possible, initial loads (shown as PT in Figure 5–5(a)) were applied to the tension chord members of the protected beam in order to replicate post-tensioning effects in accordance with Phase I and Phase II testing. Note that this model essentially represents the C-STM analysis *without* any ASR/DEF effects.

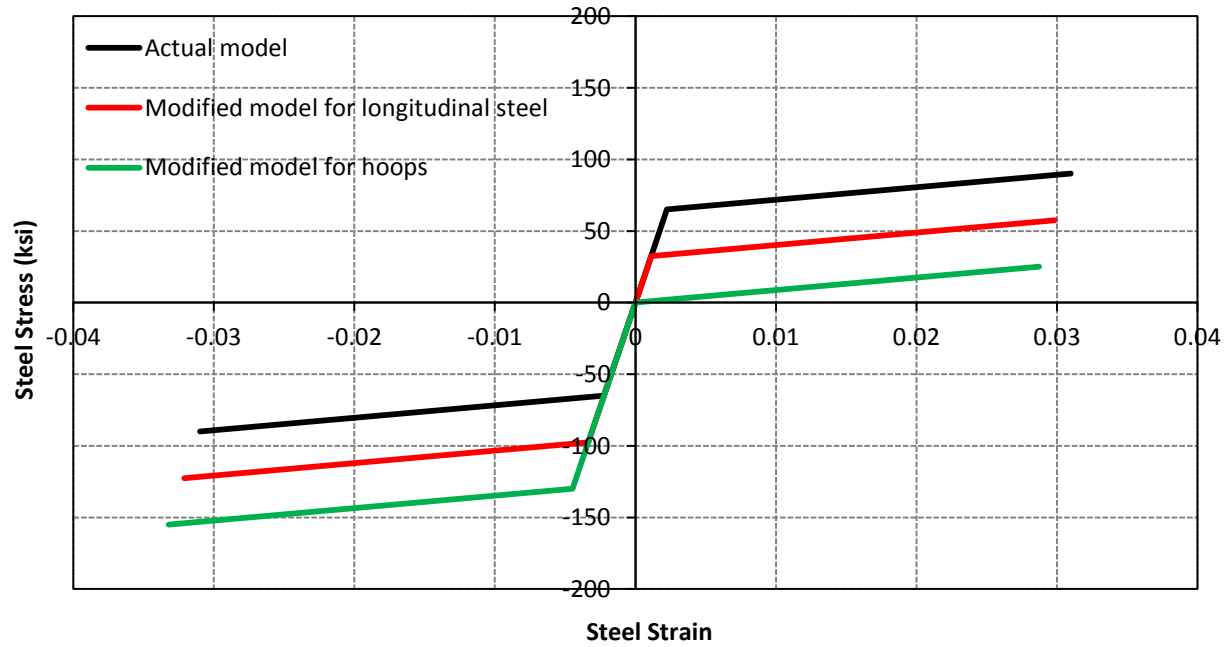
### Stage 3.2: C-STM with ASR/DEF damage

Figure 5–5(b) shows the C-STM model for C-Beam Specimen 4. *Moderate* damage due to ASR/DEF was observed in this specimen. Prestressing forces are applied on the longitudinal and transverse reinforcements in order to replicate the prestress effects that arise as a consequence of the swelling within the core concrete due to ASR/DEF effects. As per the recommendations made for *moderate* damage due to ASR/DEF effect in section 3.6.5, the strength reduction factor for cover concrete is taken as  $\lambda = 0.70$ . The confinement ratio was calculated as  $K_{cc} = 1.28$  for the beam and  $K_{cc} = 1.35$  for the column core concrete. The prestress in the longitudinal reinforcement is taken as  $0.5 f_y$  and that of the hoops is taken as  $1.0 f_y$ , as per the recommendations for moderate damage due to ASR/DEF. The modified stress-strain relation of longitudinal and transverse reinforcing steel due to prestressing effects is shown in Figure 5–7.

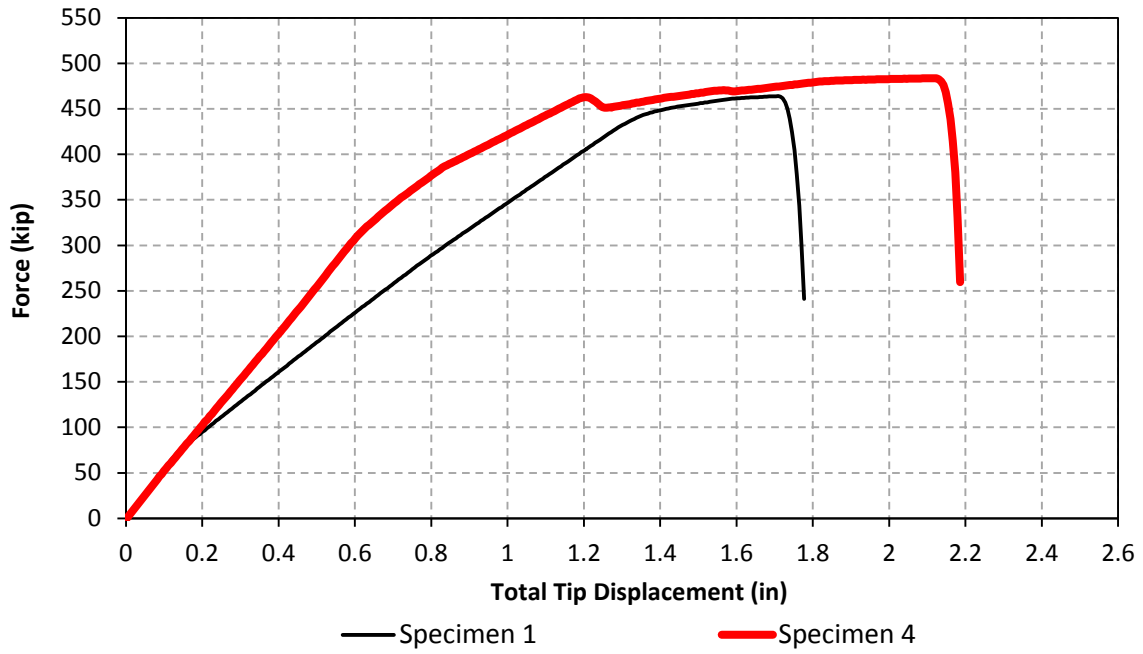
## 5.6 C-STM RESULTS AND DISCUSSION

Figure 5–8(a) shows the modeled results for the C-STM response for C-Beam Specimens 1 and 4. In Specimen 1 it is evident that there is a stiffness change at about 100 kip; this is due to first cracking in concrete. For Specimen 4, however, this apparent stiffness change is at 310 kip. This higher level of apparent “cracking” is strictly when the decompression of the prestressed sections occurs.

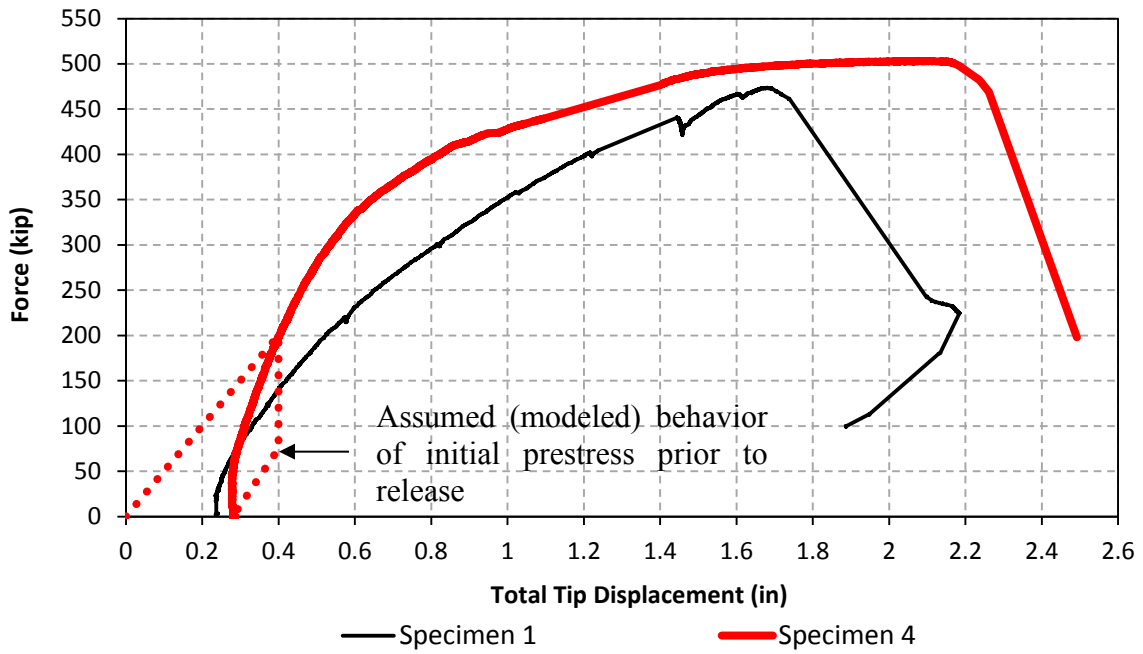
Note that after “cracking”/decompression occurs and prior to yield of the two specimens at about 450 kip, the cracked stiffness of the two specimens appears similar. These computationally modeled results with C-STM are in agreement with the experimental



**Figure 5-7: Actual and Modified Stress-Strain Models for Reinforcing Steel to Account for Prestressing Effects in C-Beam Specimen 4.**



(a) C-STM results



(b) Experimental performance

Figure 5-8: Force-Deformation Results for Specimens 1 and 4.

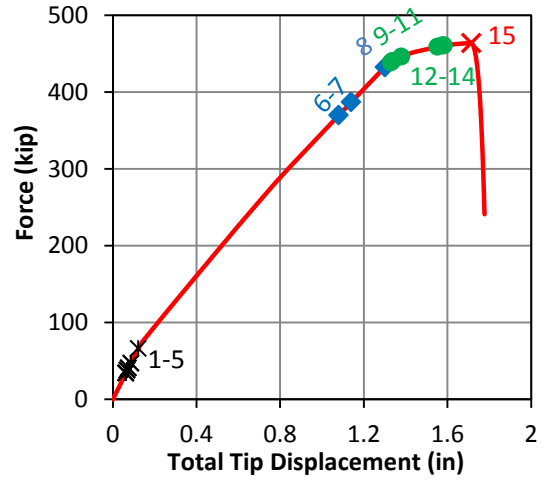
observations for the two specimens in [Figure 5–8\(b\)](#). Note that the initial prestress (field) loading in the experiments was not accurately captured, and it is for this reason the starting point of the laboratory experiment commences at a displacement of 0.25 inches.

The photograph showing the crack pattern on the strong beam of the C-Beam Specimen 1 is presented in [Figure 5–9\(a\)](#). [Figure 5–9\(b\)](#) shows the order of nonlinear hinge formation observed by the C-STM analysis. [Figure 5–9\(c\)](#) shows the force-deformation of C-Beam Specimen 1 along with the points that correspond to the formation of nonlinear hinges. The chronological progression of nonlinear behavior for C-Beam Specimen 1 is as follows ([Figure 5–9\(b\)](#)).

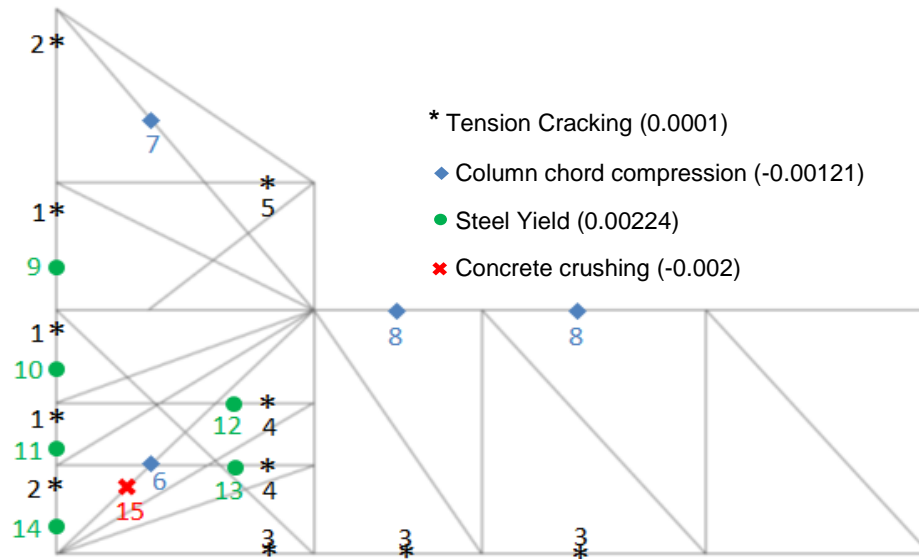
1. Longitudinal cracking first occurred in the beam. This is when the member stress exceeds the concrete tensile strength, thus initiating flexural cracking in the beam at the column face, and along the column, respectively. Tension softening refers to the concrete's ability to resist tensile strains after the development of the primary cracks.
2. Transverse cracking then occurred in the transverse concrete elements, starting in the beam column joint and then in the beam. This corresponds with diagonal shear cracking observed as a result of the flexure-shear interaction and is in agreement with experimental observations.
3. Chord compression occurred in the diagonal arch and column compression chord elements indicating that the concrete had exceeded the elastic limit of  $0.5f'_c$ .
4. Longitudinal yielding occurred in the longitudinal beam reinforcement when the stress exceeds the specified yield stress  $f_y$ .
5. Transverse steel yielding in the beam-column joint U-bars were the next member in the C-STM to respond nonlinearly.
6. With the yielding of transverse reinforcement in the beam-column joint the load-carrying capacity of the truss mechanism is limited, and the stress flow occurs through the corner-to-corner arch diagonal in the beam-column joint.



(a) Photograph of crack pattern at incipient failure near end of experiment.



(c) Force-deformation with nonlinear hinge formation events



(b) Order of nonlinear hinge formation

**Figure 5-9: Failure Analysis of C-Beam Specimen 1.**



7. The final event, which results in the collapse of the concrete bridge pier, is compression softening of the main corner-to-corner (arch) strut in the beam-column joint.

A similar mechanism is observed in C-Beam Specimen 4, which is modeled to include the effects of ASR/DEF.

## 5.7 CONCLUDING REMARKS ON WORKED EXAMPLE 2

The results of the analysis are summarized in [Table 5-5](#).

From the results presented in [Table 5-5](#) and the C-STM results presented in [Figure 5-8](#), it is observed that the flexural analysis predicts the yield force accurately. However, the sectional shear approach had the largest discrepancy and did not accurately represent the specimen capacity. These predictions are unduly harsh because the shear capacity is calculated in a D-region where the theory breaks down. It is for this reason a SAT analysis needs to be conducted. This analysis would imply that the joint would fail even before the beam yielded, thus suggesting that the structure fails in a very brittle manner. However, this is not the case as can be seen from the experimental results ([Figure 5-8](#)). The effects of ASR/DEF damage cannot be analyzed using any of these techniques.

On the other hand, the C-STM simulates the behavior of the specimen quite well and also overcomes the difficulties associated with trying to model the failure mechanism using present conventional strength-based analysis techniques used in [AASHTO LRFD \(2010\)](#) for design. The effects of ASR/DEF were modeled into the C-STM analysis technique, and the results are in good agreement with the experimental observations. Additionally, the C-STM provides the additional insight in terms of the sequence of behavior and whether the behavior is ductile or brittle.

Finally, providing the applied factored loads  $1.25D+1.75(L+I)$  are less than  $\phi P_{C-STM} = 318$  kip then the performance of the structure can be deemed *acceptable*. This is in spite of the moderate level of ASR/DEF damage observed.

**Table 5–5: Result for C-Beam Specimens 1 and 4.**

		Specimen 1		Specimen 4		
Stage		Capacity (kip)	Factored Capacity (kip)	Capacity (kip)	Factored Capacity (kip)	Comments
Stage 1: Beam Theory	$P_y^b$	430	---	428	---	External load based on yield flexural of the beam.
	$P_n^f$	481	433	476	428	External load based on nominal flexural capacity of the beam.
	$V_n^s$	281	253	266	239	Beam shear capacity.
	$V_n^j$	532	479	472	425	Joint shear capacity.
Stage 2: SAT	$P_n^{SAT}$	318	223	236	165	External load based on critical CTT node.
	$P_y^{SAT}$	429	N/A	429	N/A	External load based on yield of longitudinal steel in beam.
Stage 3: C-STM	$P_{C-STM}$	<b>454*</b>	318 <sup>+</sup>	<b>484*</b>	339	Compression failure due to diagonal splitting/compression in the beam-column joint zone. $\phi = 0.70$ (assumed).
Experiment	$P_{Failure}^{Expt}$	474	---	503	---	Maximum load at incipient failure due to failure in beam-column joint zone.

\* Bold typeface = critical case.

<sup>+</sup> Value assumed for overall structural load rating.

## 6. CLOSURE

From the analysis presented in the earlier sections, it can be seen that the strength-based analysis does not give a conclusive estimate of the ultimate strength of bridge piers. Also, none of these analysis techniques takes the effects of ASR/DEF damage into account. However, the compatibility based strut-and-tie model that was developed as a computational method of analyzing the nonlinear flexure-shear interaction of deep beams and other disturbed regions gives a good estimate of the behavior of shear critical concrete bridge piers. The computational truss modeling technique developed has the following highlights:

- i. Incorporates a method for apportioning the interaction of different truss and arch shear resisting mechanisms.
- ii. Incorporates the contribution of both flexural steel and concrete in compression chord members transformed from conventional stress block methods, which in turn defines nodal coordinates.
- iii. Incorporates a direct method of modeling the softened constitutive relations of cracked reinforced concrete struts, which does not require an iterative process to obtain convergence.
- iv. Enables to model the effects of ASR/DEF into the analysis.
- v. Accurately simulates the global force-deformation response of the structure without and with ASR/DEF damage.
- vi. Enables to “see” the nonlinear mechanism that progressively develops in the structure and precisely pinpoints the failure point and mechanism.



## REFERENCES

- AASHTO. (2002). "Standard Specifications for Highway Bridges." 17th edition, *American Association of State Highway and Transportation Officials*, Washington DC.
- AASHTO. (2010). "LRFD Bridge Design Specifications and Commentary." third edition, *American Association of State Highway and Transportation Officials*, Washington DC, 1264 pp.
- ACI Committee 318. (2011). "Building Code Requirements for Structural Concrete (ACI 318-11) and Commentary." *American Concrete Institute*, Farmington Hills, MI, 2008.
- Arnold, D.M. (2004). "Development and Experimental Testing of a Seismic Damage Avoidance Designed Beam to Column Connection Utilizing Draped Unbonded Post-tensioning." M.S. thesis, University of Canterbury, Christchurch, New Zealand.
- Bentz, E.C., Vecchio, F.J., and Collins, M.P. (2006). "Simplified Modified Compression Field Theory for Calculating Shear Strength of Reinforced Concrete Elements." *ASCE J Struct Div*, 104(4), 649-666.
- Bracci, J.M., Keating, P.B., and Hueste, M.B.D. (2000). "Cracking in RC Bent Caps." *Texas Transportation Institute*, Texas A&M University.
- Collins, M.P. (1978). "Towards a Rational Theory for RC Members in Shear." *ASCE J Struct Div*, 104(4), 649-666.
- Collins, M.P., and Mitchell, D. (1991). *Prestress Concrete Structures*. Prentice Hall, Englewood Cliffs, NJ.

- Dilger, W. (1966). "Veränderlichkeit der Biege- und Schubsteifigkeit bei Stahlbetontragwerken und ihr Einfluß auf Schnittkraftverteilung und Traglast bei statisch unbestimmter Lagerung." Deutscher Ausschuss für Stahlbeton, Heft 179, Berlin, Germany.
- Drucker, D.C. (1961). "On Structural Concrete and the Theorems of Limit Analysis." *International Association for Bridge and Structural Engineering (IABSE)*. Zürich, Abhandlungen 21.
- FIP-Commission 3. (1996). "Practical Design of Structural Concrete." SETO, distributed by fib, London, UK.
- Holden, T., Restrepo, J., and Mander, J.B. (2003). "Seismic Performance of Precast Reinforced and Prestressed Concrete Walls." *Journal of Structural Engineering*, 129(3), 286-296.
- Hsu, T.T.C. (1996). "Toward a Unified Nomenclature for Reinforced-Concrete Theory." *Journal of Structural Engineering*, 122(3), 275-283.
- Hsu, T.T.C., and Zhang, L.X. (1997). "Nonlinear Analysis of Membrane Elements by Fixed-Angle Softened-Truss Model." *ACI Structural Journal*, 94(5), 483-492.
- Hwang, S.J., Lu, W.Y., and Lee, H.J. (2000) "Shear Strength Prediction for Deep Beams." *ACI Structural Journal*, 97(3), 367-376.
- Karthik, M.M., and Mander, J.B. (2011) "Stress-Block Parameters for Unconfined and Confined Concrete Based on a Unified Stress-Strain Model." *ASCE Journal of Structural Engineering*, 137(28), 270-273.
- Kim, J.H., and Mander, J.B. (1999). *Truss Modeling of Reinforced Concrete Shear-Flexure Behavior*. Technical Report MCEER - 99-0005, University at Buffalo, NY.

- Kim, J.H., and Mander, J.B. (2000). "Cyclic Inelastic Strut-Tie Modeling of Shear-Critical Reinforced Concrete Members." *American Concrete Institute*, V. SP Vol. 193, 707-728.
- Kim, J.H., and Mander, J.B. (2007). "Influence of Transverse Reinforcement on Elastic Shear Stiffness of Cracked Concrete Elements." *Engineering Structures*, 29(8), 1798-1807.
- MacGregor, J.G. (1992). *Reinforced Concrete Mechanics and Design*. 2<sup>nd</sup> Ed., Prentice-Hall, Englewood Cliffs, NJ.
- Mander, J.B. (1983). "Seismic Design of Bridge Piers." Ph.D. Thesis, Univ. of Canterbury, New Zealand.
- Mander, J.B., Priestley, M.J.N., and Park, R. (1988). "Theoretical Stress-Strain Model for Confined Concrete." *ASCE Journal of Structural Engineering*, 114(8), 1804-1826.
- Mau, S.T., and Hsu, T.T.C. (1987). "Shear Strength Prediction for Deep Beams with Web Reinforcement." *ACI Structural Journal*, 84(6), 513-523.
- Mörsch, E. (1909). *Concrete-Steel Construction*, McGraw-Hill, NY.
- Park, R., and Paulay, T. (1975). *Reinforced Concrete Structures*. Wiley, NY.
- Paulay, T. (1971). "Coupling Beams of Reinforced Concrete Shear Walls." *Journal of the Structural Division*, ASCE, 97(ST3), 843-862.
- Petersson, P.E. (1980). "Fracture Energy of Concrete: Practical Performance and Experimental Results." *Cement and Concrete Research*, 10(1), 91-101.

- Powanusorn, S., and Bracci, J.M. (2006). "Behavior of Reinforced Concrete Members Prone to Shear Deformations: Part I - Effect of Confinement." *ACI Structural Journal*, 103(5), 736-46.
- Ritter, W. (1899). "Die Bauweise Hennebique (The Hennebique system)." *Schweizerische Bauzeitung* (Zürich).
- Rots, J.G., Nauta, P., Kusters, G.M.A., and Blaauwendraad, J. (1985). "Smearred Crack Approach and Fracture Localization in Concrete." *Heron*, 30(1), 1-48.
- Salem, H.M., and Maekawa, K. (2006). "Computer-Aided Analysis of Reinforced Concrete Using a Refined Nonlinear Strut-and-Tie Model Approach." *Journal of Advanced Concrete Technology*, 4(2), 325-336.
- SAP2000™ (1995). Advanced 14.0.0, Computer and Structures, Inc, Berkeley, CA.
- Scott, R.M. (2010). *Experimentally Validated Compatibility Strut-and-Tie Modeling of Reinforced Concrete Bridge Piers*. M.S. Thesis, Texas A&M University: College Station, TX.
- Sritharan, S., and Ingham, J.M. (2003). "Application of Strut-and-Tie Concepts to Concrete Bridge Joints in Seismic Regions." *PCI Journal*, 48(4), 66-90.
- Thürlimann, B., Marti, P., Pralong, J., Ritz, P., and Zimmerli, B. (1983). "Application of the Theory of Plasticity to Reinforced Concrete (Anwendung der plastizitätstheorie auf stahlbeton)." *Institute of Structural Engineering, ETH Zürich*.
- Vecchio, F.J. (2000). "Analysis of Shear-Critical Reinforced Concrete Beams." *ACI Structural Journal*, 97(1), 102-110.



- Vecchio, F.J., and Collins, M.P. (1986). "The Modified Compression-Field Theory for Reinforced Concrete Elements Subjected to Shear." *Journal of the American Concrete Institute*, 83(2), 219-231.
- Vecchio, F.J., and Collins, M.P. (1993). "Compression Response of Cracked Reinforced Concrete." *Journal of Structural Engineering*, 119(12), 3590-3610.
- Young, B.S., Bracci, J.M., Keating, P.B., and Hueste, M.B.D. (2002). "Cracking in Reinforced Concrete Bent Caps." *ACI Structural Journal*, 99(4), 488-498.
- Yun, Y.M. (2000). "Nonlinear Strut-Tie Model Approach for Structural Concrete." *ACI Structural Journal*, 97(4), 581-590.
- Zhu, R.R.H., Wanichakorn, W., Hsu, T.T.C., and Vogel, J. (2003). "Crack Width Prediction Using Compatibility-Aided Strut-and-Tie Model." *ACI Structural Journal*, 100(4), 413-421.



## APPENDIX A: STAGE 1–3 ANALYSIS–C-BEAM SPECIMEN

This appendix presents the analysis procedure followed for the C-Beam specimens. The computations for Stage 1 (beam theory), Stage 2 (SAT analysis), and Stage 3 (C-STM analysis) are included.

**Table C–1: Material Properties for C-Beam Specimens.**

	Specimen 1	Specimen 4
$f'_c$ (ksi) (at time of testing)	5.40	4.00
$f'_t$ (ksi)	0.30	0.23
$E_c$ (ksi)	4190	3605
$f_y$ (ksi)	65	65
$E_s$ (ksi)	29000	29000

### STAGE 1: ANALYSIS USING BEAM THEORY

Step 1: Determine first yield flexural capacity,  $M_y^b$ .

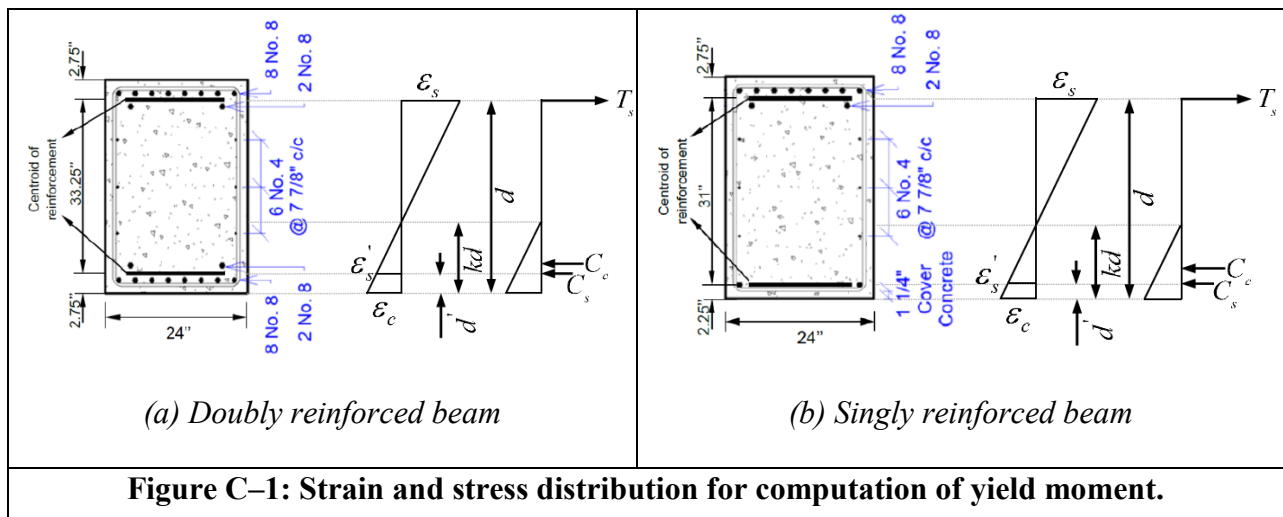


**Table C-2: Computation of First Yield Flexural Capacity and Corresponding Axial Load.**

	<b>Specimen 1</b>		<b>Specimen 4</b>	
	<i>Doubly reinforced</i>	<i>Singly reinforced</i>	<i>Doubly reinforced</i>	<i>Singly reinforced</i>
$A_s (in^2)$	7.854	7.854	7.854	7.854
$A'_s (in^2)$	7.854	1.571	7.854	1.571
$b (in)$	24	24	24	24
$d (in)$	33.25	33.25	33.25	33.25
$d' (in)$	2.75	2.25	2.75	2.25
$jd = d - d' (in)$	30.5	31	30.5	31
$\rho_L = \frac{A_s}{bd}$	0.00984	0.00984	0.00984	0.00984
$\rho'_L = \frac{A'_s}{bd}$	0.00984	0.00197	0.00984	0.00197
$n = E_s / E_c$	6.92		8.04	
$k = \sqrt{(\rho_L + \rho'_L)^2 n^2 + 2(\rho_L + \rho'_L d'/d)n} - (\rho_L + \rho'_L)n$				
$k$	0.271	0.299	0.285	0.317
$kd (in)$	9.01	9.94	9.48	10.54
$\varepsilon_c = \frac{\varepsilon_y(kd)}{d - kd}$	0.00083	0.00096	0.00089	0.00104
$\varepsilon'_s = \frac{\varepsilon_y(kd - d')}{d - kd}$	0.00058	0.00074	0.00063	0.00082
$C_c (kip) = \frac{1}{2} \varepsilon_c E_c (kd)b$	-377	-480	-366	-474
$C_s (kip) = A'_s \varepsilon'_s E_s$	-132	-34	-144	-37
$T_s (kip) = A_s f_y$	511	511	511	511
$M_y^b = T_s (d - kd / 3) + C_s (kd / 3 - d')$				
$M_y^b (kip.in)$	15474	15319	15420	15228
$P_y^b = M_y^b / L_b$ where $L_b = 36 in$				
$P_y^b (kip)$	430	425	428	423

Step 2 and Step 3: Determine nominal flexural moment,  $M_n^f$  and externally applied load based on flexure,  $P_n^f$ .

For an accurate estimate of the nominal moment, calculations were performed in a spreadsheet considering the contribution of each layer of steel. The spreadsheets are presented below for both doubly and singly reinforced beam for both the specimens.

**Table C-3: Computation of Flexural Moment and Corresponding Axial Load Demand for Doubly Reinforced Beam: Specimen 1.**

Input Parameters						Calculated Variables	
Section Properties		Reinforcement Details		Reinforcement Properties		$\alpha$	0.85
Breadth (in)	24	Reinforcement	Diameter (in)	Es (ksi)	29000	$\beta$	0.78
a (shear span) (in)	36	Longitudinal	1	fy (ksi)	65		
<b>Concrete Properties</b>		Distribution	0.5			Assume NA depth for equilibrium, c (in)	4.145
f'c (ksi)	5.4	Stirrups	0.5				
Analysis							
Layer	No. of bars	Area (in <sup>2</sup> )	Dist to layers from bottom (in)	Strain	Stress in Steel (ksi)	Force in Concrete/ Steel (kip)	Moment (kip-in)
Concrete (Bottom)	-----	-----	1.617	-0.0030	-----	-356.16	-575.75
1	8	6.28	2.250	-0.0014	-39.77	-249.91	-562.30
Steel 2	2	1.57	4.750	0.0004	12.70	19.95	94.75
Steel 3	2	0.39	10.125	0.0043	64.96	25.51	258.29
Steel 4	2	0.39	18.000	0.0100	64.96	25.51	459.18
Steel 5	2	0.39	25.875	0.0157	64.96	25.51	660.06
Steel 6	2	1.57	31.250	0.0196	64.96	102.04	3188.72
Steel 7	8	6.28	33.750	0.0214	64.96	408.16	13775.26
						$M_n^f$ (kip-ft)	<b>1441.52</b>
						$P_n^f$ (kip)	<b>480.51</b>

**Table C-4: Computation of Flexural Moment and Corresponding Axial Load Demand for Singly Reinforced Beam: Specimen 1.**

Input Parameters						Calculated Variables	
<i>Section Properties</i>		<i>Reinforcement Details</i>		<i>Reinforcement Properties</i>		$\alpha$	0.85
Breadth (in)	24	<i>Reinforcement</i>	<i>Diameter (in)</i>	Es (ksi)	29000	$\beta$	0.78
a (shear span) (in)	36	Longitudinal	1	fy (ksi)	65		
<i>Concrete Properties</i>		Distribution	0.5			Assume NA depth for equilibrium, c (in)	5.845
fc (ksi)	5.4	Stirrups	0.5				
Analysis							
<i>Layer</i>	<i>No: of bars</i>	<i>Area (in<sup>2</sup>)</i>	<i>Dist to layers from bottom (in)</i>	<i>Strain</i>	<i>Stress in Steel (ksi)</i>	<i>Force in Concrete/ Steel (kip)</i>	<i>Moment (kip-in)</i>
Concrete (Bottom)	-----	-----	2.280	-0.0030	-----	-502.23	-1144.86
1	2	1.57	2.250	-0.0018	-53.46	-83.97	-188.93
Steel 2	0	0.00	4.750	-0.0006	-16.30	0.00	0.00
Steel 3	2	0.39	10.125	0.0022	62.08	24.38	246.83
Steel 4	2	0.39	18.000	0.0062	64.96	25.51	459.18
Steel 5	2	0.39	25.875	0.0103	64.96	25.51	660.06
Steel 6	2	1.57	31.250	0.0130	64.96	102.04	3188.72
Steel 7	8	6.28	33.750	0.0143	64.96	408.16	13775.26
						$M_n^f$ (kip-ft)	<b>1416.36</b>
						$P_n^f$ (kip)	<b>472.12</b>

**Table C-5: Computation of Flexural Moment and Corresponding Axial Load Demand for Doubly Reinforced Beam: Specimen 4.**

Input Parameters						Calculated Variables	
<i>Section Properties</i>		<i>Reinforcement Details</i>		<i>Reinforcement Properties</i>		$\alpha$	0.85
Breadth (in)	24	Reinforcement	Diameter (in)	Es (ksi)	29000	$\beta$	0.85
a (shear span) (in)	36	Longitudinal	1	fy (ksi)	65		
<i>Concrete Properties</i>		Distribution	0.5			Assume NA depth for equilibrium, c (in)	4.555
f <sub>c</sub> (ksi)	4	Stirrups	0.5				
Analysis							
<i>Layer</i>	<i>No: of bars</i>	<i>Area (in<sup>2</sup>)</i>	<i>Dist to layers from bottom (in)</i>	<i>Strain</i>	<i>Stress in Steel (ksi)</i>	<i>Force in Concrete/ Steel (kip)</i>	<i>Moment (kip-in)</i>
Concrete	-----	-----	1.936	-0.0030	-----	-315.93	-611.61
(Bottom) 1	8	6.28	2.250	-0.0015	-44.02	-276.61	-622.38
Steel 2	2	1.57	4.750	0.0001	3.72	5.85	27.79
Steel 3	2	0.39	10.125	0.0037	64.96	25.51	258.29
Steel 4	2	0.39	18.000	0.0089	64.96	25.51	459.18
Steel 5	2	0.39	25.875	0.0140	64.96	25.51	660.06
Steel 6	2	1.57	31.250	0.0176	64.96	102.04	3188.72
Steel 7	8	6.28	33.750	0.0192	64.96	408.16	13775.26
						<b><math>M_n^f</math> (kip-ft)</b>	<b>1427.94</b>
						<b><math>P_n^f</math> (kip)</b>	<b>475.98</b>

**Table C-6: Computation of Flexural Moment and Corresponding Axial Load Demand for Singly Reinforced Beam: Specimen 4.**

Input Parameters						Calculated Variables	
<i>Section Properties</i>		<i>Reinforcement Details</i>		<i>Reinforcement Properties</i>		$\alpha$	0.85
Breadth (in)	24	Reinforcement	Diameter (in)	Es (ksi)	29000	$\beta$	0.85
a (shear span) (in)	36	Longitudinal	1	fy (ksi)	65		
<i>Concrete Properties</i>		Distribution	0.5			Assume NA depth for equilibrium, c (in)	6.985
f <sub>c</sub> (ksi)	4	Stirrups	0.5				
Analysis							
<i>Layer</i>	<i>No: of bars</i>	<i>Area (in<sup>2</sup>)</i>	<i>Dist to layers from bottom (in)</i>	<i>Strain</i>	<i>Stress in Steel (ksi)</i>	<i>Force in Concrete/ Steel (kip)</i>	<i>Moment (kip-in)</i>
Concrete	-----	-----	2.969	-0.0030	-----	-484.48	-1438.24
(Bottom) 1	2	1.57	2.250	-0.0020	-58.58	-92.01	-207.03
Steel 2	0	0.00	4.750	-0.0010	-27.84	0.00	0.00
Steel 3	2	0.39	10.125	0.0013	39.11	15.36	155.50
Steel 4	2	0.39	18.000	0.0047	64.96	25.51	459.18
Steel 5	2	0.39	25.875	0.0081	64.96	25.51	660.06
Steel 6	2	1.57	31.250	0.0104	64.96	102.04	3188.72
Steel 7	8	6.28	33.750	0.0115	64.96	408.16	13775.26
						$M_n^f$ (kip-ft)	<b>1382.79</b>
						$P_n^f$ (kip)	<b>460.93</b>



Step 4: Determine beam shear capacity,  $V_n^s$ .

**Table C-7: Computation of Beam Shear Capacity.**

	Specimen 1		Specimen 4	
	<i>Doubly</i>	<i>Singly</i>	<i>Doubly</i>	<i>Singly</i>
$f'_c$ (ksi) (at time of testing)	5.40		4.00	
$f_y$ (ksi)	65		65	
$b_v$ (in)	24		24	
$A_v$ (in <sup>2</sup> )	0.393		0.393	
$s$ (in)	4.5		4.5	
$\beta$ (per AASHTO Method 1)	2		2	
$\theta$ (degrees) (per AASHTO Method 1)	45		45	
	<i>Doubly</i>	<i>Singly</i>	<i>Doubly</i>	<i>Singly</i>
$d_v = jd$ (in)	30.5	31	30.5	31
$V_c = 0.0316 \beta \sqrt{f'_c} b_v d_v$ (kip)	108	109	93	94
$V_s = A_v f_y \frac{d_v}{s} \cot \theta$ (kip)	173	176	173	176
$V_n^s = V_c + V_s$ (kip)	281	285	266	270

Step 5: Check strength hierarchy.

**Table C-8: Checking Strength Hierarchy.**

	Specimen 1		Specimen 4	
	<i>Doubly</i>	<i>Singly</i>	<i>Doubly</i>	<i>Singly</i>
$\phi_v$	0.90 (AASHTO 5.5.4.2)			
$V_n^s$ (kip)	281	285	266	270
$\phi_f$	0.90 (AASHTO 5.5.4.2)			
$P_n^f$ (kip)	481	472	476	461
$\phi V_n^s$ (kip)	253	256	239	243
$\phi_f P_n^f$ (kip)	433	425	428	415

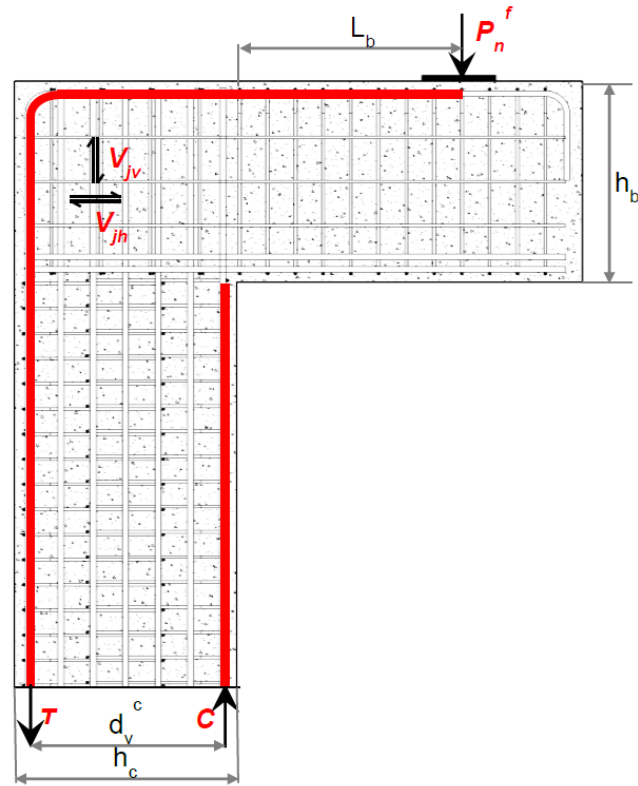
In all of the above cases  $\phi_v V_n^s < \phi_f P_n^f$ , which implies that the dependable shear capacity may be insufficient leading to a shear failure of the bridge pier.

*Step 6: Determine the shear capacity of the beam-column joint region.*

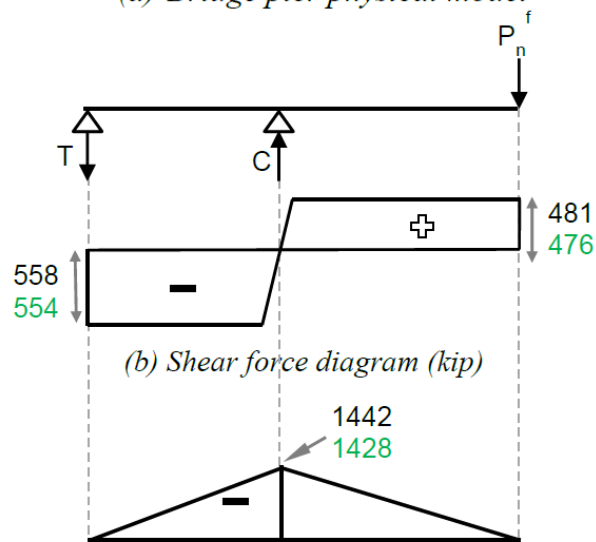
The vertical shear in the joint ( $V_{jv}$ ) caused by the axial load based on flexure can be determined from the shear force diagram of the equivalent beam model of the bridge pier shown in [Figure C-2](#). The horizontal shear  $V_{jh}$  can be computed from  $V_{jv}$ .

**Table C-9: Computing the Vertical and Horizontal Shear in the Beam-Column Joint Caused by Flexural Axial Load Demand.**

	Specimen 1		Specimen 4	
	<i>Doubly</i>	<i>Singly</i>	<i>Doubly</i>	<i>Singly</i>
$P_n^f$ (kip)	481	472	476	461
$V_{jv}$ (kip)	558	548	554	535
$h_c = h_b$ (in)	36		36	
$V_{jh} = \frac{h_c}{h_b} V_{jv}$ (kip)	558	548	554	535



(a) Bridge pier physical model



(c) Bending moment diagram (kip-ft) of cap beam

**Figure C-2: Approach to determine shear in the beam-column joint for Specimen 1 and Specimen 4.**

The computation for assessing the joint shear capacity is as follows:

**Table C-10: Assessing the Joint Shear Capacity.**

	Specimen 1		Specimen 4	
$\sum A_{sv} \text{ (in}^2\text{)}$ (total area of hoops/ties in the joint region)	1.571		1.571	
$f_y \text{ (ksi)}$	65		65	
$f'_c \text{ (ksi)}$	5.4		4.0	
$b_v \text{ (in)}$	24		24	
	<i>Doubly</i>	<i>Singly</i>	<i>Doubly</i>	<i>Singly</i>
$jd \text{ (in)}$	30.5	31	30.5	31
$V_{truss} \text{ (kip)}$	102	102	102	102
$V_{arch} \text{ (kip)}$	430	437	370	376
$V_n^j \text{ (kip)} = V_{arch} + V_{truss}$	532	539	472	478
$\phi_v$	0.90			
$\phi_v V_n^j \text{ (kip)}$	479	485	425	430
$\phi_f$	0.90			
$\phi_f V_{jv} \text{ (kip)}$	502	493	498	481

In the above cases  $\phi_v V_n^j < \phi_f V_{jv}$ , which implies that the joint capacity is less than the demand, and hence there could be a shear joint failure.

From the above analysis it is determined that the beam and the beam-column joint are shear critical. Therefore a strut-and-tie analysis is performed. It is also required by the code to perform a SAT as the  $a/d$  ratio for the specimen is 1.08.

## STAGE 2: STRUT-AND-TIE ANALYSIS

*Step 1: Determine the node geometry.*

The computation of the node dimensions and geometry for the two specimens follows.

*CCT node:*

- The width of the CCT node is taken equal to the width of the bearing pad = 12".
- The depth of the back face of the CCT node =  $2 \times$  distance from the extreme tension face to the centroid of the tension reinforcement =  $2 \times 2.75 = 5.5"$ .

*CTT Node:*

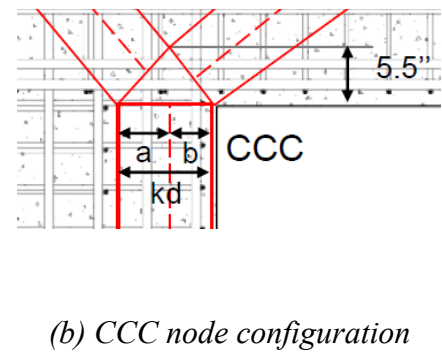
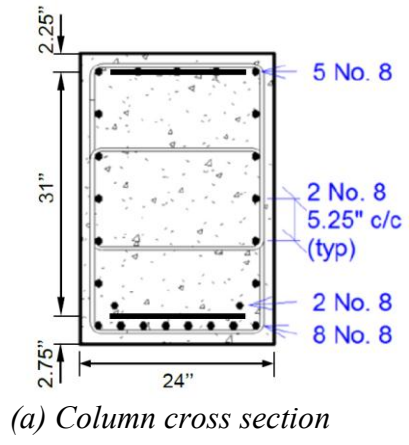
- Width of the CTT node =  $\sqrt{2 \times (R + d_b / 2)^2}$  where  $R$  = bar bending radius = 4" and  $d_b$  = diameter of the column longitudinal rebar = 1".

*CCC Node:*

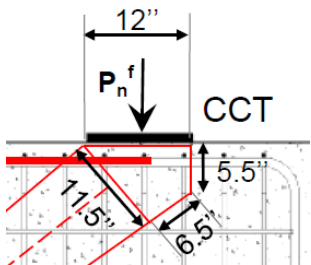
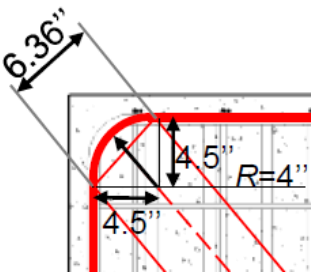
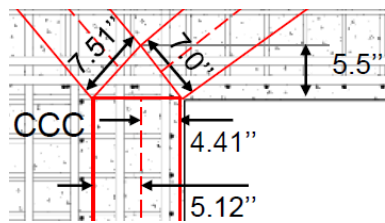
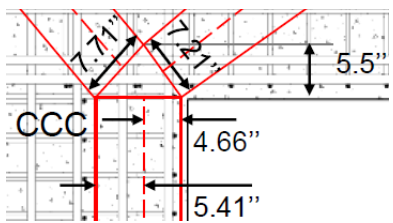
- The width of the bottom face of the CCC node is equal to the depth of compression zone of the column ( $kd$ ), which is determined based on the equation for the elastic compression zone coefficient  $k$ .
- The bottom face is proportioned based on the ratio of  $a/b = V_{jv} / P_n^f$  (Figure in [Table C-11](#)) obtained from Stage 1 of the analysis.
- Since the horizontal force in the CCC node is equal to the horizontal force in the CCT node, the height of the CCC node is assumed to be equal to the depth of the back face of the CCT node =  $2 \times 2.75 = 5.5"$ .
- Knowing the above, the other sides of the CCC node can be determined.

**Table C-11: Computations for Sizing the CCC Node.**

	<b>Specimen 1</b>	<b>Specimen 4</b>
$A_s$ (in <sup>2</sup> )	7.854	
$A'_s$ (in <sup>2</sup> )	3.927	
$b$ (in)	24	
$d$ (in)	33.25	
$d'$ (in)	2.25	
$\rho_L = \frac{A_s}{bd}$	0.00984	0.00984
$\rho'_L = \frac{A'_s}{bd}$	0.00492	
$n = E_s / E_c$	6.92	8.04
$k = \sqrt{(\rho_L + \rho'_L)^2 n^2 + 2(\rho_L + \rho'_L d'/d)n} - (\rho_L + \rho'_L)n$		
$k$	0.287	0.303
$kd$ (in)	9.5	10.1
$V_{jv}$ (kip)	558	554
$P_n^f$ (kip)	481	476
$V_{jv} / P_n^f$	1.16	1.16
$a$ (in)	5.12	5.41
$b$ (in)	4.41	4.66



**Table C-12: Geometry and Dimensions of Nodes.**

<p style="writing-mode: vertical-rl; transform: rotate(180deg);"><b>CCT Node</b></p>		
<p style="writing-mode: vertical-rl; transform: rotate(180deg);"><b>CCT Node</b></p>		
<p style="writing-mode: vertical-rl; transform: rotate(180deg);"><b>CCC Node</b></p>	<p style="text-align: center;"><b>Specimen 1</b></p> 	<p style="text-align: center;"><b>Specimen 4</b></p> 

Step 2: Solve the determinate truss-determine strut and tie forces

**Table C-13: Forces in the Struts and Ties of the SAT Model.**

CCT Node	<b>Node forces based on steel yield</b>		
	$A_s$ ( $in^2$ )	7.854	
	$f_y$ ( $ksi$ )	65	
	$\theta_b$ ( $degrees$ )	40	
	$\theta_j$ ( $degrees$ )	45	
	$T = A_s f_y$ ( $kip$ )	511	
	$D_b = T / \cos(\theta_b)$ ( $kip$ )	667	
$P^{SAT} = D_b \sin(\theta_b)$ ( $kip$ ) = $P_y^{SAT}$	429		
CCC Node	$C' = D_b \cos(\theta_b)$ ( $kip$ )	511	
	$D_j = C' / \cos(\theta_j)$ ( $kip$ )	723	
	$P_v^j = D_j \sin(\theta_j)$ ( $kip$ )	511	

Step 3 and Step 4: Determine minimum externally applied load causing node failure and determine shear demand.

Allowable stresses in the nodes based on [AASHTO \(2010\)](#) are presented in [Table C-14](#). From the allowable node stresses, the CCT node is found to be the critical node. The axial load required to cause the failure of the CCT node can be back calculated based on the allowable nodal stress and the area of the node. The results are presented in [Table C-14](#).



**Table C–14: Allowable Node Stresses and Axial Load Required to Cause CTT Node Failure.**

	<b>Specimen 1</b>	<b>Specimen 4</b>
$f'_c$ (ksi)	5.40	4.00
<b>Allowable Stresses</b>		
CCC Node $f_{cu} = 0.85f'_c$	4.60	3.40
CCT Node $f_{cu} = 0.75f'_c$	4.05	3.00
CTT Node $f_{cu} = 0.65f'_c$	3.51	2.60
Node capacity $D_{j(node)} \text{ (kip)} = F_{cu}$	536	397
Axial load that causes nodal failure, $P_n^{SAT} \text{ (kip)} = P_y^{SAT} D_{j(node)} / D_j$	318	236

For both the specimens it is evident that  $P_n^{SAT}$  computed from the SAT analysis is lesser than  $P_n^f$  calculated from the beam flexure theory. Also,  $\phi_v P_n^{SAT} < \phi_f P_n^f$  for both the specimens. However from the experimental results, it was observed that the load at failure for Specimen 1 and 4 was  $P_{Failure}^{Expt} = 474$  kip and 503 kip, respectively. It is apparent from Stage 1 and Stage 2 of the analysis that they do not give a good prediction of the load carrying capacity of the specimens. Therefore, a C-STM analysis is performed to evaluate the performance of the structure.

**STAGE 3: ANALYSIS USING COMPATIBILITY STRUT-AND-TIE METHOD**

The computation of member and material properties of the C-STM model are presented below for Specimen 1 (control specimen) followed by Specimen 4 (with ASR/DEF damage).

**Computation for C-Beam Specimen 1**

A few of the section properties have to be determined beforehand to set up the C-STM geometry. These computations follow.

*Step 1: Calculate section properties.*

**Table C-15: Computation of Section Properties for C-STM.**

	Doubly Reinforced	Column	Singly Reinforced
<b>CROSS-SECTION</b>			
Compression Chord	8-#8 Bars	5-#8 Bars	2-#8 Bars
$h$ (in)	36	36	36
$d'$ (in)	2.25	2.25	2.25
$d$ (in)	33.25	33.25	33.25
$A_s'$ (in <sup>2</sup> )	6.28	3.93	1.57
Steel contributing to tension chord	10-#8 Bars 2 sets of 2-#4	10-#8 Bars 2 sets of 2-#4	10-#8 Bars 2 sets of 2-#8
$A_{s(total)}$ (in <sup>2</sup> )	8.64	11.00	8.64
$\bar{y}$ (in) (centroid of $A_{s(total)}$ )	3.78	4.86	3.78
$A_s$ (in <sup>2</sup> ) = $A_{s(total)} \frac{h - d' - \bar{y}}{d - d'}$	8.35	10.25	8.35
$jd = d - d'$ (in)	31.0	31.0	31.0

Determine the depth of compression zone ( $kd$ ) of the singly and doubly reinforced beams and column using the equation:

$$k = \sqrt{\left(\rho_L + \rho'_L + \left(\frac{P}{f_c'bd}\right)\left(\frac{f_c'}{f_s}\right)\right)^2 n^2 + 2\left(\rho_L + \rho'_L\left(\frac{d'}{d}\right) + \left(\frac{P}{f_c'bd}\right)\left(\frac{f_c'}{f_s}\right)\right)n - \left(\rho_L + \rho'_L + \left(\frac{P}{f_c'bd}\right)\left(\frac{f_c'}{f_s}\right)\right)n}$$

For the beams the axial load  $P$  is zero.

**Table C–16: Determining the Depth of the Compression Zone for Specimen 1.**

$f_c' = 5.4$ ksi	Compression Steel			Tension Steel				Axial Load	Elastic Depth	
	$A_s'$ (in <sup>2</sup> )	$d'$ (in)	$\rho'$	$A_s$ (in <sup>2</sup> )	$d$ (in)	$b$ (in)	$\rho$	$P$ (kip)	$k$	$kd$ (in)
Single Beam	1.57	2.25	0.00197	8.35	33.25	24	0.01046	-	0.307	10.19
Double Beam	6.28	2.25	0.00787	8.35	33.25	24	0.01046	-	0.283	9.42
Column	3.92	2.25	0.00492	10.25	33.25	24	0.01284	430	0.394	13.10

*Step 2: Determine C-STM geometry based on Step 1.*

The tension ties (AK and K1K2 in [Figure C–3](#)) and compression chords (BH and L1L2 in [Figure C–3](#)) in the beams and the column are placed along the centroids of the tension and compression steel determined in [Table C–15](#). The C-STM geometry is the same in both the singly and double reinforced beams. The overhang portion of the specimen is modeled using the single-point Gauss truss model as presented in [Chapter 3](#). The position of tie CB is determined based on the coefficients for the single point Gauss model. In the beam-column joint region, the ties GF and IH are placed along the position of the U-Bars to better represent the specimen. All the dimensions of the C-STM are shown in [Figure C–3](#).

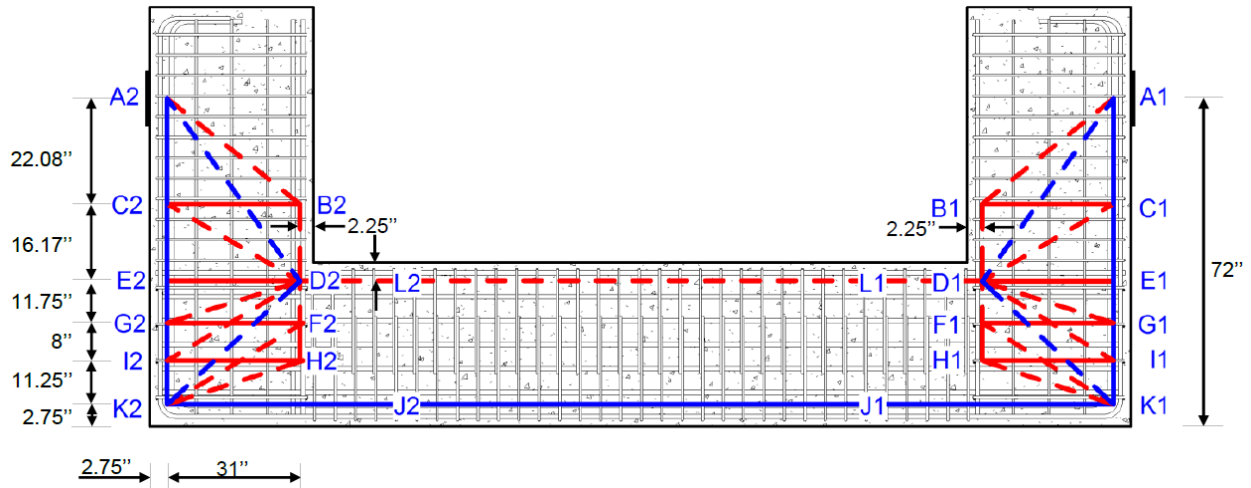


**Figure C-3: C-STM Model for C-Beam Specimen 1.**

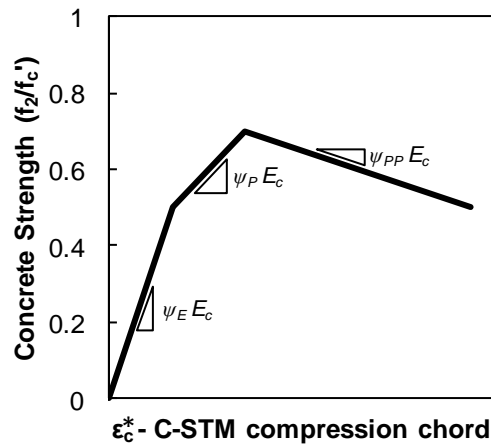
*Step 3: Determine axial rigidities.*

The next step in the C-STM analysis is to determine the axial rigidities of each of the members constituting the C-STM model.

To model the combined response of steel and concrete in the compression chord members, the compatibility correction factor is calculated in [Table C-17](#). Based on these correction scalars, the modified stress-strain relation of the compression chord is determined.

**Table C-17: Computation of Compatibility Correction Scalar for Specimen 1.**

	<b>Singly Reinforced</b>	<b>Double Reinforced</b>	<b>Column</b>
$d'$ (in)	2.25	2.25	2.25
$kd$ (in)	10.19	9.42	13.10
$f'_c$ (ksi)	5.4	5.4	5.4
$\psi_E = \frac{\sqrt{f'_c} (psi)}{168(1-d'/kd)}$	0.561	0.575	0.528
$\psi_P = \frac{\sqrt{f'_c} (psi)}{480(1-d'/kd)}$	0.196	0.201	0.185
$\psi_{PP} = -\frac{\sqrt{f'_c} (psi)}{1500(1-d'/kd)}$	-0.063	-0.064	-0.059



The arch breadth scalar is calculated to determine the area that needs to be assigned to the inclined arch and struts in the beam and beam-column joints.

**Table C–18: Computing Arch Breadth Scalar.**

$\eta = \frac{V_{Arch}}{V_{Arch} + V_{Truss}} = \frac{\rho_L f_y}{\rho_L f_y + \rho_T f_{yh} j \cot^2 \alpha}$			
	<b>Singly Reinforced</b>	<b>Double Reinforced</b>	<b>Column</b>
$d$ (in)	33.25	33.25	33.25
$b$	24	24	24
$s$	4.5	4.5	8
$jd$ (in)	31.0	31.0	31.0
$j$	0.93	0.93	0.93
$f_y = f_{yh}$ (ksi)	65	65	65
$A_s$ (in <sup>2</sup> )	8.35	8.35	10.25
$A_{sh}$ (in <sup>2</sup> )	0.393	0.393	0.393
$\rho_T = A_{sh}/b_w s$	0.00364	0.00364	0.00205
$\rho_L = A_s/bd$	0.0105	0.0105	0.0128
$\alpha$ (degrees)	39.02	39.02	45
$\eta$	0.671	0.671	0.87 (0.75 used)

Based on the properties computed above and the theory presented in [Chapter 3](#), the axial rigidities are computed. The equations used are presented in [Table 3–2](#).

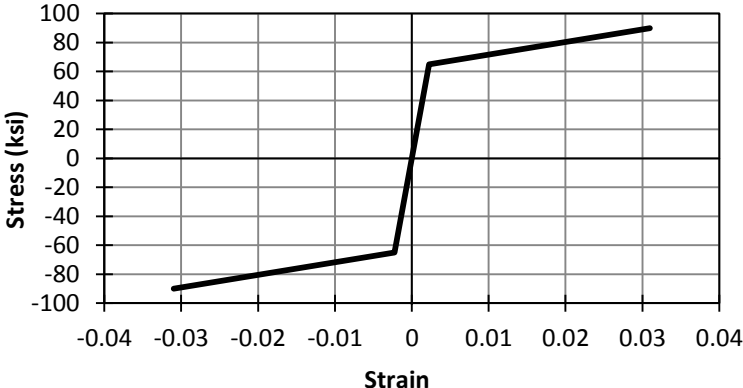
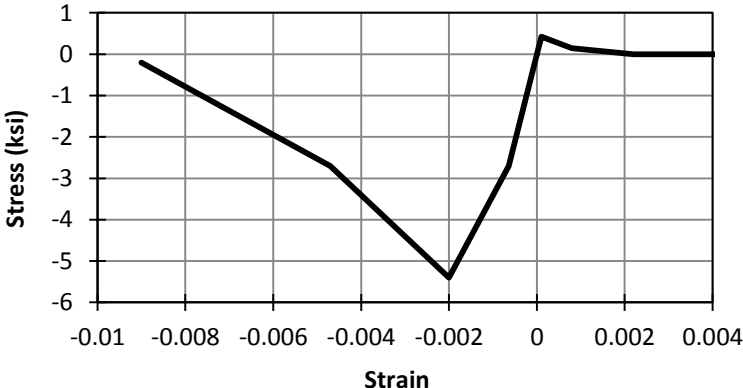
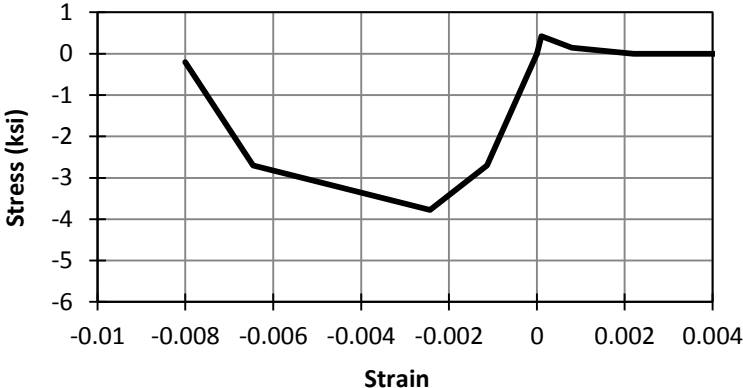
**Table C–19: Axial Rigidities of C-STM Elements: Specimen 1.**

	MEMBER	Steel		Concrete		Comments
		E (ksi)	A (in <sup>2</sup> )	E (ksi)	A (in <sup>2</sup> )	
<b>Beam</b>	A-E (D)	29000	8.35	4190	226.00	Tension Chord
	A-E (S)	29000	8.35	4190	245.00	
	B-D (D)	29000	6.28	2409	226.00	Compression Chord
	B-D (S)	29000	1.57	2351	245.00	
	BC	29000	2.36	4190	162.00	Transverse Steel
	AD	-	-	4190	240.60	Concrete Arch
	AB	-	-	4190	110.52	Concrete Truss
	CD	-	-	4190	118.14	
<b>Beam-Column Joint</b>	E-K (D)	29000	8.35	4190	226.00	Tension Chord
	E-K (S)	29000	8.35	4190	245.00	
	D-H (D)	29000	6.28	2409	226.00	Compression Chord
	D-H (S)	29000	1.57	2351	245.00	
	FG&HI	29000	0.39	4190	54.00	Transverse Steel
	DK	-	-	4190	295.92	Concrete Arch
	DG	-	-	4190	73.64	Concrete Truss
	DI	-	-	4190	78.46	
	FK	-	-	4190	78.15	
HK	-	-	4190	73.90		
<b>Column</b>	JJ	29000	10.25	4190	314.40	Tension Chord
	LL	29000	3.93	2212	314.40	Compression Chord
Beam: $N_h = 6$ and beam-column joint: $N_h = 2$						
<i>(D) Doubly reinforced beam (S) Singly reinforced beam</i>						

*Step 4: Determine constituent material properties.*

The stress-strain models used for the members in Phase 1 of Specimen 1 are as follows. The only difference for Phase 2 of the specimen is that the concrete tensile strength was reduced to 0.2 *ksi* to account for the minor concrete cracking that had occurred in Phase 1 of the experiment.

**Table C-20: Stress-Strain Models Used for C-STM Members: Phase 1 of Specimen 1.**

Member	Stress-Strain Model
All steel members.	 <p>The graph shows Stress (ksi) on the y-axis ranging from -100 to 100 and Strain on the x-axis ranging from -0.04 to 0.04. The curve is bilinear, starting at approximately (-0.03, -90), passing through the origin (0,0), and reaching a peak of about 90 ksi at a strain of 0.03.</p>
All concrete members, except the beam and column compression chord members. AB, CD, GD, ID, FK, HK, AD, CB, GF, IH, J1J2, and AK.	 <p>The graph shows Stress (ksi) on the y-axis ranging from -6 to 1 and Strain on the x-axis ranging from -0.01 to 0.004. The curve is parabolic-rectangular, starting at approximately (-0.009, -0.5), reaching a minimum of about -5.5 ksi at a strain of -0.002, crossing the origin (0,0), and peaking at approximately 0.5 ksi at a strain of 0.001.</p>
Beam compression chord. BH	 <p>The graph shows Stress (ksi) on the y-axis ranging from -6 to 1 and Strain on the x-axis ranging from -0.01 to 0.004. The curve is parabolic-rectangular, starting at approximately (-0.009, -0.5), reaching a minimum of about -4 ksi at a strain of -0.002, crossing the origin (0,0), and peaking at approximately 0.5 ksi at a strain of 0.001.</p>



**Table C-20: Stress-Strain Models Used for C-STM Members: Phase 1 of Specimen 1 (continued).**

<p>Column compression chord. L1L2</p>	<p>Stress (ksi)</p> <p>Strain</p>
<p>Softened concrete model for the beam-column joint concrete arch. DK (In Phase 2)</p>	<p>Stress (ksi)</p> <p>Strain</p>

### ***Computation for C-Beam Specimen 4.***

C-Beam Specimen 4 was subjected to moderate amounts of ASR/DEF damage. While the procedure for calculating the member and material properties remains the same as in the case of Specimen 1, certain modifications are required to account for the effects of ASR/DEF in the specimens. The modifications are based on the recommendations made in [Chapter 3](#).

*Step 1: Compute modified material properties to account for ASR/DEF.*

To account for the effects of ASR/DEF on the C-Beam specimens, modified material properties are calculated based on the recommendations presented in [Section 3.6.5](#).

- *Diagonal truss concrete:*

**Table C–21: Modified Concrete Strength for Concrete Truss Members of the C-STM.**

	<b>Specimen 4</b>
ASR/DEF damage level	Moderate
$f'_c$ (ksi)	4.0
$\lambda$	0.70
$f'_{cASR}$ (ksi) = $\lambda f'_c$	2.80

The stress-strain of the following members ([Figure C–3](#)) is modified based on the reduced concrete strength of the diagonal truss: AK, AB, CD, GD, ID, FK, HK, CB, GF, and IH.

- *Compute prestress in the beam and column ties:*

Based on the recommendations made in [3.6.5](#) the prestress in the longitudinal bars and the hoops are calculated.

**Table C–22: Prestress in Longitudinal Bars and Hoops Due to ASR/DEF.**

	<b>Specimen 4</b>
ASR/DEF damage level	Moderate
$f_y = f_{yh}$ (ksi)	65
Prestress in longitudinal bar (ksi)	$f_{ps} = 0.5f_y = 32.5$
Prestress in hoops (ksi)	$f_{ps} = 1.0f_{yh} = 65$

Knowing the prestress in the ties and the tie area, the prestress force to be applied in the C-STM model is computed.

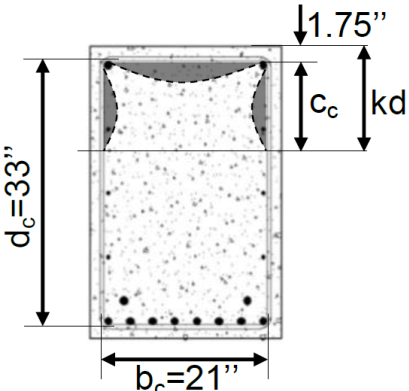
**Table C–23: Prestress Forces Applied to the C-STM Model.**

	<b>Prestress Force (kip)</b>
<b>MEMBER</b>	<b>Specimen 4</b>
<b>A-K</b>	$32.5 \times 8.35 = 271.38$
<b>B-H (D)</b>	$32.5 \times 6.28 = 204.10$
<b>B-H (S)</b>	$32.5 \times 1.57 = 51.03$
<b>BC</b>	$65 \times 2.36 = 153.40$
<b>FG&amp;HI</b>	$65 \times 0.393 = 25.35$
<b>JJ</b>	$32.5 \times 10.25 = 333.13$
<b>LL</b>	$32.5 \times 3.93 = 127.73$

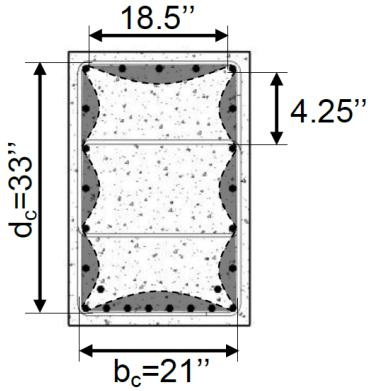
- Compute confinement ratio for the beam and the column:

To account for the confinement caused by the swelling of core concrete, the confinement ratios are computed for the beam and the column.

**Table C-24: Calculating Confinement Ratio of the Beam.**

	
	<b>Specimen 4</b>
$f'_c$ (ksi)	4.0
$kd$ (in)	11.20
$A_{cc}$ (in <sup>2</sup> ) = $(c_c + d_s / 2) \times b_c$	200.70
$A_e$ (in <sup>2</sup> ) = $(c_c + d_s / 2) \times b_c$ - area of shaded region	122.86
$k_e = A_e / A_{cc}$	0.603
$f_{lx}$ (ksi)	0.176
$f_{ly}$ (ksi)	0.162
Smallest confining stress ratio $f_{ly} / f'_c$	0.041
Largest confining stress ratio $f_{lx} / f'_c$	0.44
$K = f'_{cc} / f'_c$	1.28

**Table C–25: Calculating Confinement Ratio of the Column.**

	
	<b>Specimen 4</b>
$f'_c$ (ksi)	4.0
$kd$ (in)	11.20
$A_{cc}$ (in <sup>2</sup> ) = $b_c d_c$	693
$A_e$ (in <sup>2</sup> ) = $b_c d_c$ – area of shaded region	560.85
$k_e = A_e / A_{cc}$	0.81
$f_{lx}$ (ksi)	0.278
$f_{ly}$ (ksi)	0.219
Smallest confining stress ratio $f_{ly} / f'_c$	0.055
Largest confining stress ratio $f_{lx} / f'_c$	0.069
$K = f'_{cc} / f'_c$	1.35

*Step 2: Compute section properties.*

The steel areas computed in [Table C–15](#) for Specimen 1 hold good for Specimen 4 as well. However, the depth of compression zone ( $kd$ ) has to be recalculated to account for the prestress forces that are applied on the ties.

**Table C-26: Determining the Depth of the Compression Zone for Specimen 4 With ASR/DEF Damage.**

	Compression Steel			Tension Steel				Axial Load	Elastic Depth	
	$A_s'$ ( $in^2$ )	$d'$ ( $in$ )	$\rho'$	$A_s$ ( $in^2$ )	$d$ ( $in$ )	$b$ ( $in$ )	$\rho$	$P$ ( $kip$ )	$k$	$kd$ ( $in$ )
Single Beam	1.57	2.25	0.00197	8.35	33.25	24	0.01046	51.0	0.337	11.21
Double Beam	6.28	2.25	0.00787	8.35	33.25	24	0.01046	204.1	0.343	11.40
Column	3.92	2.25	0.00492	10.25	33.25	24	0.01284	763.1	0.458	15.22

*Step 3: Determine C-STM geometry.*

The geometry of the C-STM remains the same as Specimen 1. However, axial loads are applied at the nodes to account for the ASR/DEF effects. The C-STM model for Specimen 4 is shown in Figure C-4.

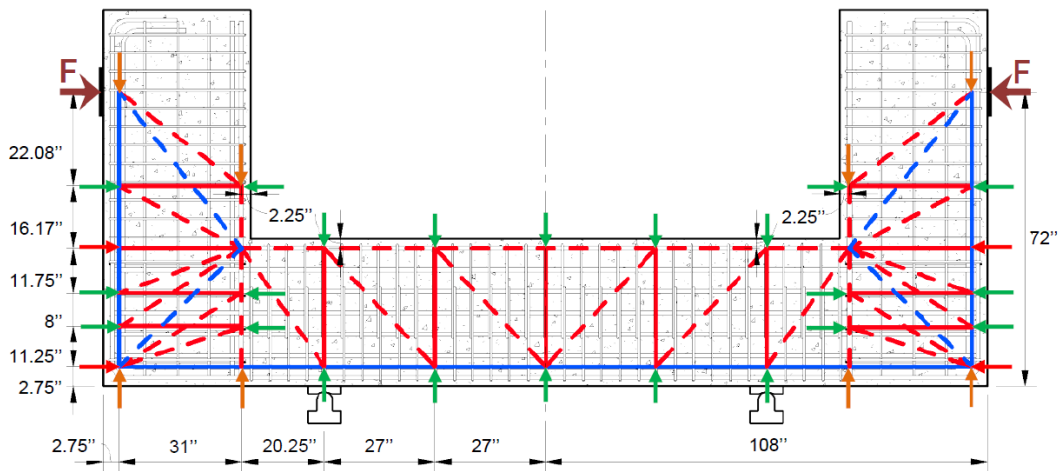


**Figure C-4: C-STM Model for C-Beam Specimen 4.**

*Step 4: Determine axial rigidities.*

The compatibility correction factor for Specimen 4 is recalculated.

**Table C-27: Computation of Compatibility Correction Scalar for Specimen 4.**

	<b>Singly Reinforced</b>	<b>Double Reinforced</b>	<b>Column</b>
$d' (in)$	2.25	2.25	2.25
$kd (in)$	11.21	11.40	15.22
$f'_c (ksi)$	4.0	4.0	4.0
$\psi_E = \frac{\sqrt{f'_c (psi)}}{168(1-d'/kd)}$	0.471	0.469	0.442
$\psi_P = \frac{\sqrt{f'_c (psi)}}{480(1-d'/kd)}$	0.165	0.164	0.155
$\psi_{PP} = -\frac{\sqrt{f'_c (psi)}}{1500(1-d'/kd)}$	-0.053	-0.053	-0.049

The arch-breadth scalar remains the same as in [Table C-18](#).

The axial rigidities are recomputed based on the modified properties calculated above for Specimen 4.

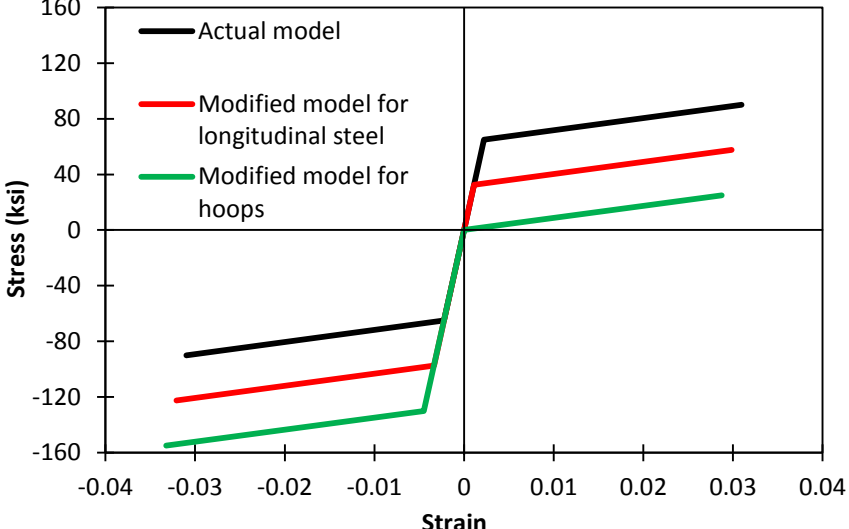
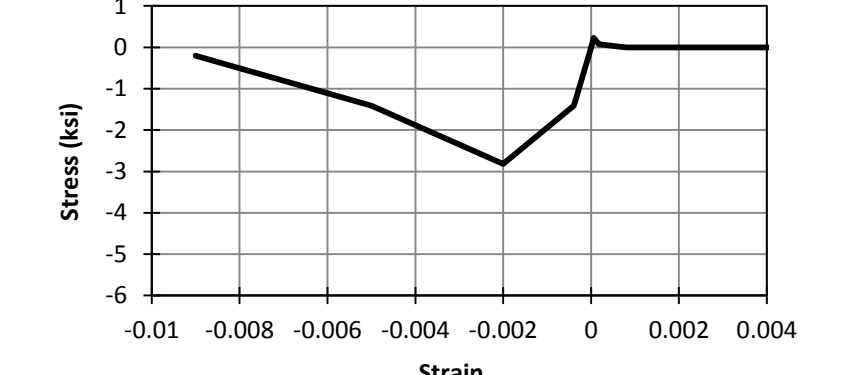
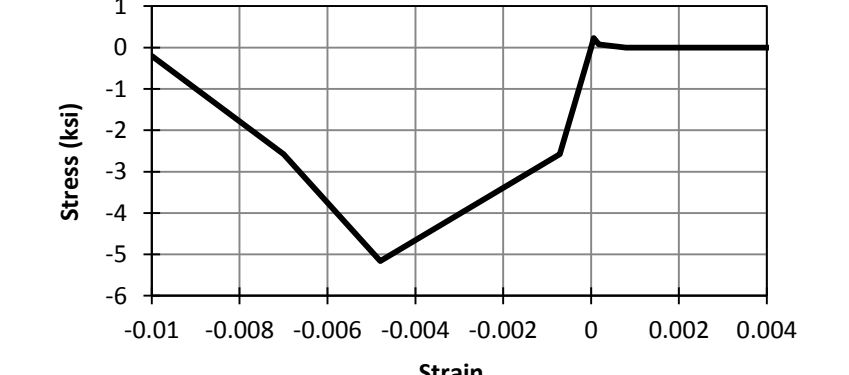
**Table C–28: Axial Rigidities of C-STM Elements: Specimen 4.**

	MEMBER	Steel		Concrete		Comments
		E (ksi)	A (in <sup>2</sup> )	E (ksi)	A (in <sup>2</sup> )	
<b>Beam</b>	<b>A-E (D)</b>	29000	8.35	4190	273.60	Tension Chord
	<b>A-E (S)</b>	29000	8.35	4190	269.04	
	<b>B-D (D)</b>	29000	6.28	1690	273.60	Compression Chord
	<b>B-D (S)</b>	29000	1.57	1698	269.04	
	<b>BC</b>	29000	2.36	4190	162.00	Transverse Steel
	<b>AD</b>	-	-	4190	240.60	Concrete Arch
	<b>AB</b>	-	-	4190	110.52	Concrete Truss
	<b>CD</b>	-	-	4190	118.14	
<b>Beam-Column Joint</b>	<b>E-K (D)</b>	29000	8.35	4190	273.60	Tension Chord
	<b>E-K (S)</b>	29000	8.35	4190	269.04	
	<b>D-H (D)</b>	29000	6.28	1690	273.60	Compression Chord
	<b>D-H (S)</b>	29000	1.57	1698	269.04	
	<b>FG&amp;HI</b>	29000	0.39	4190	54.00	Transverse Steel
	<b>DK</b>	-	-	4190	295.92	Concrete Arch
	<b>DG</b>	-	-	4190	73.64	Concrete Truss
	<b>DI</b>	-	-	4190	78.46	
	<b>FK</b>	-	-	4190	78.15	
<b>HK</b>	-	-	4190	73.90		
<b>Column</b>	<b>JJ</b>	29000	10.25	4190	365.28	Tension Chord
	<b>LL</b>	29000	3.93	1593	365.28	Compression Chord
Beam: $N_h = 6$ and beam-column joint: $N_h = 2$						
<i>(D) Doubly reinforced beam (S) Singly reinforced beam</i>						



Step 5: Determine constituent material properties.

**Table C-29: Stress-Strain Models for the Elements of the C-STM Model: Specimen 4.**

Member	Stress-Strain Model
All members	 <p>The graph shows Stress (ksi) on the y-axis (ranging from -160 to 160) versus Strain on the x-axis (ranging from -0.04 to 0.04). Three curves are plotted: a black line for the 'Actual model', a red line for the 'Modified model for longitudinal steel', and a green line for the 'Modified model for hoops'. All curves show a sharp increase in stress at zero strain, with the actual model reaching the highest peak stress of approximately 90 ksi.</p>
Concrete truss members in the beam. AK, AB, CD, GD, ID, FK, HK, CB, GF, and IH.	 <p>The graph shows Stress (ksi) on the y-axis (ranging from -6 to 1) versus Strain on the x-axis (ranging from -0.01 to 0.004). A single black curve shows a non-linear relationship, reaching a minimum stress of about -3 ksi at a strain of -0.002, and a maximum stress of about 0.5 ksi at a strain of 0.001.</p>
For remaining concrete members in the beam.	 <p>The graph shows Stress (ksi) on the y-axis (ranging from -6 to 1) versus Strain on the x-axis (ranging from -0.01 to 0.004). A single black curve shows a non-linear relationship, reaching a minimum stress of about -5 ksi at a strain of -0.005, and a maximum stress of about 0.5 ksi at a strain of 0.001.</p>

**Table C-29: Stress-Strain Models for the Elements of the C-STM Model: Specimen 4 (continued).**

<p>Column members.</p>	
<p>Softened concrete model for the beam-column joint. DK</p>	